

UNIVERSITY OF NAPOLI FEDERICO II

Doctorate School in Molecular Medicine

**Doctorate Program in
Genetics and Molecular Medicine
Coordinator: Prof. Lucio Nitsch
XXVIII Cycle**

***“Drosophila dyskerin is cell-autonomously
required for formation of the larval intestinal
stem cell niche”***

**Candidate: Arianna Petrizzo
Tutor: Prof. Maria Furia**



Napoli 2016

TITLE:

“Drosophila dyskerin is cell-autonomously required for formation of the larval intestinal stem cell niche”

TABLE OF CONTENTS

LIST OF PUBLICATIONS	pag. 4
ABSTRACT	pag. 6
1. BACKGROUND	pag. 7
1.1. Dyskeratosis Congenita (DC): clinical and genetic heterogeneity	pag. 7
1.2. The X-linked Dyskeratosis Congenita (DC)	pag. 8
1.3. The <i>DKC1</i> gene and the molecular mechanisms underlining X-DC	pag. 10
1.4. <i>Drosophila melanogaster</i> as a model for the study of dyskerin telomerase-independent functions	pag. 13
1.5. <i>Drosophila</i> larval midgut	pag. 14
1.5.1. Morphogenesis of <i>Drosophila</i> midgut	pag. 15
1.6. Autophagy	pag. 18
1.6.1. Autophagic machinery	pag. 19
1.6.2. Functions and regulation of autophagy	pag. 21
2. AIMS OF THE STUDY	pag. 23
3. MATERIALS AND METHODS	pag. 25
3.1. <i>Drosophila</i> strains	pag. 25
3.2. Sectioning	pag. 25
3.3. Flp-out/Gal4 analysis	pag. 25
3.4. Immunofluorescence stainings	pag. 26
3.5. Z-stack analysis	pag. 26
3.6. Quantification of <i>esg</i> ⁺ cells in entire midguts	pag. 27
3.7. Quantification of <i>esg</i> ⁺ <i>pros</i> ⁻ cells in frames of midguts	pag. 27

3.8. Quantification of GFP+ differentiated midgut cells	pag. 27
4. RESULTS	pag. 28
4.1. Drosophila dyskerin (the MFL protein) is required for the formation of larval midgut stem niches (the imaginal islands)	pag. 28
4.2. Formation of imaginal islands requires <i>mfl</i> expression specifically within the <i>esg+</i> cells	pag. 29
4.3. The absence of the islands is a cell-autonomous effect of <i>mfl</i> silencing	pag. 30
4.4. Quantitative reduction of MFL-depleted <i>esg+</i> cells	pag. 34
4.5. MFL-depleted <i>esg+</i> cells are not EEs but AMPs not aggregated into islands	pag. 39
4.6. Reduction in the AMP number occurs during the first amplification phase	pag. 40
4.7. The loss of imaginal islands is not due to AMP premature differentiation	pag. 42
4.8. MFL-depleted AMPs preserve their stem-cell identity	pag. 45
4.9. MFL-depletion does not affect AMP growth	pag. 49
4.10. Alteration of AMP maintenance is not due to apoptosis	pag. 53
4.11. MFL-depleted AMPs activate autophagy in a cell-specific manner	pag. 55
5. DISCUSSIONS	pag. 61
6. CONCLUSIONS	pag. 67
7. ACKNOWLEDGMENTS	pag. 68
8. REFERENCES	pag. 69
9. ORIGINAL PAPERS	pag. 80

LIST OF PUBLICATIONS RELATED TO THE THESIS:

Rosario Vicidomini¹, Annamaria Di Giovanni¹, Arianna Petrizzo, Liliana Felicia Iannucci, Giovanna Benvenuto, Anja C. Nagel, Anette Preiss and Maria Furia. Loss of *Drosophila* pseudouridine synthase triggers apoptosis-induced proliferation and promotes cell-nonautonomous EMT. *Cell Death Dis.* 2015; 6:e1705

¹ These authors contributed equally to this work

LIST OF ABBREVIATIONS:

AED, after eggs deposition
AMPs, adult midgut precursors
DC, dyskeratosis congenita
EBs, enteroblasts
ECs, enterocytes
EEs, enteroendocrine cells
EMT, epithelial-mesenchymal transition
frt, flippase recombinant target
ISCs, intestinal stem cells
MET, mesenchymal-epithelial transition
PCD, programmed cell death
PCs, peripheral cells
rRNP, ribosomal ribonucleoparticles
scaRNPs, small Cajal body ribonucleoparticles
sdrRNAs, sno-derived RNAs
snoRNPs, small nucleolar ribonucleoparticles
UAS, upstream activation sequence
VM, visceral muscle
X-DC, X-linked dyskeratosis congenita

ABSTRACT

Loss of function mutations of human *DKC1* gene cause Dyskeratosis Congenita X-linked (X-DC), a multisystemic syndrome accompanied by telomerase defects, premature aging, increased cancer susceptibility and stem cell dysfunction. The protein encoded by *DKC1*, called dyskerin, is a pseudouridine synthase belonging to a highly evolutionarily conserved family. Dyskerin participates to the formation of the H/ACA snoRNP complexes involved in a variety of cellular functions, including pseudouridylation and processing of rRNAs, transcriptional control and telomere elongation. The striking evolutionary conservation of snoRNP functions, coupled with a highly divergent mechanism of telomere lengthening, makes *Drosophila* a suitable system in which to assess the mechanisms by which pseudouridine synthases regulate stemness maintenance. Since *Drosophila* midgut has recently emerged as an ideal model for the study of the molecular mechanisms underlying somatic stem cell maintenance, it provides an useful system to evaluate the effects caused by loss of function of genes involved in this process. I thus used the GAL4/UAS system to silence *in vivo* *Nop60b/mfl*, the *Drosophila* ortholog of *DKC1*, and investigate in detail the effects triggered by gene silencing on the formation of larval Adult Midgut Precursor (AMPs) cells. I found that *mfl* silencing totally disrupts the formation of larval imaginal islands, the typical stem niches in which AMPs are organized. MFL-depleted AMPs are strongly reduced in their number and appear dispersed into the epithelium, but they still retain the expression of stemness markers as *escargot* (a member of the Snail/Slug superfamily of Zinc finger proteins), Delta and Arm/ β -catenin, indicating that they preserve stem cell identity. Instead, *mfl* activity proved to be specifically required within cells expressing the stemness marker *escargot* to allow AMPs to proliferate and expand their number. Interestingly, upon *mfl* silencing depleted AMPs do not present evident cell-growth defects, do not prematurely differentiate or die; instead, they activate a cell-specific autophagy that correlates with their amplification impairment.

Altogether, these data establish for the first time a strict link between depletion of the eukaryotic pseudouridine synthase component of H/ACA snoRNPs and stem cell maintenance in a telomerase-lacking organism as *Drosophila*. Thus, loss of stemness can be regarded as an evolutionarily conserved telomerase-independent effect of pseudouridine synthase dysfunction.

1. BACKGROUND

1.1. Dyskeratosis Congenita (DC): clinical and genetic heterogeneity

Dyskeratosis Congenita (DC) is a highly heterogeneous syndrome initially defined as a mucocutaneous disorder characterized by a classical triad of features such as nail dystrophy, oral leukoplakia and abnormal skin pigmentation, which are present in around 80-90% of cases. However, another common feature is bone marrow failure which develops in 85% of cases and is responsible of 80% of mortality (Kirwan and Dokal 2009) (Figure 1).

The minimal clinical criteria for diagnosis of DC include the presence of at least two of the four major features mentioned above and two or more of the other somatic features known to occur in DC, including developmental delay; mental retardation; pulmonary disease; short stature; extensive dental loss; premature hair greying; malignancy; liver disease; enteropathy; ataxy; cerebellar hypoplasia; hypogonadism (Vulliamy et al. 2006). DC exhibits great heterogeneity also at genetic level, in fact mutations in seven genes

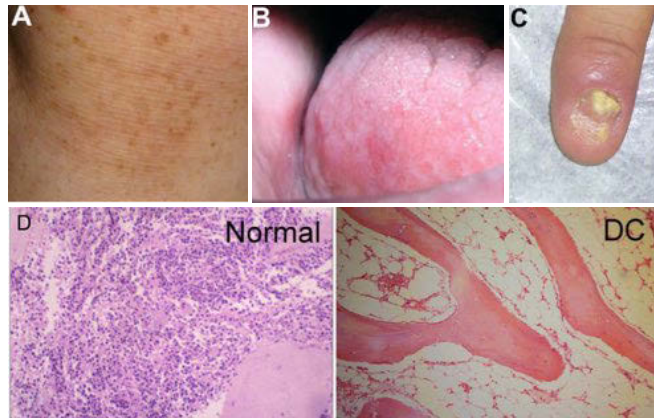


Figure 1. The main clinical features of DC: (A) Abnormal skin pigmentation; **(B)** Oral leukoplakia; **(C)** Nail dystrophy (from García and Teruya-Feldstein 2014); **(D)** Hypoplastic bone marrow (from Kirwan and Dokal 2009).

(*TERC*, *TERT*, *TINF2*, *WRAP53*, *NHP2*, *NOP10* and *DKC1*) are known to be causative of the disease with three kinds of inheritance modes: Autosomal Dominant (AD), Autosomal Recessive (AR) and X-linked recessive (XR). Table 1 reports the proportion of DC attributed to mutations in the different

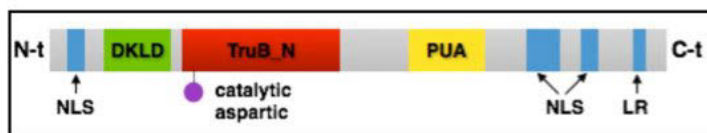


Figure 2. Structure of human dyskerin. In blue, low complexity regions corresponding to NLSs and Lysine Reach domains (LR); in green, the DKLD domain; in red, the TruB_N domain; in purple, aspartic 125 within the catalytic site; in yellow the PUA domain.

genes and the respective inheritance mode.

The products of all the seven genes are involved in telomeres maintenance because they are components

of the active telomerase complex or, in the case of *TINF2*, component of the shelterin telomere complex (Podlevsky et al. 2008). In addition, *DKC1*, *NHP2* and *NOP10* encoded proteins which are also components of H/ACA snoRNP and H/ACA scaRNPs complexes known to be involved in several important cellular functions (Kiss et al. 2006).

1.2 The X-linked Dyskeratosis Congenita (DC)

The X-linked Dyskeratosis Congenita (X-DC) is caused by hypomorphic mutations in the *DKC1* gene and is undoubtedly the most widespread form of DC (see Table 1). *DKC1* was identified as the causative gene in 1998,

Table 1. Summary of the different forms of DC

Gene	Inheritance mode	Proportion of DC attributed to mutations in this gene
<i>TERC</i>	AD	6-10%
<i>TERT</i>	AD and AR	1-7%
<i>TINF2</i>	AD	11-24%
<i>WRAP53</i>	AR	3%
<i>NHP2</i>	AR	<1%
<i>NOP10</i>	AR	<1%
<i>DKC1</i>	XR	17-36%

* 1. Data from Vulliamy et al. 2006; Walne et al. 2007; Savage et al. 2008; Vulliamy et al. 2008; Walne et al. 2008

when a screening of cDNA from different patients unveiled mutations in its coding region (Heiss et al. 1998). It encodes for a protein, named dyskerin, in which the Pfam databank (<http://pfam.sanger.ac.uk/> accession O60832) identifies at least three well conserved functional domains: the dyskerin-like domain (DKLD; 48-106 aa), typical of the proteins of the dyskerin family, whose function is currently unknown; the TruB_N pseudouridine

synthase catalytic domain (110-226 aa) that includes the active site directly involved in the process of pseudouridylation; the PUA domain (297-370 aa) that is a RNA binding domain involved in the recognition of the H/ACA ncRNAs. In addition, four low complexity regions (aa 11-20, 421-455, 467-480, 498-507), rich in lysine and arginine, are identified within the nuclear localization signals (NLSs) located at both the N- and C-terminus positions (Figure 2).

More than 40 pathologic allelic variants are described for *DKC1*; the majority are due to missense mutations that are dispersed along the sequence, although

mainly localized in the N-terminal region, in the PUA domain and in the C-terminal region. Also mutations falling in *DKC1* promoter that reduce wild type dyskerin protein levels are identified as causative of X-DC (Knight et al. 1999; Salowsky et al. 2002).

In Table 2 are reported the locations within the nucleotide and protein sequence, the amino acid substitutions and the original literature citations that are linked to the known mutations within dyskerin (Podlevsky et al. 2008).

Table 2. *DKC1* Pathologic allelic variants

Domain	Mutation	AA substitution	Exon	Reference
URR	c.-141C>G	n/a	5' URR	Knight et al., 2001
	c.-142C>G	n/a	5' URR	Dokal et al., 2000
	c.5C>T	p.Ala2Val	1	Knight et al., 1999.1
	c.16+592C>G r. 16_17ins247, 16+343_589	p.Val6AlafsX5	IVS1	Knight et al., 2001
	c.29C>T	p.Pro10Leu	2	Vulliamy et al., 2006
	c.85-5C>G	p.(?)	IVS2	Knight et al., 2001
	c.91C>G	p.Gln31Glu	3	Wong et al., 2004
	c.106T>G	p.Phe36Val	3	Heiss et al., 1998
	c.109_111delCTT	p.Leu37del	3	Heiss et al., 1998
	c.113T>C	p.Ile38Thr	3	Cossu et al., 2002
	c.115A>G	p.Lys39Glu	3	Knight et al., 1999.1
	c.119C>G	p.Pro40Arg	3	Heiss et al., 1998
	c.121G>A	p.Glu41Lys	3	Knight et al., 1999.1
	c.127A>G	p.Lys43Glu	3	Heiss et al., 2001
	c.146C>T	p.Thr49Met	3	Knight et al., 1999.2
	c.194G>C	p.Arg65Thr	4	Knight et al., 1999.1
	c.196A>G	p.Thr66Ala	4	Knight et al., 1999.1
	c.200C>T	p.Thr67Ile	4	Vulliamy et al., 2006
	c.204C>A	p.His68Gln	4	Vulliamy et al., 2006
c.214_215CT>TA	p.Leu72Tyr	4	Heiss et al., 1998	
TruB	c.361A>G	p.Ser121Gly	5	Knight et al., 1999.2
	c.472C>T	p.Arg158Trp	6	Knight et al., 2001
	c.838A>C	p.Ser280Arg	9	Knight et al., 2001
	c.911G>A	p.Ser304Asn	10	Du et al., 2009
	c.941A>G	p.Lys314Arg	10	Vulliamy et al., 2006

Domain	Mutation	AA substitution	Exon	Reference
	c.949C>T	p.Leu317Phe	10	Marrone et al., 2003
	c.949C>G	p.Leu317Val	10	Du et al., 2009
PUA	c.961C>G	p.Leu321Val	10	Knight et al., 1999.1
	c.965G>A	p.Arg322Gln	10	Marrone et al., 2003
	c.1049T>C	p.Met350Thr	11	Knight et al., 1999.1
	c.1050G>A	p.Met350Ile	11	Knight et al., 1999.1
	c.1058C>T	p.Ala353Val	11	Knight et al., 1999.1
	c.1069A>G	p.Thr357Ala	11	Knight et al., 1999.1
	c.1075G>A	p.Asp359Asn	11	Vulliamy et al., 2006
	c.1133G>A	p.Arg378Gln	11	Vulliamy et al., 2011
	c.1150C>T	p.Pro384Ser	11	Marrone et al., 2003
	c.1151C>T	p.Pro384Leu	11	Knight et al., 2001
	c.1156G>A	p.Ala386Thr	12	Vulliamy et al., 2006
	c.1193T>C	p.Leu398Pro	12	Hiramatsu et al.,
	c.1204G>A	p.Gly402Arg	12	Knight et al., 1999.1
	c.1205G>A	p.Gly402Glu	12	Heiss et al., 1998
	c.1223C>T	p.Thr408Ile	12	Vulliamy et al., 2006
	c.1226C>T	p.Pro409Leu	12	Ding et al., 2004
	c.1226C>G	p.Pro409Arg	12	Alder et al., 2013
	c.1258_1259AG>TA	p.Ser420Tyr	12	Vulliamy et al., 2006
	c.1477-2A>G	p.(?)	IVS14	Vulliamy et al., 2006
	c.1476+51_oMPP1:c. (?)del	p.Asp493ValfsX 12	15	Vulliamy et al., 1999

1.3 The *DKC1* gene and the molecular mechanisms underlining X-DC

The human X-DC causative gene, *DKC1*, encodes a 58 kDa nucleolar protein, named dyskerin, and belongs to a highly conserved family that includes yeast *Cfb5*, rat *Nap57*, and *Drosophila mfl/Nop60b* (Heiss et al., 1998). Within the nucleus, mammalian dyskerin participates in at least three essential complexes: the H/ACA small nucleolar ribonucleoproteins (snoRNPs, Kiss et al. 2006); the H/ACA small Cajal body ribonucleoproteins (scaRNPs, Richard et al. 2003) and the active telomerase holoenzyme (Cohen et al. 2007).

In H/ACA snoRNP complexes dyskerin associates with three highly conserved proteins (NOP10, NHP2 and GAR1) and one molecule of small nucleolar RNA (snoRNA) of the H/ACA class (Kiss et al. 2006) (Fig. 3).

In the pseudouridylation process, dyskerin acts as catalytic pseudouridine synthase, directing the isomerization of specific uridines to pseudouridines, while each assembled snoRNA acts as a guide and selects by base complementarity the target RNA molecule and the specific site to be pseudouridylated (Lafontaine and Tollervy 1998). Pseudouridylation can influence folding and activity of target RNAs, such as tRNAs, rRNAs, snRNAs and also mRNA (Arnez and Steitz 1994; Newby and Greenbaum 2002; Schwartz et al. 2014). The most common targets of pseudouridylation are rRNAs, which are also targets of the endonucleolytic cleavages required for their maturation, directed by specific snoRNP complexes linked to the essential E1, E2 and E3 snoRNAs (Lestrade and Weber, 2006).

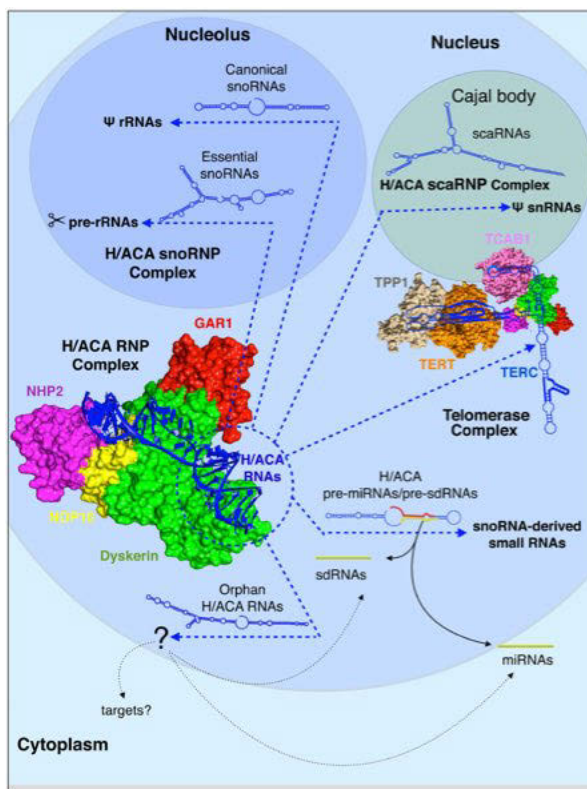


Figure 3. The diverse dyskerin-containing nuclear complexes.

Mature H/ACA snoRNPs are composed by a dyskerin-NOP10-NHP2-GAR1 tetramer assembled with a molecule of H/ACA RNA. In the nucleolus, RNPs assembled with essential snoRNAs direct pre-rRNA processing; those assembled with canonical snoRNAs direct RNA pseudouridylation. When associated with orphan H/ACA RNAs, the complexes might either guide modification of cellular RNAs or act as precursors of smaller regulatory RNAs (miRNAs/sdRNAs). H/ACA snoRNAs already identified as miRNA/sdRNA precursors are referred to as H/ACA pre-miRNAs or pre-sdRNAs. If assembled with a scaRNAs,

the tetramer composes the scaRNPs, that localize in the Cajal bodies and directs pseudouridylation of snRNAs. The whole tetramer also participates in the formation of the telomerase active complex, together with the reverse transcriptase TERT, the TCAB1 protein, that directs the complex to the Cajal bodies, and the TPP1 protein, that binds the DNA template. Within the telomerase holoenzyme, dyskerin binds the TERC 3' H/ACA domain. (from Angrisani et al., 2014)

However, functions of dyskerin extend beyond ribosome biogenesis, since it binds in the Cajal bodies a specific subgroup of small RNAs, called scaRNAs,

thus forming Cajal body ribonucleoparticles (scaRNPs), together with NOP10, NHP2 and GAR1. In this cellular compartment, the scaRNPs are responsible for pseudouridylation of snRNAs of the U1 spliceosome involved into splicing (Richard et al. 2003).

Beside acting in RNA modification processes, snoRNAs can be matured to produce short regulatory RNAs able to modulate alternative splicing (Khanna and Stamm 2010), or microRNAs (miRNAs) involved in post-transcriptional gene regulation (Ender et al. 2008; Taft et al. 2009).

Furthermore, through its ability to bind the telomerase RNA component (TERC), which harbours a 3' H/ACA domain, dyskerin participates to the formation of the active telomerase holoenzyme that is assembled in the Cajal bodies and thus plays a well established role in maintenance of telomere integrity (Cohen et al. 2007) (Figure 3).

Beyond its well-documented role in ribosome and telomerase biogenesis, more recently dyskerin has been associated to cotranscriptional functions. The snoRNP complex occupies enhancers and promoters and regulates expression of key pluripotency-related genes, such as *Oct4*, *Sox2* and *Nanog*, that are critical for self-renewal in mammalian embryonic stem cells. The snoRNA molecule determines the functionality of the RNP complex also in that transcriptional role. In fact, gene expression could be activated or repressed depending on the snoRNA molecules bound to the complex (Fong et al. 2014).

Since dyskerin is involved in several cellular functions so far described, the molecular mechanisms of X-DC pathogenesis are still not well defined.

Many authors affirm that X-DC is mainly caused by defects in telomerase function. In fact, both in mouse and in human cells, it has been observed that dyskerin mutations lead to lower telomerase RNA (TERC) levels (Wong and Collins 2006; Mochizuki et al. 2004). However, pathogenic *DKC1* mutations affect not only telomere maintenance, but also rRNA processing and pseudouridylation of cellular RNAs. Studies on mice and also on X-DC patient cells suggest that defects in ribosome biogenesis or in pseudouridylation may contribute to the DC phenotype (Ruggero et al. 2003; Bellodi et al. 2013). Moreover, specific *DKC1* mutations have been associated to a decrease in the accumulation of distinct classes of H/ACA RNAs in a tissue-specific manner, suggesting that small RNA defects may at least in part underlie the pleiotropic manifestation of X-DC (Bellodi et al. 2013).

1.4 *Drosophila melanogaster* as a model for the study of dyskerin telomerase-independent functions

One of the main challenges posed by the pathogenesis of X-DC is to distinguish the effects caused by telomere shortening from those caused by alteration of other dyskerin functions. In this respect, *Drosophila melanogaster* represents an excellent model organism with which to dissect the multiple roles

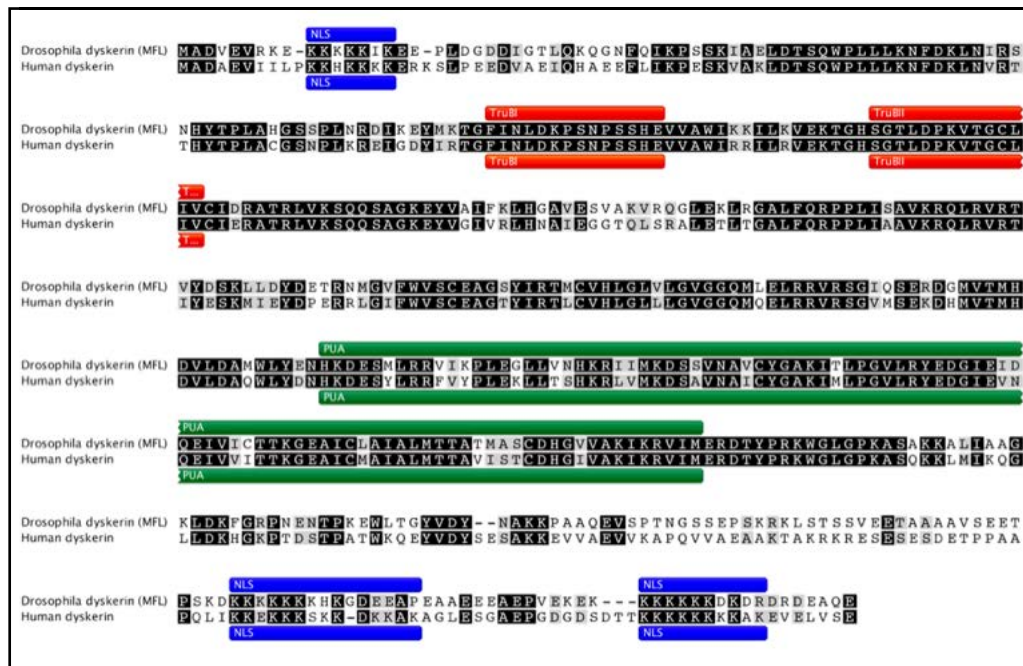


Figure 4. Alignment of human dyskerin and drosophila MFL sequences. Black boxed letters highlight identical amino acids. Blue boxes at N- and at C-terminal ends represents the NLS (nuclear localization signals); the TruB_ N e PUA domains are represented respectively in red and in green.

played by the proteins of the dyskerin family. Indeed, the *Drosophila* homologue of dyskerin, encoded by the *Nop60B/minifly (mfl)* gene, is 66% identical to human dyskerin (Figure 4) and is equally involved in rRNA processing and pseudouridylation. In addition, the most frequent missense mutations founded in patients affected by X-DC fall in regions of identity between *DKC1* and *mfl* (Giordano et al. 1999). Despite these similarities, telomere maintenance in *Drosophila* is not performed by a canonical telomerase, but by a unique transposition mechanism involving two telomere-associated retrotransposons, HeT-A and TART, which are attached specifically to the chromosome ends (Pardue et al. 2005). Therefore, the conservation of rRNP/snoRNP functions, coupled with a different mechanism of telomere

maintenance, makes *Drosophila* a useful model system to evaluate the telomerase-independent roles played by pseudouridine synthases. Hypomorphic mutations of *mfl* gene causes developmental delay, defective maturation of rRNA, small body size, alterations of the abdominal cuticle and reduced fertility, while null mutations cause larval lethality. Reduction of viability and fertility gets complicated the analysis of the molecular mechanisms that underlie this complex phenotype. However, these aspects can be overcome by triggering RNA interference (RNAi) *in vivo*, by means of a system routinely used to knock down gene expression in specific regions of the transgenic fly: the Gal4-UAS system (Fischer et al. 1988; Brand and Perrimon 1993). This system relies on two components: a transcriptional activator from yeast, Gal4, which can be expressed in a tissue-specific manner, and a transgene under the control of the upstream activation sequence (UAS) recognized by GAL4. The two components are brought together in a simple genetic cross between the transgenic line (called driver line) which expresses GAL4 and a second transgenic line (the responder line) containing the UAS-dependent transgene (the transgene of interest). In the progeny of the cross, the transgene of interest (i.e. a *sh*-RNA for gene silencing) is transcribed only in cells or tissues expressing the GAL4 protein. In previous works this approach, that allows to mimic reduced levels of wild type dyskerin, has been extensively used to induce tissue-specific silencing in the *Drosophila* wing imaginal disc/adult wing system and the results obtained revealed that MFL depletion causes specific alterations of developmental patterns (Tortoriello et al. 2010). More recently, by monitoring the effects of RNAi-mediated *mfl* silencing, we noted that gene knock-down induces apoptosis and extensive tissue remodeling, adding new light on the still unexplained tumor predisposition that characterizes X-DC (Vicidomini et al. 2015).

1.5 *Drosophila* larval midgut

The *Drosophila* gut, like its mammalian counterpart, is lined by an epithelial monolayer specialized for nutritional uptake and protection from the environment. The gut is comprised of three distinct anatomical regions: foregut, midgut, and hindgut. While foregut and hindgut are ectodermally derived, the midgut is of endodermal origin and corresponds to the mammalian small intestine (Lucchetta and Ohlstein 2012). The midgut contains both absorptive and secretory cells, which are maintained by a hierarchically organized intestinal stem cell lineage (Micchelli and Perrimon 2006; Ohlstein and Spradling 2006) (Fig. 5). After recent identification of key morphological

and molecular markers of the different cell types, the midgut has emerged as an advantageous model system for the study of the intestinal stem cell lineage, particularly useful to the discovery of genes required for stem cell maintenance and differentiation. These premises prompted me to investigate the role played by *mfl* gene in the processes governing stemness in the *Drosophila* midgut, an issue particularly relevant considering that loss of stemness is one of the pathological features of X-DC.

1.5.1 Morphogenesis of *Drosophila* midgut

During embryogenesis, endoderm is first specified as two distinct primordia positioned at the anterior and posterior termini of the embryo. Cells of the endodermal rudiment first invaginate and then undergo an epithelial-mesenchymal transition (EMT) to produce two masses of mesenchymal cells which migrate towards each other and meet in the middle of the embryo. Midgut cells are then deposited on the surface of two lateral sheets of visceral muscle (VM) flanking the embryo and undergo a mesenchymal-epithelial transition (MET). These cellular sheets close over at their dorsal and ventral aspects to form the embryonic-larval midgut, that is retained through the course of larval development until metamorphosis. During metamorphosis, larval midgut delaminates from the visceral mesoderm and basement membrane and is shed into the gut lumen. Only the so called “Adult Midgut Precursor” cells (AMPs) survive at this degeneration and fuse to form the presumptive adult midgut epithelium (Micchelli 2012).

Both molecular and morphological criteria have been employed to identify AMPs during early stages of embryonic and larval development. Initially, the relatively small cell size and the spindle shape has been used to follow AMPs (Technau and Campos-Ortega 1986; Hartenstein et al. 1992; Tepass and Hartenstein 1994; Tepass and Hartenstein 1995). However, more recent studies demonstrate that *escargot* (*esg*), a member of the Snail/Slug superfamily of zinc finger transcription factors, is an AMP marker gene (Jiang and Edgar 2009; Takashima et al. 2011). *esg* expression marks AMPs since the early embryonic stages (10-11 stages), as endoderm invagination occurs (Takashima et al. 2011). Subsequently, the endoderm splits into an outer and inner layer of cells. The outer layer gives rise to the absorptive cells of the larval gut, the enterocytes (ECs) (Tepass and Hartenstein 1994; 1995). In contrast, the inner layer contains the precursors of the larval enteroendocrine cells (EEs), which begin to express the enteroendocrine marker *prospero* (*pros*), and the AMPs, which remain in the lumen of the embryo midgut until stage 16, when they

translocate to the basal surface of the midgut epithelium (Takashima et al. 2011). AMPs maintain *esg* expression during both larvae and pupal stages (Jiang and Edgar 2009; Micchelli et al. 2011) and *esg* is expressed also in the adult intestinal stem cells, called ISCs (Micchelli and Perrimon 2006).

Another important AMP marker is the Notch ligand encoded by *Delta* (*Dl*). Since the early phases of embryogenesis, cell fate decision between the three major midgut cell types (ECs, EEs and AMPs) is in fact dependent on balanced activation of the Notch signaling. In particular, Notch activity is required for enterocytes and at the same time restricts the number of enteroendocrine cells. (Takashima et al. 2011). *Dl* expression is detected in the endoderm of stage 11 embryos and is retained in the larval undifferentiated AMPs and in the adult ISCs (Takashima et al. 2011; Jiang and Edgar 2009; Mathur et al. 2010) (Fig. 5).

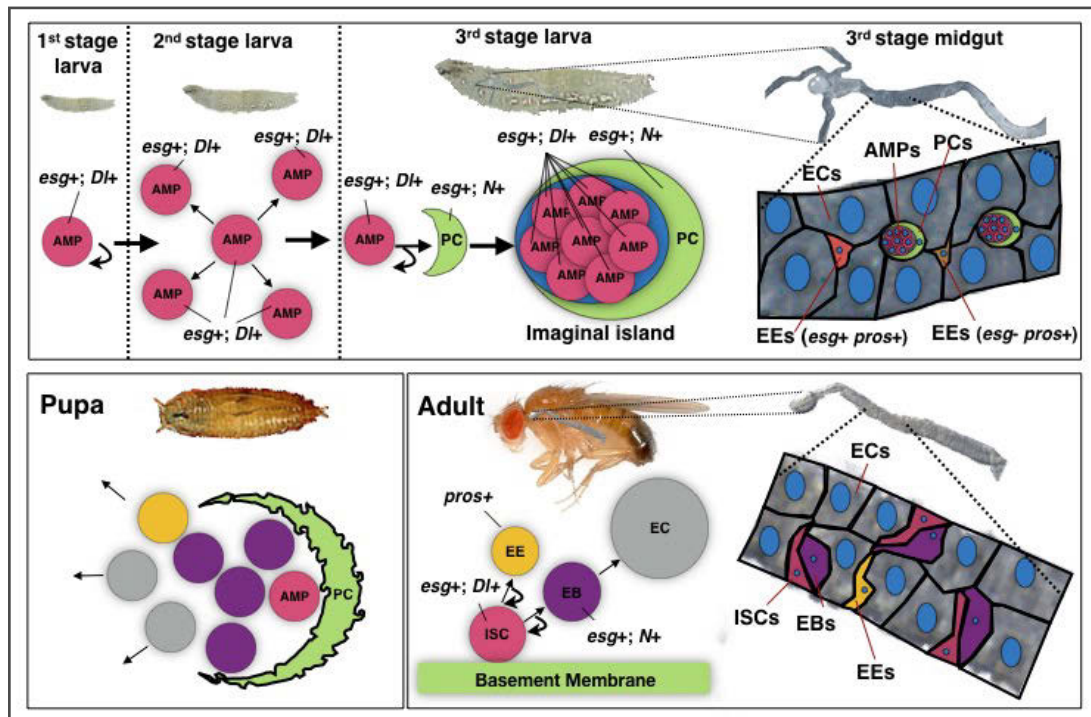


Figure 5. AMP cell lineage in larval and adult midgut. During the first two larval stages (top-left panels) AMPs, marked by *escargot* (*esg*) and *Delta* (*Dl*) expression, divide symmetrically and increase their number. During the third larval stage (top-right panel), AMPs undergo an asymmetric division to produce a Peripheral Cell (PC), which is *esg*-positive and activates Notch (N) signaling. The PC surrounds an expanded cluster of AMPs, forming the imaginal island, a transient niche in which AMPs amplify. During metamorphosis (bottom-left panel), AMPs are released from the island and begin to differentiate into enterocytes (ECs) and enteroendocrine cells (EEs) of the adult midgut. One AMP per island becomes the future adult intestinal stem cell (ISC, *esg*+;*Dl*+) which divides asymmetrically to produce both an ISC and a new differentiating cell of the adult midgut. The differentiating cell can be either a N-positive enteroblast (EB), in the way of becoming an absorptive EC, or a *prospero* (*pros*)-positive enteroendocrine cell (EE).

Recently, the use of a combination of molecular markers and cell lineage-tracing experiments have begun to clarify our understanding of AMP cell lineage. In 2011, Micchelli and coworkers have focused on the precise identification of AMPs. In their work, they demonstrated that at least three distinct classes of small midgut cells can be defined at the embryonic/larval transition on the basis of differential marker gene expression: *esg+pros-*, *esg+pros+*, *esg-pros+*. The *esg+pros+* and the *esg-pros+* cells correspond to the enteroendocrine cells, whose function is to secrete peptide hormones (Takashima et al. 2011). The *esg+pros-* cells were instead identified as AMPs for their capacity to originate all the adult midgut cells (Micchelli et al. 2011). In the embryonic-larval midgut AMPs can be identified also because they are diploid and thus appear much smaller than the large polyploid enterocytes (ECs). In addition, AMPs express the marker genes *esg* and *Dl*, and are easily distinguishable from the EEs because they do not express the enteroendocrine marker *pros*. During the first two larval stages (24-72 hours After Egg Deposition, AED), AMPs increase their number through a series of symmetric divisions (about 4 divisions) and disperse into the epithelium (Jiang and Edgar 2009; Micchelli et al. 2011). However, at the beginning of the third larval stage (96 hours AED) AMPs undergo an asymmetric division that produces two daughter cells, one that retains the AMP fate, and the other that develops as a peripheral cell (PC), in which Notch signaling is activated (Mathur et al. 2010). The newly formed AMP then undergoes a few rounds of symmetric divisions (from 3 to 5 divisions) generating an expanded cluster of cells (from 4 to 16 AMPs) that is closely surrounded by one or at least two falcet-shaped PCs to compose a sort of stem niche called “imaginal island”. Within the island, BMP signaling (Dpp signaling in *Drosophila*) from the PC promotes self-renewal and prevents differentiation of AMPs. Genetic analysis has shown that the main signaling controlling AMP amplification is the EGFR signaling. In fact, blocking the EGFR signaling in larvae at the third larval stage leads to a decrease in both the number and size of the AMP clusters (Jiang and Edgar 2009). Moreover, AMP clusters normally express high levels of *Drosophila* β -catenin (*Armadillo*, *Arm*), suggesting that cadherin-mediated interactions between AMPs facilitate the formation of the islands (Mathur et al. 2010; Issigonis and Matunis 2010). During metamorphosis, when larval midgut degenerates, AMPs are released from the islands and begin to differentiate into the ECs and the EEs that will form the adult midgut epithelium (Mathur et al. 2010; Micchelli et al. 2011). Only one AMP per island does not undergo differentiation and becomes the future ISC which guarantees the adult midgut homeostasis. In fact, ISC asymmetric divisions produce both ISCs and new ECs or EEs, in a Notch-dependent manner (Mathur et al. 2010; Micchelli and Perrimon 2006; Ohlstein and Spradling 2006; Guo and Ohlstein 2015) (Fig. 5).

1.6 Autophagy

Since in the present work I observed activation of autophagy upon *mfl* gene silencing in the larval midgut stem cells, in the following paragraphs I will describe in summary what is actually known about this process.

Autophagy is an evolutionarily conserved catabolic process in which cytoplasmic materials, organelles and proteins are delivered to lysosomes for degradation. Three main types of autophagy are usually distinguished: chaperone-mediated autophagy, microautophagy, and macroautophagy (Mizushima and Komatsu 2011). Chaperone-mediated autophagy, currently identified only in mammalian cells, is a process in which a subset of individual proteins bearing a KFERQ amino acid sequence are unfolded and selectively imported into lysosomes by interacting with chaperon proteins (Kaushik and Cuervo 2012). Microautophagy is a process in which parts of the cytosol or

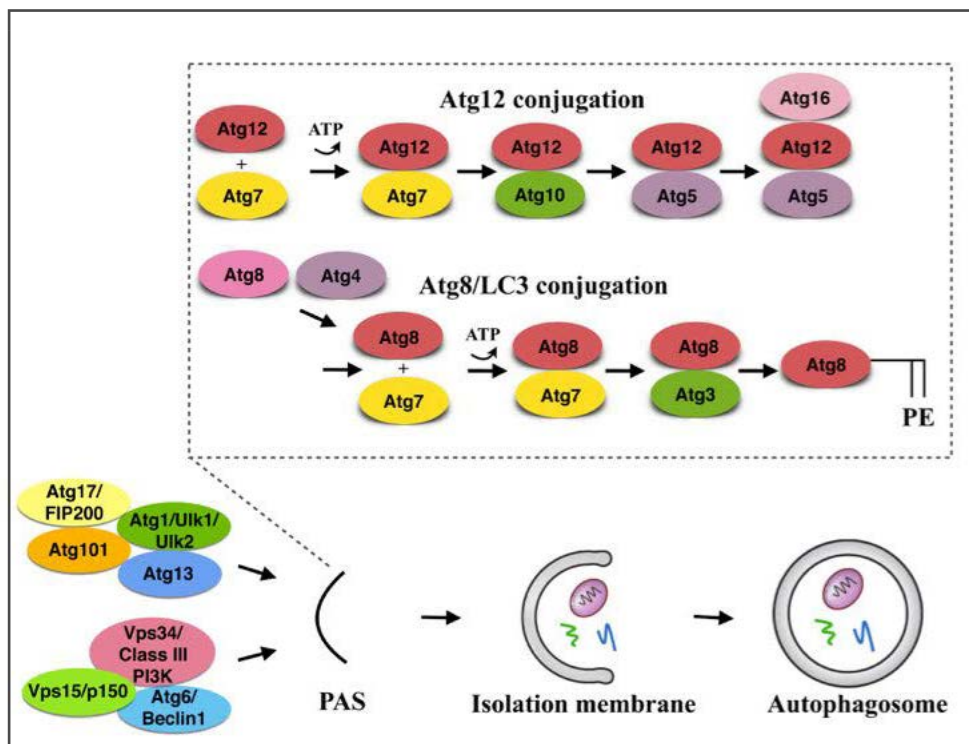


Figure 6. Core pathways that regulate autophagy. Atg1 and its interacting proteins, Vps34 and its interacting proteins, and two ubiquitin-like conjugation systems are required to originate the phagophore assembly site (PAS) and to allow elongation of the isolation membrane and formation of an autophagosome.

selected organelles, such as mitochondria (micromitophagy), peroxisomes (micropexophagy) or pieces of nucleus (micronucleophagy) are directly invaginated into lysosome for degradation (Mijaljica et al. 2011). However, the molecular mechanisms and physiological relevance of these processes are not well understood. Finally, macroautophagy is a process in which the delivery of cytoplasmic material to the lysosome involves membrane fusion events. First an isolation membrane, also known as a phagophore, must be initiated from a membrane source, known as the phagophore assembly site (PAS) (Fig. 6). Several studies indicate that the smooth endoplasmic reticulum is the principal source of autophagosome membrane (de Duve and Wattiaux 1966; Axe et al. 2008). However, recent findings suggest that additional membranes derived from the Golgi complex, the mitochondria, and the plasma membrane also contribute to autophagosome formation (Mizushima and Komatsu, 2011). Then, the elongating isolation membrane surrounds cargo that is ultimately enclosed in the double membrane autophagosome (Fig. 6). Once the autophagosome is formed, it fuses with lysosomes to form autolysosomes in which the cargo is degraded by hydrolases (Yu et al. 2010). Since in this thesis I focus on macroautophagy, I will hereafter refer to macroautophagy as autophagy for matter of simplicity.

1.6.1 Autophagic machinery

Thanks to genetic analysis performed in yeast, the major genes essential for autophagy have been identified and referred to as autophagy-related (*Atg*) genes (Klionsky, 2007). The first study demonstrating that an *Atg* gene homolog is required for autophagy in a multicellular animal was performed in *Drosophila* (Juhász et al. 2003), where 17 *Atg* genes were later identified (Melendez and Neufeld, 2008). *Atg* gene products form distinct multi-subunit complexes, controlling different steps of autophagosome formation. The Atg1 complex is usually considered to act most upstream in the hierarchy of *Atg* gene products and contains the serine/threonine kinase Atg1 (the homolog of mammalian ULK1 and ULK2 proteins) whose catalytic activity is important for autophagy induction (Kamada et al. 2000). Atg13 is the regulatory subunit of the Atg1 kinase complex that also includes Atg101 and FIP200 (also known as RB1CC1 in mammals and Atg17 in flies) in animals (Weidberg et al. 2010). The Vps34 regulatory complex is comprised of the lipid kinase Vps34 (also known as class III phosphatidylinositol 3 (PI3) kinase), Atg6 (known as Beclin-1 in mammals), and the regulatory protein Vps15 (p150 in mammals), which has a serine/threonine kinase domain (Simonsen and Tooze 2009). This

complex regulates the formation of PI3 phosphate (PI3P) lipids, and is required for multiple intracellular vesicle trafficking pathways, including endocytosis and autophagy. The Vps34 complex associates with different proteins depending on the specific vesicle process that is regulated. In the context of autophagy, these proteins include Atg14 and Vps38 (UVRAG in mammals). The Vps34 complex components have been localized to the PAS, and are required for the formation of autophagosomes (Juhász et al. 2008).

Two ubiquitin-like conjugation pathways are required for autophagy, and involve the ubiquitin-like proteins Atg8 and Atg12 (Ohsumi 2001). Atg8 and its homologs (Atg8a and Atg8b in *Drosophila*, and LC3 and GABARAP family proteins in mammals) are the most commonly used markers in studies on autophagy. In fact, Atg8 is covalently bound to autophagosome membranes, making it possible to visualize these structures using tagged reporters or antibodies against endogenous proteins (Klionsky et al. 2012). More precisely, the carboxy-terminal glycine of Atg8 is covalently bound to phosphatidylethanolamine (PE). The C-terminal amino acid(s) following the glycine residue of Atg8 are cleaved by the Atg4 family of cysteine proteases. Subsequently, the exposed glycine is conjugated to the E1-like enzyme Atg7 and is transferred to the E2-like Atg3. In parallel, Atg12 is activated by Atg7 as well, and then the E2-like Atg10 catalyzes the formation of an Atg5-Atg12 conjugate (Ichimura et al., 2000). Then, a multimeric complex of Atg5-Atg12 and Atg16 forms and enhances the covalent conjugation of Atg8 to the membrane lipid PE (Matsushita et al. 2007) (Fig. 6).

Atg8-PE is associated with both the isolation membrane and autophagosome, whereas the Atg12, Atg5, and Atg16 complex is only associated with the isolation membrane. Although autophagy was long considered a bulk degradation process with limited specificity, recent studies have clearly shown that specific cargoes can be recruited to autophagosomes for destruction (Johansen and Lamark, 2011). Several factors required for selection of specific proteins as cargo for autophagosomes have been identified, including p62/SQSTM1/Ref(2)P, Nbr1, and Alfy (Bjørkøy et al. 2005; Kirkin et al. 2009; Filimonenko et al. 2010).

The formation of autophagosomes is followed by docking and fusion with the lysosomes to form the autolysosomes; this process uses the Rab-SNARE system and other molecules that regulate membrane fusion (Nair et al. 2011). Subsequently, lysosomal hydrolases degrade the cargo in the acidic environment of the autolysosomes, and the resulting macromolecules are released into the cytosol for further recycling. Therefore, the rate of autophagy, also known as autophagic flux, depends on both the number of autophagosomes that are formed, the degradative capacity of lysosomes, and the turnover of autophagic cargo within the cell (Das et al. 2012).

1.6.2 Functions and regulation of autophagy

Autophagy is often considered a cell survival process. In fact, under starvation or energy deficient conditions, an enhanced autophagic degradation and recycling of cellular components is induced and provides an internal source of nutrients to maintain cell homeostasis (Levine and Klionsky, 2004; Lum et al. 2005). It is well known that starvation-induced autophagy is regulated by the TOR family of Ser-Thr kinases, central components of a conserved nutrient sensing pathway (Jacinto and Hall 2003). Inactivation of TOR by mutation or by treatment with the drug rapamycin induces autophagy despite the large presence of nutrients, indicating that TOR suppresses autophagy under non-starvation conditions. In yeast, TOR is thought to control the autophagic machinery, in part by regulating the activity of a complex containing the Ser-Thr kinase Atg1 (Kamada et al. 2000) and the expression of Atg8 (Kirisako et al. 1999). In higher eukaryotes, including *Drosophila*, starvation-induced autophagy is also suppressed by components of the insulin/PI3K pathway upstream of TOR, including the insulin receptor, PI3K, and Akt, whereas autophagy is promoted by the tumor suppressor PTEN, a negative regulator of insulin/PI3K signaling. In addition, the activity of a critical downstream effector of TOR, the ribosomal protein S6 kinase (S6K), has been shown to negatively correlate with induction of autophagy (Scott et al. 2004).

Recently, much interest has been focused on autophagy as a mechanism by which cells defend themselves against environmental stresses. The c-Jun NH₂-terminal kinase (JNK) pathway plays an important role in this response. In particular, JNK participates in multiple stimulation-induced autophagic events, including endoplasmic reticulum stress, nutrition deficiency, oxidative stress, cytokines and growth factors decrease and exposition to neurotoxic drugs (Zhou et al. 2015). At the molecular level, JNK mediates phosphorylation of Bcl-2, which in turn dissociates from Beclin-1 disrupting the Bcl-2/Beclin-1 complex and activating autophagy (Wei et al. 2008). The JNK pathway has been related to the so-called autophagic-induced cell death, that has been described as a non-apoptotic or necrotic programmed cell death (PCD) in which autophagy serves as a cell death mechanism (Zhou et al. 2015). This kind of death occurs in cells that are protected against apoptosis, particularly in the absence of the pro-apoptotic proteins of the Bcl-2 family, Bax and Bak (Shimizu et al. 2004). Autophagy is involved also in tissue remodeling during development. Its activation is in fact observed in dying cells throughout mammalian development, including the regression of the corpus luteum, the

involution of mammary and prostate gland and the regression of Mullerian duct structures during male genital development (Clarke, 1990).

The contribution of autophagy to cell death during development has been studied most in *Drosophila*, in which an increase of the steroid hormone ecdysone triggers the destruction of larval tissues at the end of larval period (Jiang et al. 1997). During larval salivary gland degradation, autophagy and caspases cooperate to efficiently clear dying cells. Therefore, impaired function of either autophagy or caspases results in partially degraded salivary gland cells, and decreased function of both of these processes results in intact salivary glands. These data indicate that autophagy and caspases function in parallel genetic pathways to degrade salivary glands. By contrast, caspases act upstream of autophagy to direct both starvation-induced ovarian cell death (Hou et al. 2008) and degradation of amnioserosa embryonic membrane (Mohseni et al. 2009). In addition, autophagy selectively degrades the caspase inhibitor dBruce to activate caspases and execute cell death in the *Drosophila* ovary (Nezis et al. 2009; Nezis et al. 2010).

However, autophagy plays a more prominent role in the death of fly midgut cells. In particular, during metamorphosis, larval midgut degradation is neither disrupted by expression of the pan-caspase inhibitor p35 nor by mutation of multiple caspases, indicating that apoptosis is dispensable for midgut degradation. Interestingly, midgut destruction is blocked in animals with impaired Atg1, Atg2, or Atg18 function, directly implicating autophagy as a crucial process in steroid-induced degradation of larval midgut differentiated cells, such as enterocytes (ECs) and enteroendocrine cells (EEs) (Denton et al. 2009; Das et al. 2012). As previously described, the adult midgut precursors (AMPs) are the only larval midgut cells which survive to this destroying process to give rise the adult midgut epithelium.

Intriguingly, in the present work I observed, for the first time, an unexpected cell-specific autophagic activation in the stemness compartment of *Drosophila* larval midgut, unveiling a link among depletion of the *Drosophila* dyskerin, stemness maintenance and autophagy.

2. AIMS OF THE STUDY

The X-linked Dyskeratosis Congenita (X-DC) is a multisystemic disorder characterized by mucocutaneous features, premature aging, bone-marrow failure and loss of stemness. The disease is caused by hypomorphic mutations in the *DKCI* gene which encodes dyskerin, a member of a highly conserved protein family of pseudouridine synthases (Heiss et al. 1998). All eukaryal dyskerins described so far have a prevalent nuclear localization and constitute essential core components of the H/ACA snoRNP complexes, known to be involved in a variety of essential cellular functions, including ribosome biogenesis, pseudouridylation of cellular RNAs, biogenesis and stability of H/ACA snoRNAs (Kiss et al. 2006). Beyond these well-documented roles, mammalian dyskerin has recently been associated also to co-transcriptional functions. Within a large RNP complex, dyskerin has been shown to bind enhancers and promoters, regulating the expression of key stemness regulatory genes (Fong et al. 2014). In mammals, dyskerin is an essential component also of the active telomerase complex, and thus plays a relevant role in the maintenance of telomere integrity (Cohen et al. 2007). The distinction between the effects caused by telomere shortening and those related to impairment of other dyskerin functions is still on debate and represents one of the main challenges posed by the pathogenesis of the disease. The *Drosophila* animal model may represent an attractive system in which defining the telomerase-independent roles played by eukaryotic pseudouridine synthases. In fact, the *Drosophila* protein, encoded by the *Nop60B/minifly (mfl)* gene, is highly related to human dyskerin with which shares 66% of identity; in addition, the most frequent missense mutations identified in X-DC patients fall in regions of identity between the human *DKCI* and the *Drosophila mfl* gene (Giordano et al. 1999). However, despite these similarities, telomere maintenance in *Drosophila* is not performed by a canonical telomerase, but by a unique transposition mechanism involving two telomere-associated retrotransposons, HeT-A and TART, which are attached specifically to the chromosome ends (Pardue et al., 2005).

Previous works showed that silencing the *Drosophila mfl* gene by *in vivo* RNAi alters key developmental patterns and induces apoptosis coupled with extensive tissue remodeling (Tortoriello et al. 2010; Vicidomini et al., 2015), a finding that added new light on the still unexplained tumor predisposition that characterizes X-DC patients (Angrisani et al. 2014).

The purpose of the present study was that of using *Drosophila* as a model to better define the telomerase-independent roles of eukaryotic pseudouridine synthases in order to deepen our knowledge on the molecular mechanisms underlying X-DC pathogenesis. Since stemness maintenance is one of the major biological processes affected in X-DC patients, I focussed my research activity on the formation of *Drosophila* larval midgut stem cells, known as AMPs (Adult Midgut Precursors), which emerged as an ideal system for the study of epithelial stem cell lineage (Micchelli, 2011). On these premises, this work has been addressed to the evaluation of the effects triggered by *mfl* RNAi on AMP specification and maintenance. Potent genetic tools, such as the Gal4/UAS binary system, RNAi constructs and fluorescent reporter transgenes were used to monitor *in vivo* apoptosis, autophagy, and stem cell lineage-tracing. Moreover, the coupling of Gal4/UAS and FLP/rt systems allowed to establish the cell-autonomy of the effects induced by *mfl* silencing.

3. MATERIALS AND METHODS

3.1 *Drosophila* strains

Flies were raised on standard *Drosophila* medium at 25 °C. The following strains #36595 (UAS-IR*mfl*); #4414 (*act*-Gal4); #42732 (*tub*-Gal4); #26816 (*esg*-Gal4); #31417 (UAS-RFP); #28281 (UAS-RFP,UAS-FLP,Ubi>STOP>GFP); #30728 (NRE-GFP); #32123 (UAS-Apoliner), #37749 (UAS-mCherry-GFP-ATG8a); #37750 (UAS-mCherry-ATG8a) were obtained from Bloomington Drosophila Stock Center at Indiana University (BDSC, Bloomington, IN, USA). The *omb*-Gal4 driver line was kindly provided by A. Preiss (University of Hohenheim, Germany). The *hs*-Flp;*act*>STOP>Gal4;UAS-NLS-GFP and the *hs*-Flp;*act*>STOP>Gal4,UAS-GFP lines were kindly provided by D. Grifoni (University of Bologna, Italy). The UAS-IR*mfl* RNAi (v46282) line was obtained from Vienna Drosophila RNAi Center (VDRC, Vienna, Austria).

3.2 Sectioning

Larval midguts were collected at various developmental stages, dissected in PBS (Phosphate-Buffered Saline, pH 7.5), fixed for 2 hours in 3,7% PFA (paraformaldehyde, Sigma), washed in PBS and mounted in 70% Glycerol +Dapi for fluorescence analysis.

3.3 Flp-out/Gal4 analysis

Drosophila transgenic embryos of correct genotypes were collected in a time of deposition of 12 hours and heat shocked at 18 hours AED for 15 minutes at 37 °C to induce clones. Larval midguts from heat shocked animals were dissected at the third larval stage in wandering (120 h AED), and analyzed.

3.4 Immunofluorescence stainings

For wing disc stainings, *Drosophila* larvae were dissected in PBS and fixed in 3,7% PFA. Tissues were permeabilized in 0,1% PBT (Triton X-100 in PBS) for 45', blocked for 1 hour in 2% BSA (Bovine Serum Albumine in PBT) at room temperature and incubated overnight at 4°C in 2% BSA with primary antibody. Tissues were then incubated for 1 hour at room temperature in 2% BSA with secondary antibody. Accurate washes in 0,1% PBT were performed following each step. Wing discs were then mounted on microscopy slides in 70% Glycerol+Dapi.

For larval midgut stainings, *Drosophila* larvae were dissected in PBS, fixed for 2 hours in 3,7% PFA, permeabilized in 0,1% PBT (No permeabilization for anti-Dl), blocked in 5% NGS (Normal Goat Serum in PBT, substituted by PBS for anti-Dl) for 1 hour at room temperature and incubated overnight at 4°C in 5% NGS with primary antibody. Tissues were then incubated in 5% NGS with secondary antibody for 1 hour at room temperature. Accurate washes in 0,1% PBT (PBS for anti-Dl) were performed following each step. Midguts were then mounted in 70% Glycerol+Dapi.

Antibodies used were: customer rabbit polyclonal antibody against MFL (Sigma-Aldrich Inc., St. Louis, MO, USA; dilution 1:100); mouse monoclonal antibodies against Pros, Dl, Arm (Hybridoma Bank, University of Iowa, Iowa City, IA, USA; dil. 3-5 µg/ml); rabbit polyclonal antibodies against cleaved Caspase-3, p-S6K, p-eIF2 α (Cell Signaling Tech., Danvers, MA, USA; dilution 1:500 anti-Cas3 and anti- p-S6K, 1:50 anti-p-eIF2 α); mouse monoclonal antibody against Fib (Abcam; Cambridge, UK, dil. 1/100).

Fluorescent secondary antibodies were from Jackson ImmunoResearch (Dianova, Hamburg, Germany) and used at a final dilution of 1:250. Epifluorescent images were obtained with a Nikon Eclipse E1000 epifluorescence microscope. Confocal images were obtained with Zeiss LSM510 and with Zeiss LSM700 confocal microscopes.

3.5 Z-stack analysis

All confocal captured pictures (in RAW format) have been analyzed and processed with ImageJ v1.440 software. Z-stack analysis was performed by using STACK> ZProjection and STACK>Orthogonal views ImageJ plug-in.

3.6 Quantification of *esg*⁺ cells in entire midguts

Drosophila entire larval midguts were collected at the third larval stage, fixed in 3,7% PFA, washed in PBS and mounted in 70% Glycerol+Dapi for epifluorescence analysis. Images were acquired with a 40X objective of Nikon Eclipse E1000 epifluorescence microscope on two focal planes. The two planes were added with STACK> ZProjection ImageJ plug-in and the stacked images were pieced together with Adobe Photoshop CS5.1 to obtain the reconstruction of entire midguts from the proventriculus to the posterior gut region. The *esg*⁺ cells marked by RFP fluorescence were classified as single, doublets and clusters of at least 3 cells and counted using the cell counter Image-J plug-in. The Mann-Whitney test for variance analysis was applied using the GraphPad Prism software.

3.7 Quantification of *esg*⁺*pros*⁻ cells in frames of midguts

The *esg*⁺ cells, marked by RFP fluorescence, were counted in midguts stained with anti-Pros at 3 days AED and at the third larval stage (5 days AED for control midguts; 7 days AED for silenced midguts). It was preferred to analyze frames of midguts (at a magnification of 40X) and not entire midguts, because the immunostaining method does not allow to keep the tissue intact. The *esg*⁺ cells were classified as single, doublets and clusters of at least 3 cells and counted using the cell counter Image-J plug-in. The Mann-Whitney test for variance analysis was applied using the GraphPad Prism software.

3.8 Quantification of GFP⁺ differentiated midgut cells

The *GFP*⁺ enterocytes (ECs) and enteroendocrine cells (EEs) in midguts of the correct genotypes were counted at the third larval stage (5 days AED for control midguts; 7 days AED for silenced midguts) in frames at a magnification of 40X. The cell counter Image-J plug-in was used for counting. The Mann-Whitney test for variance analysis was applied using the GraphPad Prism software.

4 RESULTS

4.1 *Drosophila* dyskerin (the MFL protein) is required for the formation of larval midgut stem niches (the imaginal islands)

The *Drosophila* larval midgut is composed by different cell types; the most common is represented by the absorptive enterocytes (ECs), characterized by large polyploid nuclei. Rarer cell types are represented by the secretory

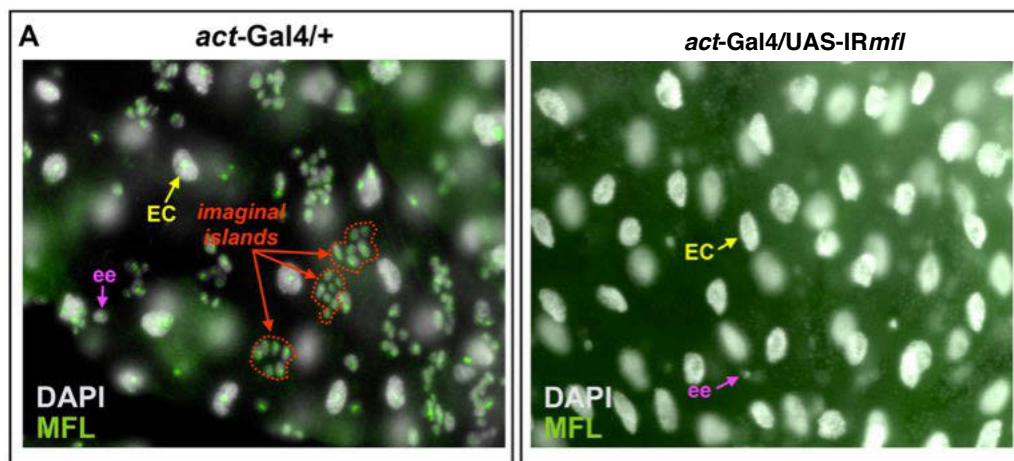


Figure 7. *mfl* ubiquitous silencing alters the formation of larval midgut stem niches (imaginal islands). (A) *act-Gal4/+* control larval midgut analyzed in epifluorescence at the third larval stage. Nuclei of three different cell types are detected: large polyploid nuclei belong to absorptive enterocytes (EC, yellow arrow); dispersed diploid nuclei belong to putative secretory enteroendocrine cells (ee, purple arrow); diploid nuclei closely associated in cluster belong to imaginal island cells (stem cell niches, red arrows). Immunostaining with anti-MFL antibody and epifluorescence analysis show that all these nuclei express the ubiquitous MFL protein. (B) *act-Gal4/UAS-IRmfl* silenced midgut at the third larval stage. *Mfl* RNAi drastically abolishes the accumulation of MFL protein in all cell types. The presence of enterocytes (yellow arrow) and putative enteroendocrine cells (purple arrows) is unaffected, but imaginal islands are no longer detectable. Dapi is in grey; anti-MFL in green.

enteroendocrine cells (EEs or ees), diploid and dispersed in the epithelium, and by the adult midgut precursor cells (AMPs), diploid and clustered within the larval midgut stem niches, called imaginal islands (Skaer 1993; Jiang and Edgar 2009; Zeng et al. 2010).

These distinct cell types can easily be distinguished morphologically, and all express the ubiquitary MFL protein (the *Drosophila* dyskerin) which, as

described for other tissues (Giordano et al. 1999), concentrates in the nucleoli (Fig. 7 A).

To check the role played by *mfl* activity on the intestinal stem cell lineage, I used the GAL4/UAS system. As previously observed, *mfl* ubiquitous silencing triggered by either *actin*-Gal4 (*act*-Gal4) or *tubulin*-Gal4 (*tub*-Gal4) drivers caused lethality at the onset of metamorphosis, underlining the crucial role played by this gene on *Drosophila* development (Tortoriello et al. 2010). In my experiments, I performed genetic crosses to couple the *act*-Gal4 (and *tub*-Gal4) driver line with an UAS-IR*mfl* responder line that already proved to be capable of knocking down efficiently all *mfl* transcripts (Riccardo et al. 2009; Tortoriello et al. 2010). In the progeny, I looked at the effects exerted by ubiquitous silencing, specifically focusing on control (genotype: *act*-Gal4/+) and silenced (genotype: *act*-Gal4/UAS-IR*mfl*) midguts at the third larval stage of development. I observed that ubiquitous silencing induced a developmental delay of about 2 days and efficiently blocked accumulation of MFL protein in each cell type. Intriguingly, ubiquitous MFL depletion dramatically elicits the disappearance of the imaginal islands (Fig. 8 B), which could not be detected even upon careful analysis at several different focal planes. This result indicates that normal accumulation levels of MFL protein are required for proper formation of larval midgut stem niches.

4.2 Formation of imaginal islands requires *mfl* expression specifically within the *esg*⁺ cells

Since both EC and EE differentiated cell types appear normally formed after *mfl* ubiquitous silencing, I supposed that gene expression was specifically required within the cells that compose the islands, i.e. the AMPs and the peripheral cells (PCs). To check this point, I restricted silencing to the population of midgut cells expressing *escargot* (*esg*), a *Drosophila* member of the *Snail/Slug* family of transcription factors whose expression in the midgut is limited to AMPs, PCs and a subset of EE cells (Zeng et al. 2010; Micchelli et al. 2011). As shown in Fig. 8, no island is formed when *mfl* silencing was directed by *esg*-Gal4 driver: the *esg*-Gal4/UAS-IR*mfl* silenced larvae have a developmental delay of about 2 days, and the number of the *esg*⁺ cells were dramatically reduced, although rare and dispersed *esg*⁺ cells which do not accumulate the MFL protein were still present (Fig. 8 B). These results thus confirmed that *mfl* expression is mandatory within the *esg*⁺ cell population for the formation of the intestinal stem niches.

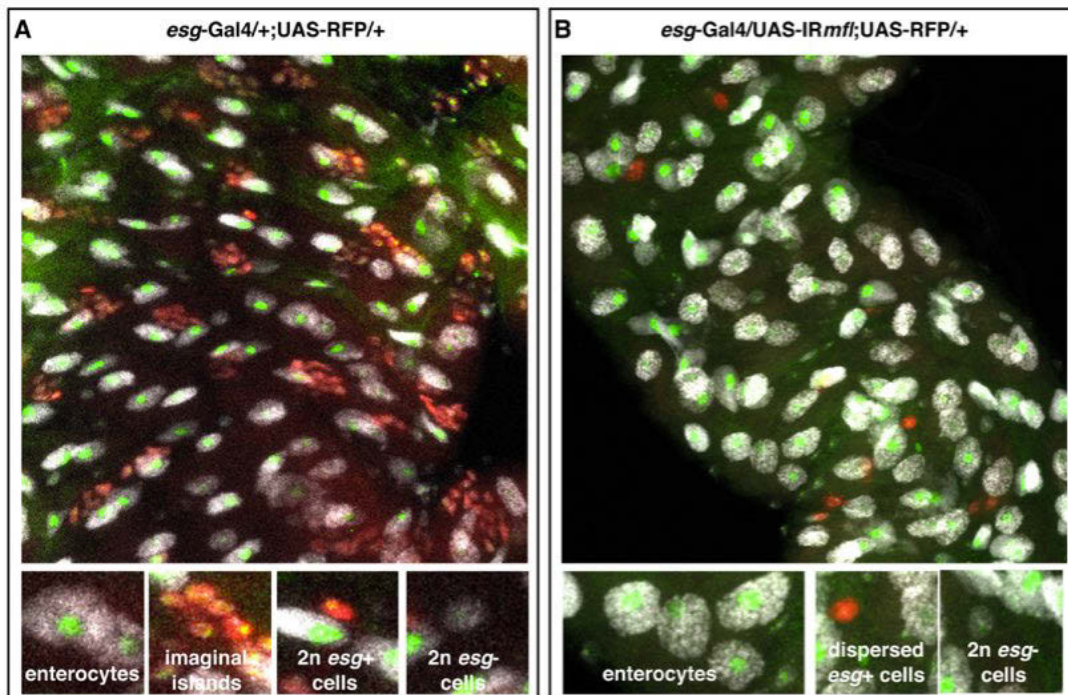


Figure 8. *mfl* silencing localized in the *esg*⁺ cells alters the formation of midgut imaginal islands. (A) *esg-Gal4/+;UAS-RFP/+* control midgut at the third larval stage. MFL protein (in green) is localized in the nucleoli of all midgut cells: polyploid ECs; diploid and clustered imaginal island cells; diploid and dispersed EEs, which are either *esg*⁺ or *esg*⁻. (B) *esg-Gal4/UAS-IRmfl;UAS-RFP/+* silenced midgut at the third larval stage. *esg-Gal4* driven silencing abolishes the accumulation of MFL protein in the population of cells expressing *esg*, marked in red. The MFL-depleted *esg*⁺ cells do not form imaginal islands but appear rare and dispersed. Dapi is in grey; anti-MFL antibody in green; *esg*-expression domain is marked by an UAS-RFP reporter line in red.

4.3 The absence of the islands is a cell-autonomous effect of *mfl* silencing

In the previous experiments, I noted that MFL-depleted *esg*⁺ cells are dispersed into the epithelium. Since also a subpopulation of enteroendocrine cells is *esg*⁺ (Micchelli et al. 2011), I attempted to establish if these dispersed cells were enteroendocrine, or instead represent AMPs not aggregated into stem niches. Furthermore, I considered the possibility that the observed loss of imaginal islands could be due to cell non-autonomous effects triggered by *mfl* silencing in a different tissue. Indeed, *act-Gal4* is an ubiquitous driver (Graveley et al. 2010) and the population of *esg*⁺ cells comprises not only cells of the imaginal islands (AMPs and PCs) and a subgroup of enteroendocrine

(EE) midgut cells but it includes cells of other organs, such as salivary glands, ring gland, and brain (Chintapalli et al. 2010) (Fig. 9 A). Thus, it could not be excluded that altered signaling from these compartments could be responsible for the loss of the midgut imaginal islands (Fig. 9 B). Indeed, it is known that the steroid hormone ecdysone, produced by ring gland, controls many events of insect morphogenesis, including AMP expansion (Micchelli et al. 2011). Defective signaling of the insulin-like peptides produced from the brain is also reported to affect either growth and adult midgut stem cell proliferation (Choi et al. 2011).

To assess this point, I performed a mitotic clonal analysis by using the Flp-out technique. According to this technique, heat-shock-induced expression of the site-specific recombinase Flippase (Flp) joins an ubiquitous promoter (i.e. *actin* promoter) to a selected coding sequence by removing an internal cassette containing a transcriptional termination site flanked on both sides by FRTs (Flippase Recognition Targets; Struhl and Basler 1993). When the Flp-out system is combined with the Gal4/UAS system, the FLP-out event activates the Gal4 transcription factor (de Celis and Bray 1997; Pignoni and Zipursky 1997). Cell clones expressing Gal4 will in turn activate any other UAS-transgene; in my experiments I added an UAS-GFP construct, to positively mark the Gal4-expressing clones, and the silencer UAS-IR*mfl* construct (Fig. 10 A). The Flp-out-Gal4 system directs *mfl* silencing only in a small and stochastic population of cells and allow to compare them to the unsilenced cells in the same gut at the same developmental time, avoiding the possibility that the results could be affected by developmental delay.

Thus, I used the Flp-out-Gal4 system to trigger gene silencing in mitotic GFP+ clones, while the surrounding GFP- cells express *mfl* normally. *Drosophila* transgenic embryos (of genotype *hs-Flp;act>STOP>GAL4,UAS-GFP/UAS-IR-mfl*) and control embryos (of genotype: *hs-Flp;act>STOP>GAL4,UAS-GFP/+*) were then subjected to heat shock at 37 °C. The timing and the duration of heat shock influence the clone formation: early clone induction generally results in larger clones, while the duration of the heat shock influences the number of cells undergoing a FLP-out event. In my experiments, I induced heat shock at 37 °C for 15 minutes on a population of embryos collected in a time of deposition of 12 hours. In particular, the heat shock was induced in embryos after they reach the stage 10 of embryonic development, which is the stage when AMPs are specified (6 hours AED, After Eggs Deposition; Takashima et al. 2011). Midguts of heat-shocked animals were then analyzed at the third larval stage (5 day AED) (Fig. 10 A). In control midguts, clones marked by GFP expression include polyploid enterocytes (ECs) and clusters of diploid cells corresponding to imaginal islands (Fig. 10 B). On the contrary, in midguts where gene silencing was mitotically induced,

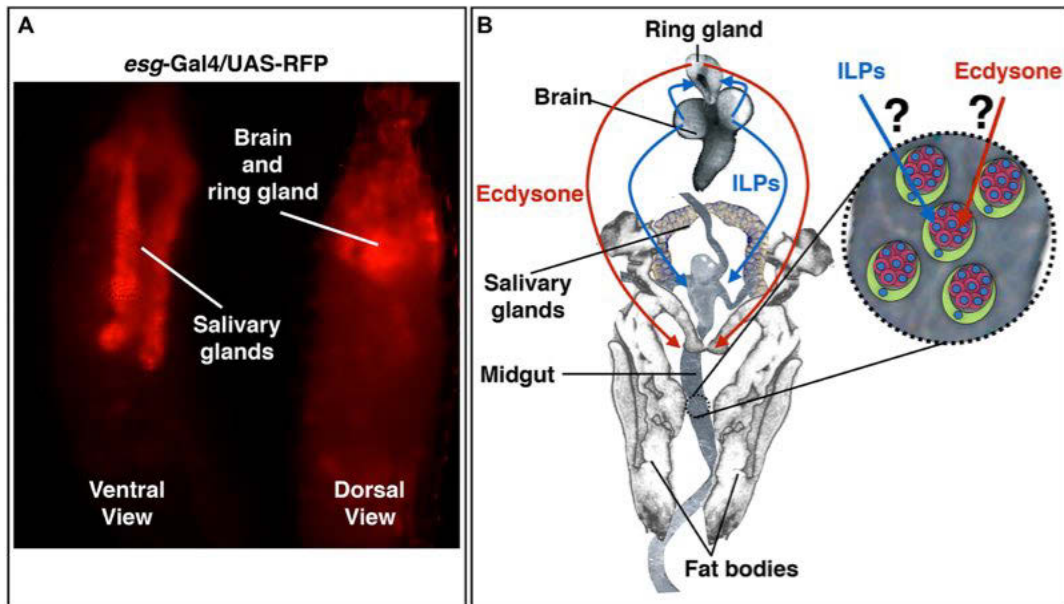


Figure 9. *esg* expression and signaling which could influence imaginal island formation. (A) Immunofluorescent image of an *esg*-Gal4/UAS-RFP larva. The UAS-RFP marks *esg* expression compartments: salivary gland (in the ventral view); brain and ring gland (in the dorsal view). (B) Schematic representation of *Drosophila* larval organs. The ecdysone signal from the ring gland and the insulins-like peptide signal from brain could influence the formation of midgut imaginal islands.

the GFP⁺ silenced clones are formed exclusively by ECs or by dispersed diploid cells, and never include imaginal islands (Fig. 10 C). These observations lead to conclude that *mfl* silencing impedes the formation of the imaginal islands in a cell-autonomous manner. Moreover, since I induced the removal of the Flp-out cassette after the developmental timing in which AMPs are specified, this result indicates that the observed loss of imaginal islands is not due to AMP specification defects. Worth noting, clonal analysis allowed to rule out the possibility that the observed loss of islands could be due to imprecise temporal staging of the silenced midguts, since I observed that imaginal islands were correctly formed in the unsilenced tissues surrounding the silenced clones.

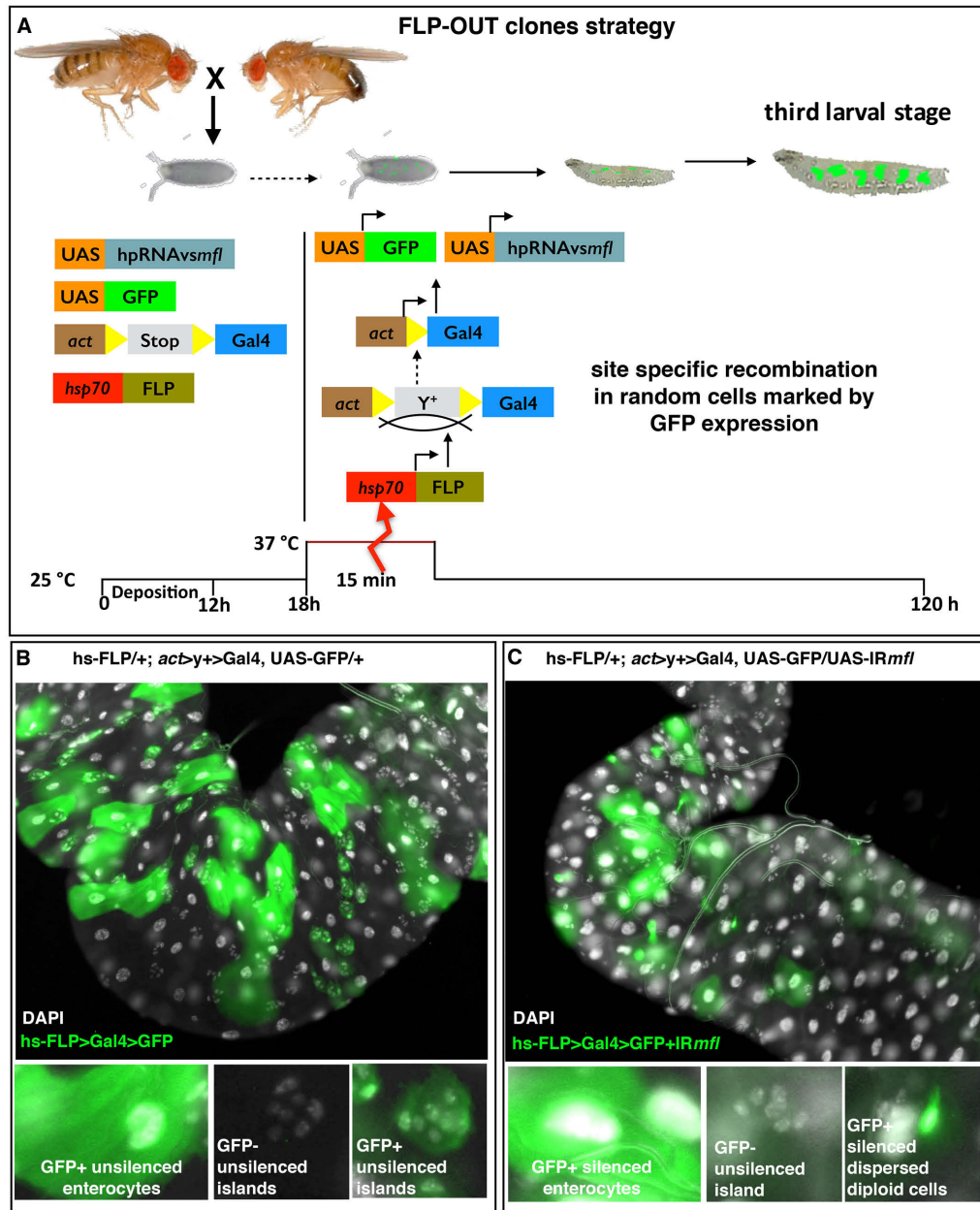


Figure 10. *mfl* silencing in mitotic clones: the absence of the islands is a cell-autonomous effect. (A) Scheme of FLP-OUT clone strategy. *Drosophila* embryos were collected in a time of deposition of 12 hours and subjected to heat shock for 15 minutes at 37 °C at 18 hours AED, i.e. after stage 10 of embryonic development. The heat-shock-induced expression of Flp fuses *actin* promoter to the Gal4 coding sequence by removing an internal cassette containing a transcriptional termination site (Stop) and flanked on both sides by FRT sites. Clones expressing Gal4 will in turn activate the UAS-GFP construct as a marker and the UAS-IR*mfl* construct for silencing. Midguts at the third larval stage (5 days AED) were stained with DAPI (in grey) and analyzed in epifluorescence. (B) In *hs-FLP/+; act>STOP>GAL4,UAS-GFP/+* control midguts GFP+ unsilenced clones include ECs and also imaginal islands. (C) In *hs-FLP/+; act>STOP>GAL4,UAS-GFP/UAS-IR-mfl* midguts GFP+ silenced clones are formed by ECs or by dispersed diploid cells but never by imaginal islands, which are always GFP- (unsilenced).

4.4 Quantitative reduction of MFL-depleted *esg*+ cells

Having established that the absence of larval intestinal stem niches is caused by MFL depletion in *esg*+ AMPs as a cell-autonomous phenomenon, I decided to quantify the reduction of the *esg*+ cells by counting them accurately in epifluorescence.

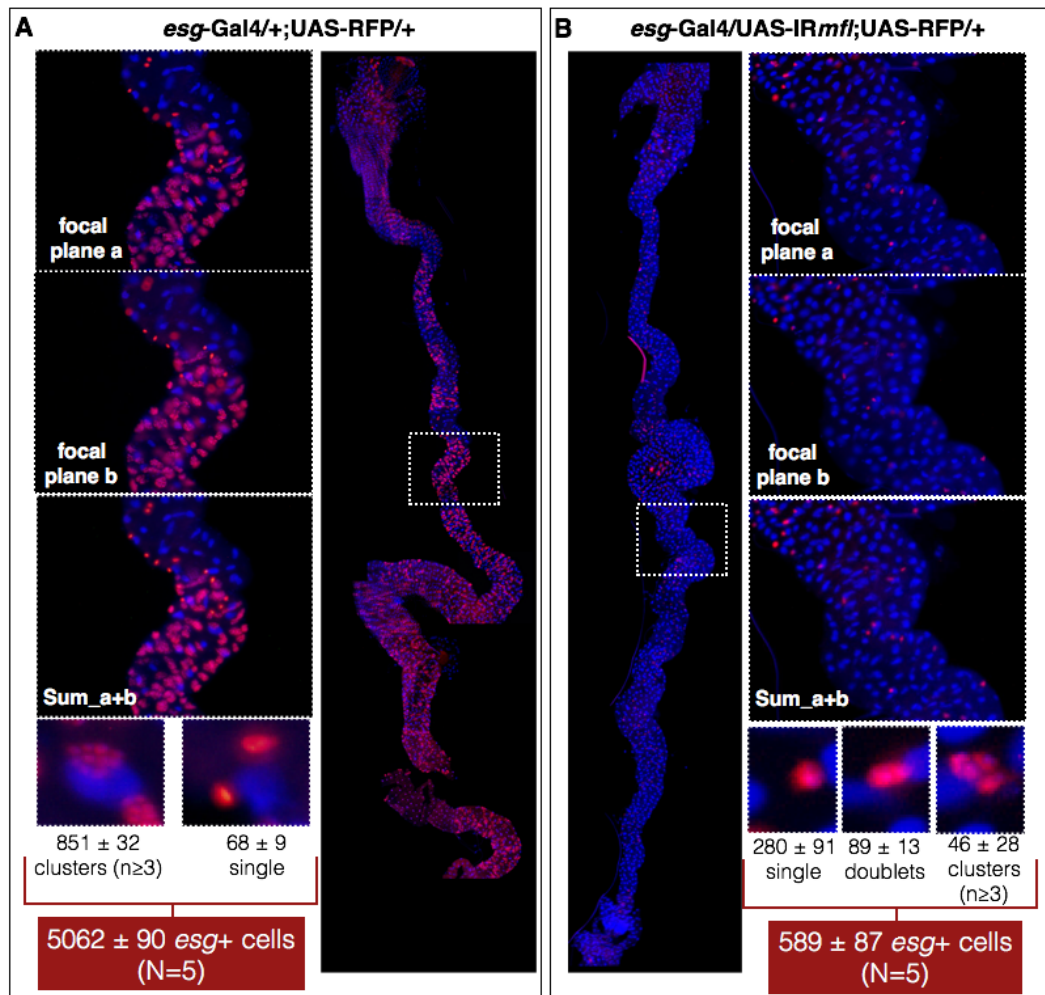


Figure 11. Reconstruction of midguts for counting the *esg*+ cells in epifluorescence. (A-B). A control (*esg-Gal4/+;UAS-RFP/+*) and a silenced (*esg-Gal4/UAS-IRmfl;UAS-RFP/+*) midgut at the third larval stage. The yellow hatched rectangles indicate fields whose magnification are shown as single focal planes and sum of the two focal planes (a and b) on both sides. 5 control and 5 silenced midguts were analyzed for counting clusters, doublets and single *esg*+ cells, marked by RFP expression. Dapi is in Blue.

To obtain solid data for a statistical analysis, I counted the *esg*⁺ cells in 5 control (*esg*-Gal4/+;UAS-RFP /+) and 5 silenced (*esg*-GAL4/UAS-IR*mfl*;UAS-RFP/+) entire midguts at the third larval stage. Since *mfl* silencing

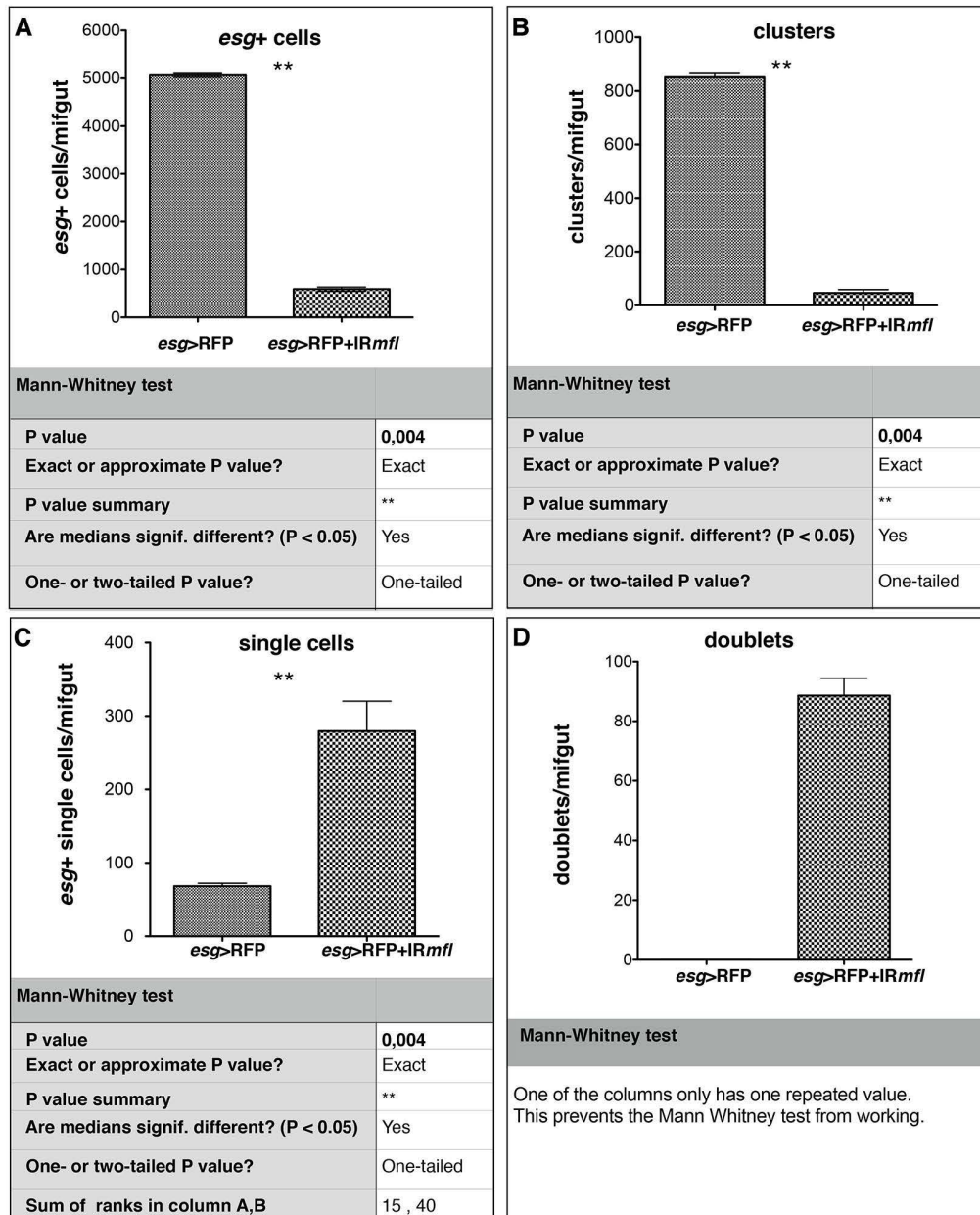


Figure 12. Estimation of the *esg*⁺ cells. The cells are counted in control (*esg*-Gal4/+;UAS-RFP/+) and silenced (*esg*-Gal4/UAS-IR*mfl*;UAS-RFP/+) entire midguts analyzed in epifluorescence at the third larval stage. **A-B-C-D).** The histograms represent the total number of the *esg*⁺ cells (A); the custers (B); the single cells (C) and the doublets (D). On the bottom of each panel, the statistical data resulting from application of Mann-Whitney test.

driven by *esg*-Gal4 induces a developmental delay of about 2 days, control midguts were collected at 5 days AED and silenced midguts at 7 days AED. Midguts were fixed, stained with DAPI and mounted for epifluorescence analysis (using a 40X objective). Since larval gut is a very thick tissue and my analysis was focussed to count the total number of the *esg*⁺ cells (marked by RFP expression) in each midgut, it was necessary to reconstruct the entire midguts by overlapping the images acquired on two different focal planes from proventriculus to the posterior region of the collected guts. The Z-Projection algorithm of the Image-J software was used to overlap planes *a* and *b*, and the different midgut fields were stacked with Adobe Photoshop software, thus obtaining the reconstruction of entire organs. All the described procedure was necessary to obtain a good resolution level to allow a precise cell count.

In Fig. 11, the reconstructions of a control midgut (A) and of a silenced midgut (B) are shown for examples. As summarized at the bottom of Fig. 11, the statistical analysis showed that in control midguts the *esg*⁺ cells appear as clusters of $n \geq 3$ cells (corresponding to the imaginal islands) or as single cells (probably corresponding to the enteroendocrine cells, EEs). In the silenced midguts, instead, the *esg*⁺ cells appear mainly as single cells, although also clusters of 2 cells (which I call “doublets”) and rare clusters of at least 3 cells were observed. The counts of the *esg*⁺ cells were statistically analyzed and the results summarized in Fig. 12. Upon *esg*-Gal4 driven *mfl* silencing, the total number of the *esg*⁺ cells is approximately reduced by 88%. In fact, 5062 ± 90 cells are counted in the control midguts, whereas only 589 ± 87 cells are counted in the silenced midguts (Fig. 12 A). The application of the Mann-Whitney test for variance analysis, using Prism software, showed that the drastic decline in the number of the *esg*⁺ cells after *mfl* silencing is highly significant. This analysis also indicated that upon *mfl* silencing the number of the clusters (formed by at least 3 *esg*⁺ cells) is dramatically reduced from 851 ± 32 in the control to 46 ± 28 in the silenced guts. This reduction, by about 95%, is highly significant (according to Mann-Whitney test) and further confirms that MFL depletion greatly alters formation and/or maintenance of midgut stem niches (Fig. 12 B). Despite the presence of a few clusters of *esg*⁺ cells detected in the silenced midguts- probably due to a local low efficiency of silencing or to stochastic fluctuations that allow few cells to form imaginal islands- it is possible to conclude that MFL depletion causes the almost total disappearance of larval intestinal stem niches.

Noticeably, despite the strong reduction in the total number of the *esg*⁺ cells (Fig. 12 A), the number of single dispersed *esg*⁺ cells increases in the silenced midgut from 68 ± 9 to 280 ± 91 cells (Fig. 12 C). This increment, slightly greater than 4 folds, is also statistically significant (according to Mann-Whitney test) and is compatible with the persistence of dispersed AMPs within

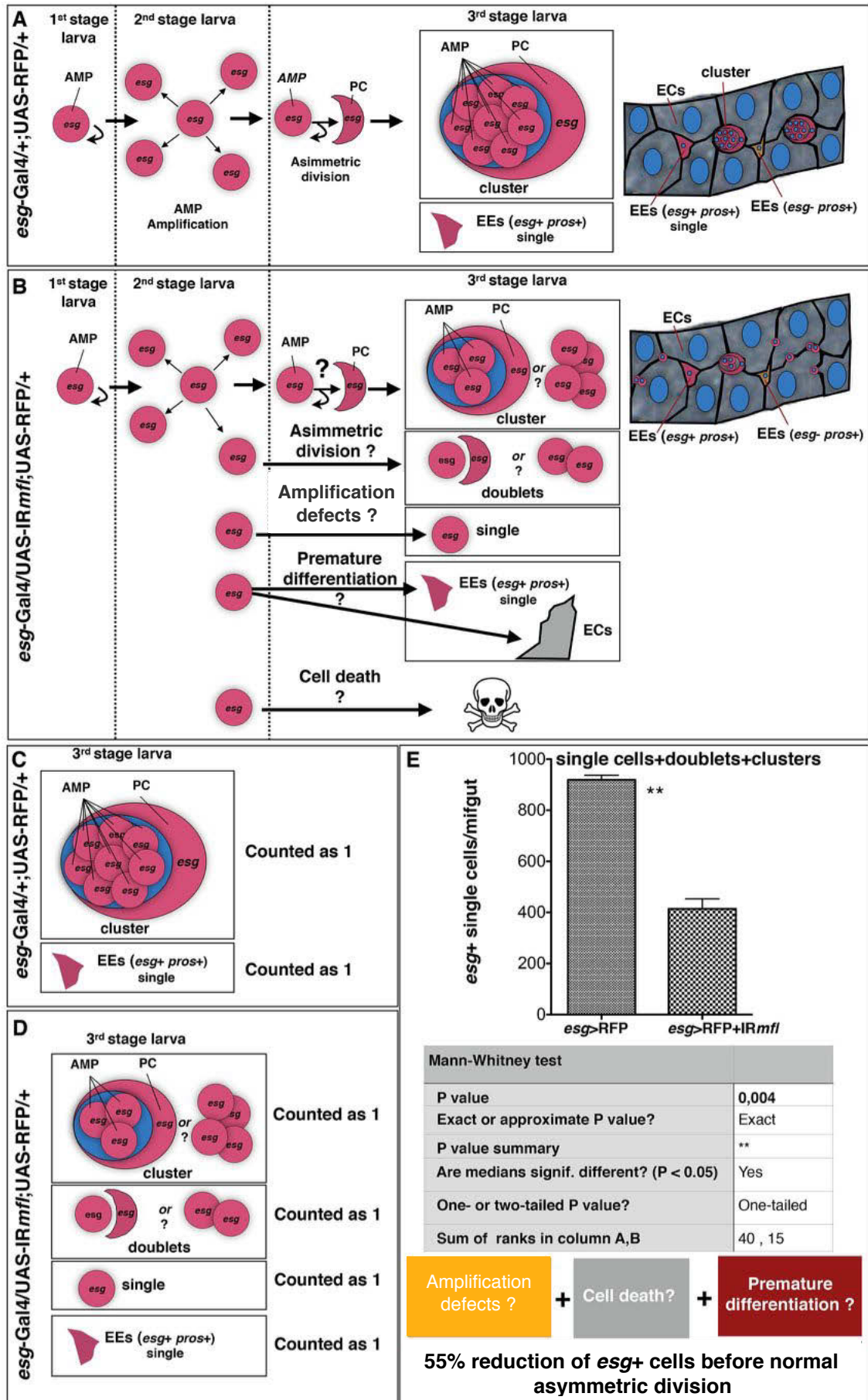
the epithelium or, alternatively, with an increase in the number of *esg*⁺ differentiated EEs.

Before verifying the nature of the dispersed *esg*⁺ cells upon *mfl* silencing, I decided to perform a further analysis based on the assumption that clusters and doublets arise from the division of a single cell. In fact, AMP amplification occurs in two phases: a first phase during early larval development (1-3 days AED), when AMPs increase their number and are dispersed or paired in doublets (two daughter AMPs deriving from a division and migrating away from each other); a second phase during the mid-third larval stage (4 days AED), when AMPs divide asymmetrically and begin to form the imaginal island clusters in which they proliferate (Jiang and Edgar, 2009).

In silenced guts at the late third larval stage (7 days AED) I noticed the presence of 89 ± 13 doublets of *esg*⁺ cells. These doublets are never present in the control guts at this stage (5 days AED), since the previous occurrence of the second amplification phase allowed the formation of fully developed islands. Hence, *mfl*-silenced doublets are likely to represent daughter AMPs unable to further proliferate. This finding was very informative, although it was impossible to apply to it a variance analysis test (because doublet's number is "zero" in the control dataset; Fig. 12 D).

Furthermore, I observed that the number of *esg*⁺ units (counting also doublets and clusters as a unit) was 919 ± 40 in control and 414 ± 88 in the silenced midguts (Fig. 13 E). This reduction, by about 55%, is again statistically significant (according Mann-Whitney test) and indicates that the strong decrease in the AMP number driven by *mfl* silencing occurs before the generation of the islands, i.e. during the first amplification phase. However, further investigation is needed to establish whether premature differentiation, cell death or cell division defects may contribute to the loss of the stem cell niches (Fig. 13).

Figure 13. Estimation of the *esg*⁺ cells before the asymmetric division phase. The cells are counted in control (*esg*-Gal4⁺;UAS-RFP/+) and silenced (*esg*-Gal4/UAS-IR*mfl*;UAS-RFP/+) entire midguts analyzed in epifluorescence at the third larval stage. **A-B).** Schematic representation of midgut development in wild type (A) or silenced (B) conditions. The silenced phenotype could be caused by amplification defects, premature differentiation and cell death and could be accompanied by asymmetric division defects. **C-D).** Schematic representation of the organization of the *esg*⁺ cells in control (A) and silenced (B) midguts. Clusters, doublets and single cells are counted as a unity. **E).** The histograms represent the sum of clusters, doublets and single *esg*⁺ cells. On the bottom, the statistical data resulting from application of Mann-Whitney test. The reduction of the *esg*⁺ cells by 55% upon *mfl* silencing could be caused by amplification defects, cell death or premature differentiation.



4.5 MFL-depleted *esg*⁺ cells are not EEs but AMPs not aggregated into islands

To characterize the nature of MFL-depleted *esg*⁺ cells and begin to clarify whether *mfl* silencing could induce a premature differentiation of AMPs in enteroendocrine cells (EEs), I followed the expression of Prospero (Pros) homeoprotein, an EE specific cell marker (Zeng et al. 2010; Micchelli et al. 2011) and observed that while in control midguts (genotype *esg*-Gal4/+;UAS-RFP/+) the dispersed diploid cells (either *esg*⁺ or *esg*⁻) always express Pros, as

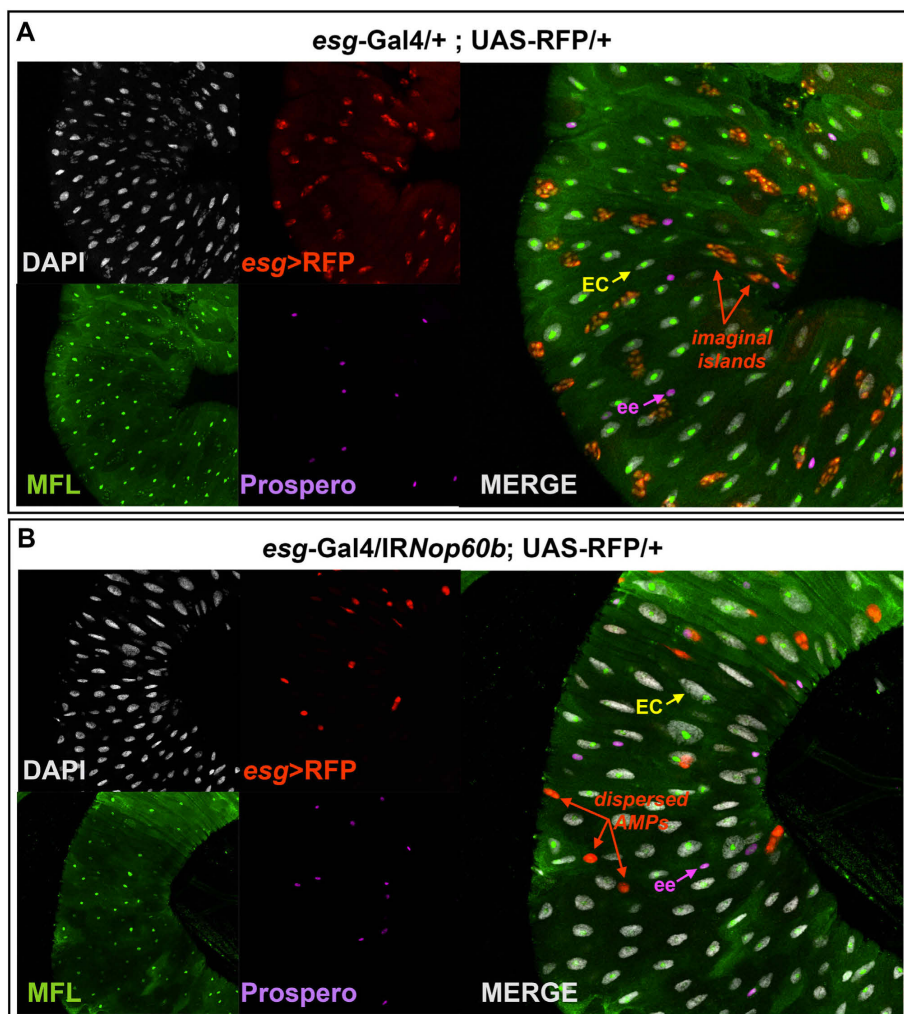


Figure 14. *esg*⁺*pros*⁻ cells (AMPs and PCs) appear rare and dispersed upon *esg*-Gal4 driven *mfl* silencing. (A) Confocal analysis of *esg*-Gal4/+;UAS-RFP/+ control midgut at the third larval stage. (B) Confocal analysis of *esg*-Gal4/UAS IR*mfl*;UAS-RFP/+ silenced midgut at the third larval stage. DAPI is in gray; *esg*-expression domain is marked by an UAS-RFP responder line (in red); staining with anti-MFL is shown in green; anti-Prospero, which specifically marks enteroendocrine cells, is in purple. Purple arrow indicates an enteroendocrine cell (ee); yellow arrow indicates an enterocyte (EC); red arrows indicate imaginal islands in A and dispersed *esg*⁺*pros*⁻ cells in B.

expected from EE cells, in the silenced midguts (genotype *esg-Gal4/UAS-IRmfl;UAS-RFP/+*) MFL-depleted *esg+* cells detected as single dispersed, doublets or rare clusters of at least three cells, are not stained for Pros (Fig. 14). This observation led to conclude that they are not differentiated EEs, but instead AMPs not organized into niches.

4.6 Reduction in the AMP number occurs during the first amplification phase

To obtain more detailed information on the effects of MFL depletion on the mechanisms involved in the formation of the intestinal stem cells (first amplification phase; grouping into niches), I decided to quantify the reduction of the *esg+* cells in midguts stained with anti-Pros at two stages of development: at 3 days after eggs deposition (AED), and at the third larval stage (5 days AED for control and 7 days AED for silenced midguts). As mentioned above, I counted the clusters of *esg+pros-* cells as a unit (because they derive from the division of a single AMP; Micchelli 2011), and used anti-Pros immunostaining to establish that the doublets and the single *esg+* cells corresponded to AMPs (*esg+pros-*) and not to EEs.

At the earlier developmental stage the AMPs are not yet aggregated into islands, but undergo symmetric divisions to amplify their number and disperse in the epithelium (Micchelli 2011; Fig. 11 A). By counting the number of the *esg+pros-* cells (corresponding to AMPs) and excluding from the count the *esg+pros+* cells (corresponding to EEs), I found that the number of the *esg+pros-* cells was reduced approximately by 60% in the silenced respect to control midguts (Fig. 16 C). The application of the Mann-Whitney test confirmed that this reduction is highly significant (Fig. 15 D).

The analysis of silenced midguts at the third larval stage showed presence of two “categories” of *esg+pros-* cells: “single dispersed cells” and “doublets”; 91% of these cells corresponds to single dispersed cells, while 9% of them are grouped into doublets (Fig. 16 A). In the control midguts, the organization into imaginal islands is instead shared by 100% of *esg+pros-* cells, that are invariably found clustered into niches. Total counting led to estimate that the number of the *esg+pros-* cells, considering also doublets and clusters as unit, is reduced by 50% in silenced midguts respect to control midguts (Fig. 16 B), a difference highly significant (Fig. 16 C, Mann-Whitney test).

Hence, the number of the *esg+pros-* cells is reduced by 60% in the early and by 50% in the later stages. This indicates that only a small proportion of *esg+pros-* cells formed in the silenced midguts (whose number is by itself strongly

reduced) is able to divide, thereby passing from single cells/doublets to clusters. Altogether these observations suggest that MFL depletion prevents stem cells from undergoing further division cycles, and confirm that stem cell reduction occurs during the first amplification phase.

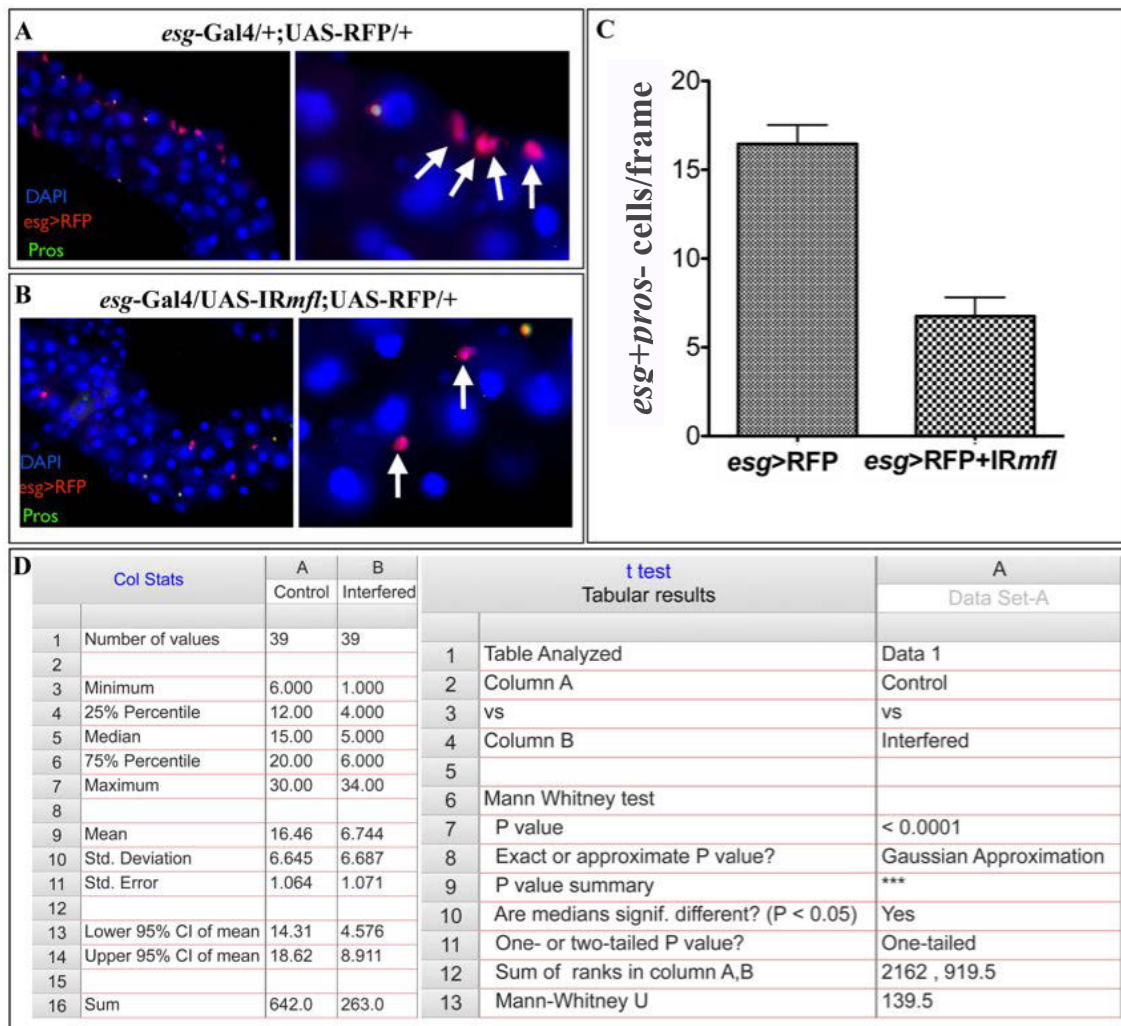


Figure 15. Estimation of the number of *esg+pros-* cells in midguts at 3 days AED. (A-B) Epifluorescence images of *esg-Gal4/+;UAS-RFP/+* control midgut (in A) and *esg-Gal4/UAS-IRmfl;UAS-RFP/+* silenced midgut (in B) at 3 days AED. DAPI is in blue; *esg*-expression domain is marked by an UAS-RFP responder line (in red); staining with anti-Prospero is shown in green. White arrows indicates the *esg+pros-* cells counted in the statistical analysis. (C) Histograms representing the number of *esg+pros-* cells counted for frame (at 40X magnification) show a 60% reduction of cells in silenced respect to control midguts. (D) Statistical data resulting from application of Mann-Whitney test.

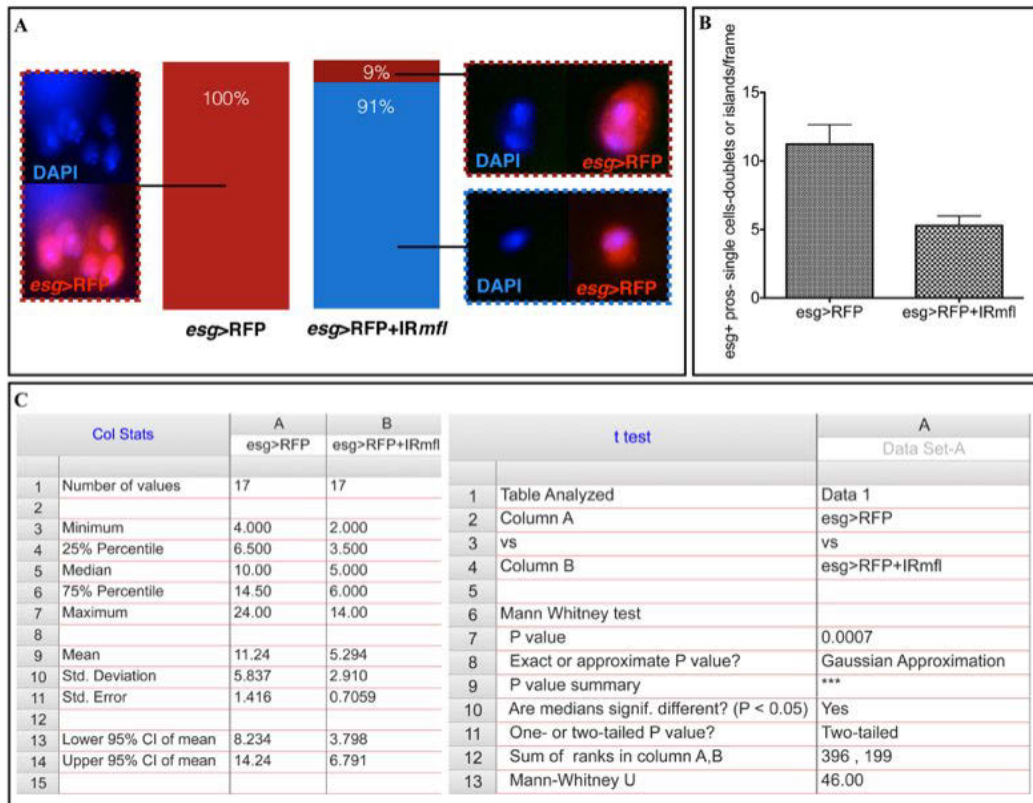


Figure 16. Estimation of the number and organization of *esg+pros-* cells in midguts at the third larval stage. (A) Percentage of the different categories of *esg+pros-* cells in *esg-Gal4/+;UAS-RFP/+* control midguts and *esg-Gal4/UAS-IRmfl;UAS-RFP/+* silenced midguts at the third larval stage. DAPI is in blue; *esg*-expression domain is marked by an UAS-RFP responder line (in red) (B) Histograms representing the number of *esg+pros-* cells counted for frame (at 40X magnification) show a 50% reduction of cells in silenced respect to control midguts. (C) Statistical data resulting from application of Mann-Whitney test.

4.7 The loss of imaginal islands is not due to AMP premature differentiation

As discussed in the previous section, MFL depletion reduces AMP number already during the early amplification phase. Once established this point, I focussed subsequent experiments to establish whether a premature differentiation may contribute to the loss of the stem cell niches (Fig. 13).

Although anti-Pros immunostaining indicated that MFL-depleted *esg+* cells do not differentiate into EEs, the possibility of a premature differentiation toward other fates could not be excluded.

Therefore, I decided to perform a lineage tracing analysis based on the use of the transcriptional activator Gal4. Gal4 mediates the expression of the red fluorescent protein (UAS-RFP) and of the site-specific recombinase Flippase (UAS-Flp). In turn, Flp removes an internal cassette and fuses the promoter of the ubiquitous gene *ubiquitin (ubi)* to the GFP coding sequence, thus allowing its expression (Evans et al. 2009). Thus, in my experiments I combined by genetic crosses the *esg*-Gal4 driver, the UAS-RFP,UAS-FLP,*ubi*>STOP>GFP/+, and the UAS-IR*mfl* silencing constructs. In these flies, the *esg*-Gal4 driver activated expression of RFP and Flp in the *esg*+ cells, leading to follow their lineage during larval development. Cells which actively express *esg* are marked by RFP expression; those derived from *esg*+ precursors which continue to express *esg* are marked by both GFP and RFP; differentiated cells derived from *esg*+ precursors, and thus do not express *esg* any more, are instead marked only by GFP (Fig. 17 A).

Control midguts (genotype: *esg*-Gal4/+;UAS-RFP,UAS-FLP,*ubi*>STOP>GFP/+) and silenced midguts (genotype: *esg*-Gal4/UAS-IR*mfl*;UAS-RFP,UAS-FLP,*ubi*>STOP>GFP/+) were then analyzed in epifluorescence (Fig. 17 B-C). In control midguts, the cells composing stem niches are marked by both GFP and RFP, as expected for cells deriving from embryonic *esg*+ precursors which still continue to express *esg*. In contrast, ECs or EEs, which derive from embryonic *esg*+ precursors but do not express *esg* anymore because of their differentiation, are marked only by GFP expression (Fig. 17 B). In contrast, single, doublets or rare clusters of three cells marked by both GFP and RFP are present in the silenced midguts; in keeping with previous results, these cells correspond to AMPs not organized into imaginal islands. I then compared the number of GFP+ differentiated cells (ECs and EEs) deriving from embryonic *esg*+ precursors in control and silenced midguts. (Fig. 17 C). When data were submitted to the Mann-Whitney test, the results indicated that neither the number of GFP+ enterocytes nor that of GFP+ EEs was significantly increased in the silenced midguts (Fig. 18 A-B). Altogether, these results rule out the possibility that the observed reduction in the AMP number was due to their premature differentiation.

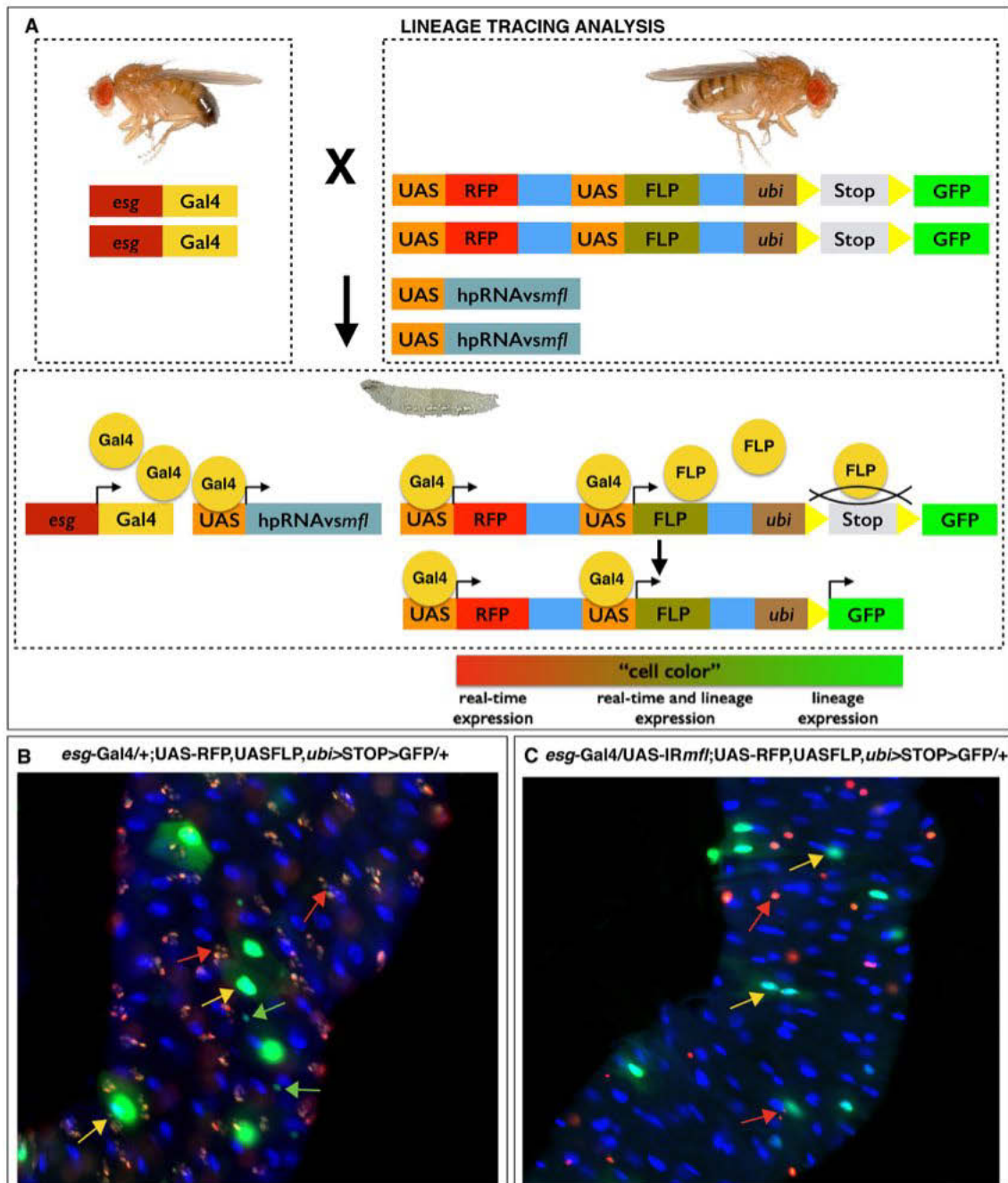


Figure 17. Lineage tracing analysis. (A) Schematic representation of lineage tracing transgenes. Genetic crosses between *esg-Gal4* driver line and *UAS-RFP,UAS-FLP,ubi>STOP>GFP/+* or *UAS-IRmfl;UAS-RFP,UAS-FLP,ubi>STOP>GFP/+* responder lines lead to obtain a progeny in which Gal4 activates expression of RFP, Flippase (FLP) and *IRmfl* in the *esg*⁺ cells. The cells which actively express *esg* are marked by RFP. The cells deriving from *esg*⁺ precursors, in which FLP has been expressed, are marked by GFP. The FLP brings the GFP coding sequence under the control of the *ubiquitin* promoter by removing an internal cassette containing a transcriptional termination site and flanked on both sides by FRT sites. The cells deriving from *esg*⁺ precursors which continue to express *esg* are marked by both GFP and RFP. (B-C) Control (*esg-Gal4/+;UAS-RFP/UAS-FLP,ubi>STOP>GFP/+*) and silenced (*esg-Gal4/UAS-IRmfl;UAS-RFP/UAS-FLP,ubi>STOP>GFP/+*) midguts at the third larval stage analyzed in epifluorescence. Dapi is in blue; RFP in red; GFP in green. Red arrows indicate *esg*⁺ imaginal island cells (in B) and *esg*⁺ dispersed cells (in C); yellow arrows indicate differentiated ECs deriving from *esg*⁺ precursors; green arrows indicate differentiated EEs deriving from *esg*⁺ precursors.

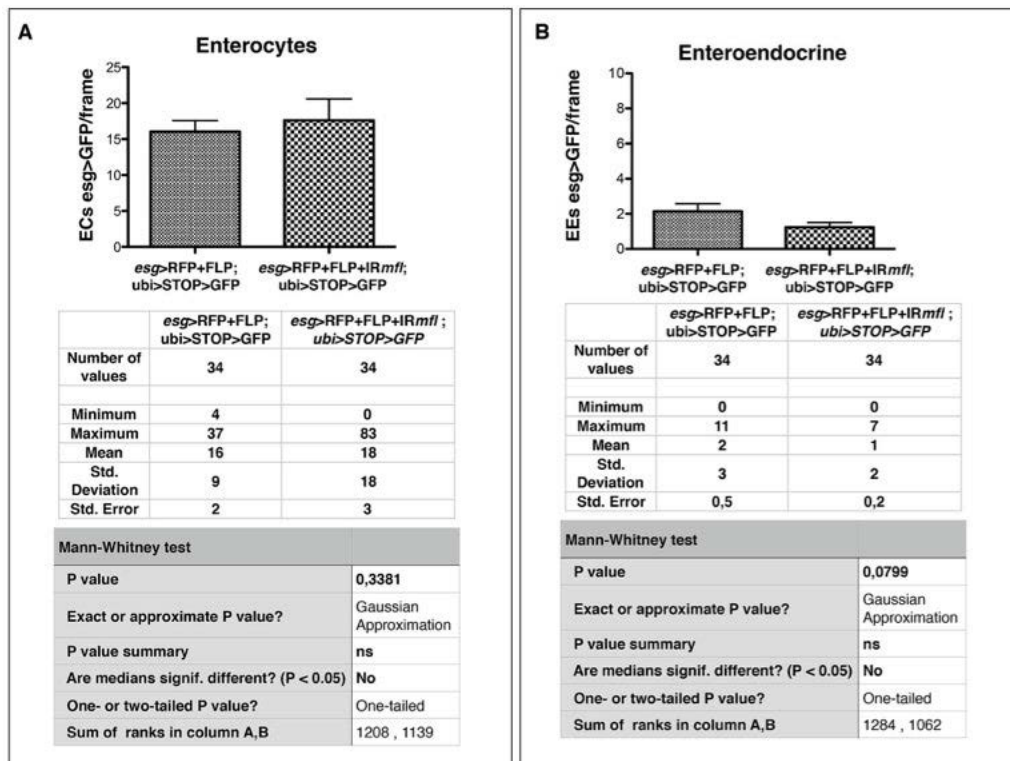


Figure 18. Estimation of the number of differentiated cells deriving from *esg*+ precursors. (A-B) Histograms and statistical data representing the number of the GFP+ Enterocytes (in A) and GFP+ Enteroendocrine cells (in B) deriving from *esg*+ precursors counted in control (*esg-Gal4/+;UAS-RFP/UAS-FLP,ubi>STOP>GFP/+*) and silenced (*esg-Gal4/UAS-IRmfl;UAS-RFP/UAS-FLP,ubi>STOP>GFP/+*) midguts at the third larval stage. The application of Mann-Whitney test estimates that the number of GFP+ ECs and EEs is not significantly increased in silenced respect to control midguts.

4.8 MFL-depleted AMPs preserve their stem-cell identity

Since MFL-depleted AMPs do not undergo a premature differentiation, I asked whether they really maintain their stemness properties. To this end, I monitored the expression of the Notch ligand Delta (Dl), a common AMP marker (Takashima et al. 2011; Jiang and Edgar 2009; Mathur et al. 2010). Control (*esg-Gal4/+;UAS-RFP/+*) and silenced (*esg-Gal4/UAS-IRmfl;UAS-RFP/+*) midguts were then immunostained with anti-Dl antibody and analyzed in confocal microscopy. As expected, in control midguts at the third larval stage Dl marks the membrane of AMPs aggregated into niches (Fig. 19 A). At the

same larval stage the MFL-depleted and dispersed AMPs detected in the silenced midguts also express DI, which appears correctly localized in membrane (Fig. 19 B). As it can be noticed from Fig. 19 B (see the yellow arrow) in some doublets DI is highly expressed in only one of the cells, as aspected after an asymmetric division (Mathur et al. 2010), indicating that the silenced *esg*⁺ cells preserve their stem cell properties.

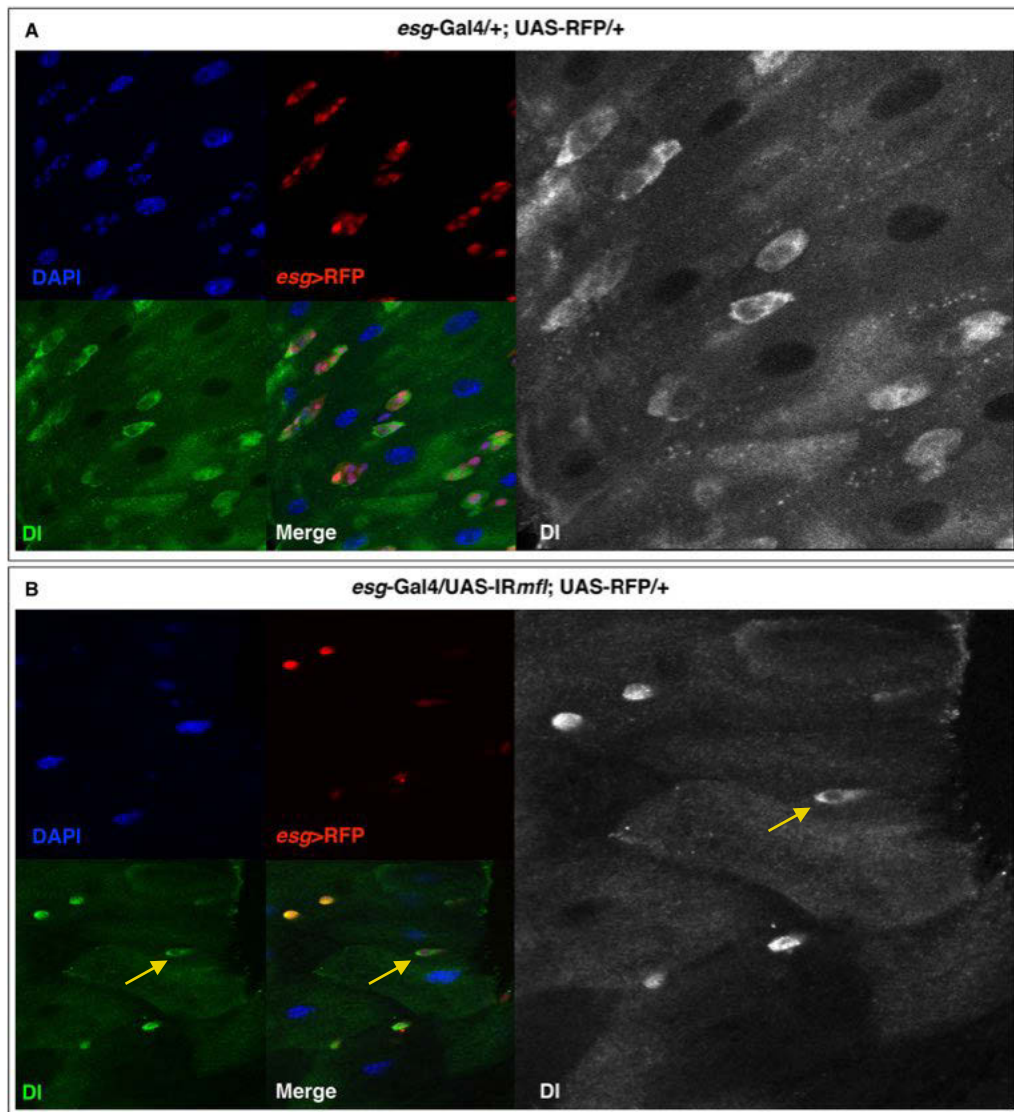


Fig. 19. Immunostaining with anti-DI A). Control midgut (*esg-Gal4/+;UAS-RFP/+*) at the third larval stage. DI localizes in membrane of *esg*⁺ imaginal island cells. **B).** Silenced midgut (*esg-Gal4/UAS-IRmfl;UAS-RFP/+*) at the third larval stage. DI is expressed and appears correctly localized in MFL-depleted *esg*⁺ single cells and in some doublets is highly expressed in only one of the cells (yellow arrow). Dapi in blue; RFP in red marks the *esg* expression domain; anti-DI in green (and in grey in the enlargements).

Since within the imaginal island AMPs normally accumulate high levels of *Drosophila* β -catenin (Armadillo, Arm) at their adherence junctions (Mathur et al. 2010; Issigonis and Matunis 2010), I also monitored Arm expression in control (*esg-Gal4/+;UAS-RFP/NRE-GFP*) and silenced (*esg-Gal4/UAS-IRmfl;UAS-RFP/NRE-GFP*) midguts. As shown in Fig. 20, Arm accumulation surrounds not only the AMPs composing the imaginal islands of wild-type midguts (Fig. 20 A), but also the *esg*⁺ cells detected as single or doublets of silenced midguts (Fig. 20 B). Worth noting, Arm immunostaining nicely confirmed that both the single dispersed *esg*⁺ cells and members of the “doublets” keep their stem-cell identity; moreover, the finding that cells belonging to the same “doublet” are linked each other by adherens junctions supports the view that they are “daughter” originating from the same division. The finding that Arm is strongly accumulated between the cells of a same doublet shows that they are tightly associated, as observed for AMPs clustered into canonical imaginal islands.

I then used NRE-GFP, a common Notch activity reporter (Saj et al. 2010), to attempt to mark the peripheral cells (PCs) which are specifically characterized by Notch activation. As shown in Fig. 20, PCs derive from the AMP asymmetric division which occurs at the early third larval stage (Fig. 20 A); once formed, the PC acquire a U-shape and surrounds the cluster of AMPs that compose the imaginal island (Fig. 20 B; Mathur et al. 2010). Interestingly, I noticed that in the silenced midguts the NRE-GFP reporter is active in only one member of the *esg*⁺ doublets, indicating that upon *mfl* silencing some AMPs remain able to divide asymmetrically. However, compared to control midguts at early third larval stage (Fig. 20 A), the asymmetric division detected in silenced midguts does not appear synchronous. This asynchrony is testified by presence of doublets without any Notch activation (Fig. 20 C central enlargement) and suggests that, although retaining their stem-cell identity, the silenced AMPs could undergo irregular cell divisions.

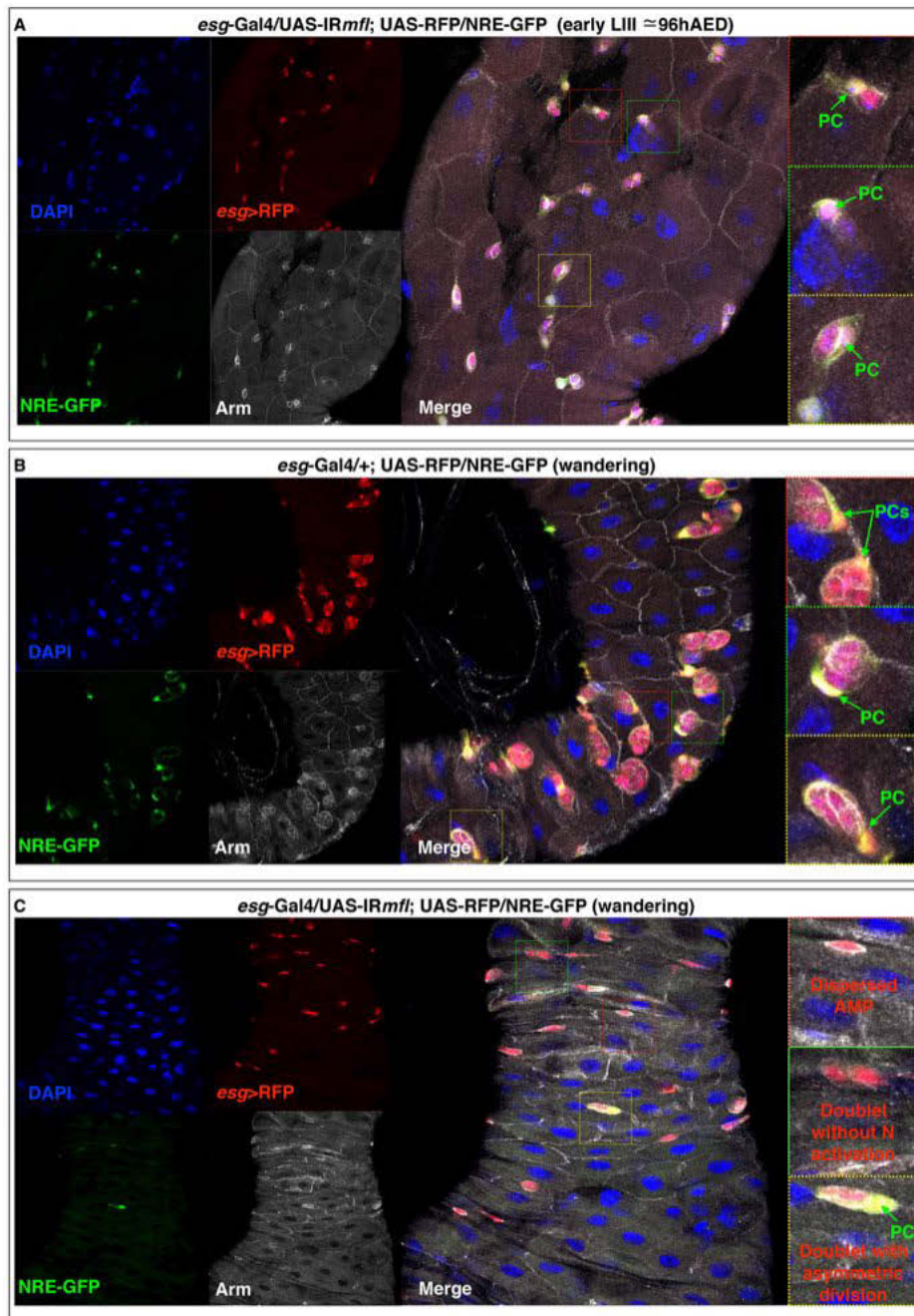


Fig. 20. Arm accumulation and Notch activation A). Control midgut (*esg-Gal4/+;UAS-RFP/NRE-GFP*) at the early third larval stage (96 h AED). Arm surrounds the *esg*⁺ cells; Notch activity, monitored by NRE-GFP reporter, marks the peripheral cell (PC) of each doublet, deriving from asymmetric division. **B).** Control midgut (*esg-Gal4/+;UAS-RFP/NRE-GFP*) at the late third larval stage (wandering stage). Arm abundantly accumulates in the adherence junctions of the *esg*⁺ imaginal island cells. Notch activity marks the peripheral cells (PCs) which surround each island. **C).** Silenced midgut (*esg-Gal4/UAS-IRmfl;UAS-RFP/NRE-GFP*) at the third larval stage. Arm surrounds the single MFL-depleted *esg*⁺ cells and abundantly accumulates at the adherence junctions of doublets. NRE-GFP expression shows the asymmetric division in some MFL-depleted doublets. Dapi in blue; RFP in red marks the *esg* expression domain; anti-Arm in grey; NRE-GFP in green.

4.9 MFL-depletion does not affect AMP growth

Since proteins belonging to the dyskerin family are involved in rRNA processing and ribosome biogenesis, it was of great importance to determine whether the reduction of AMPs observed after *mfl* silencing could be related to cell growth defects. A common way to assess cell growth is based on the evaluation of the levels of specific nucleolar markers and that of the nucleolus size (Boisvert et al. 2007; Derenzini et al. 2000).

In *Drosophila*, nucleoli are easily detectable by immunofluorescence upon immunostaining of the nucleolar protein fibrillarin (fib) a rRNA 2'-O-methyltransferase which processes pre-rRNAs (Grewal et al. 2005; Tollervey et al. 1993). It is well established that nucleolar fibrillarin levels are directly proportional to cell growth ability (Grewal et al. 2007). For this reason, I evaluated the localization and the accumulation levels of fibrillarin in the AMPs nucleoli. I thus performed a co-immunostaining with anti-MFL and anti-fib on control (*esg-Gal4/+;UAS-RFP/+*) and silenced (*esg-Gal4/UAS-IRmfl;UAS-RFP/+*) midguts at the third larval stage. As shown in Fig. 21, in control midguts fibrillarin co-localizes with MFL in the nucleoli of all midgut cells, including the imaginal island cells (marked by RFP expression). This pattern is unchanged in the silenced midguts, where fibrillarin is similarly abundantly detected in the nucleoli of MFL-depleted *esg+* cells (mainly present as doublets or single cells). Therefore, the silenced AMPs do not show evident cell growth impairment. To further investigate whether MFL depletion could be perceived as a condition that impairs the AMP growth ability, I also monitored the levels of S6K phosphorylated form (p-S6K). In fact, conditions that compromise cell growth are known to cause the repression of the Tor signaling, resulting in low levels of phosphorylation of its downstream effector, the ribosomal protein S6 kinase (S6K; Laplante and Sabatini 2009). As shown in Fig. 22, in control midguts (*esg-Gal4 +/-;UAS-RFP +/-*) at the third larval stage the level of p-S6K is high in the enterocytes, but very low in the imaginal islands, and no reduction in the level of p-S6K can be noticed in MFL-depleted *esg+* cells (genotype: *esg-Gal4/UAS-IRmfl;UAS-RFP*) respect to that observed in the control imaginal islands. Hence, *mfl* silencing does not cause any downregulation of the Tor pathway in MFL-depleted AMPs, suggesting that the Tor pathway is likely to have little or no influence on the metabolic fitness of AMPs. Consistent with this view, Jiang et al. (2009) demonstrated that AMPs amplification is not affected by alterations of Tor pathway.

Finally, growth restraints caused by nutrient deficiencies are known to induce phosphorylation of the translation initiation factor eIF2 α (Gallinetti et al. 2013). I thus monitored the accumulation levels of eIF2 α phosphorylated form (p-eIF2 α) in the *esg+* cells of both control and silenced midguts. p-eIF2 α

levels were found elevated in the enteroendocrine *esg*⁺ cells, which therefore represent a positive internal control for staining of both control and silenced tissue. Instead, the p-eIF2 α signal was very low in either the imaginal islands of control midguts (*esg-Gal4/+;UAS-RFP/+*) and the dispersed AMPs of the silenced midguts (*esg-Gal4/UAS-IRmfl;UAS-RFP/+*; Fig. 23), leading to conclude that the defective AMPs amplification observed upon *mfl* silencing is not caused by AMPs growth impairments.

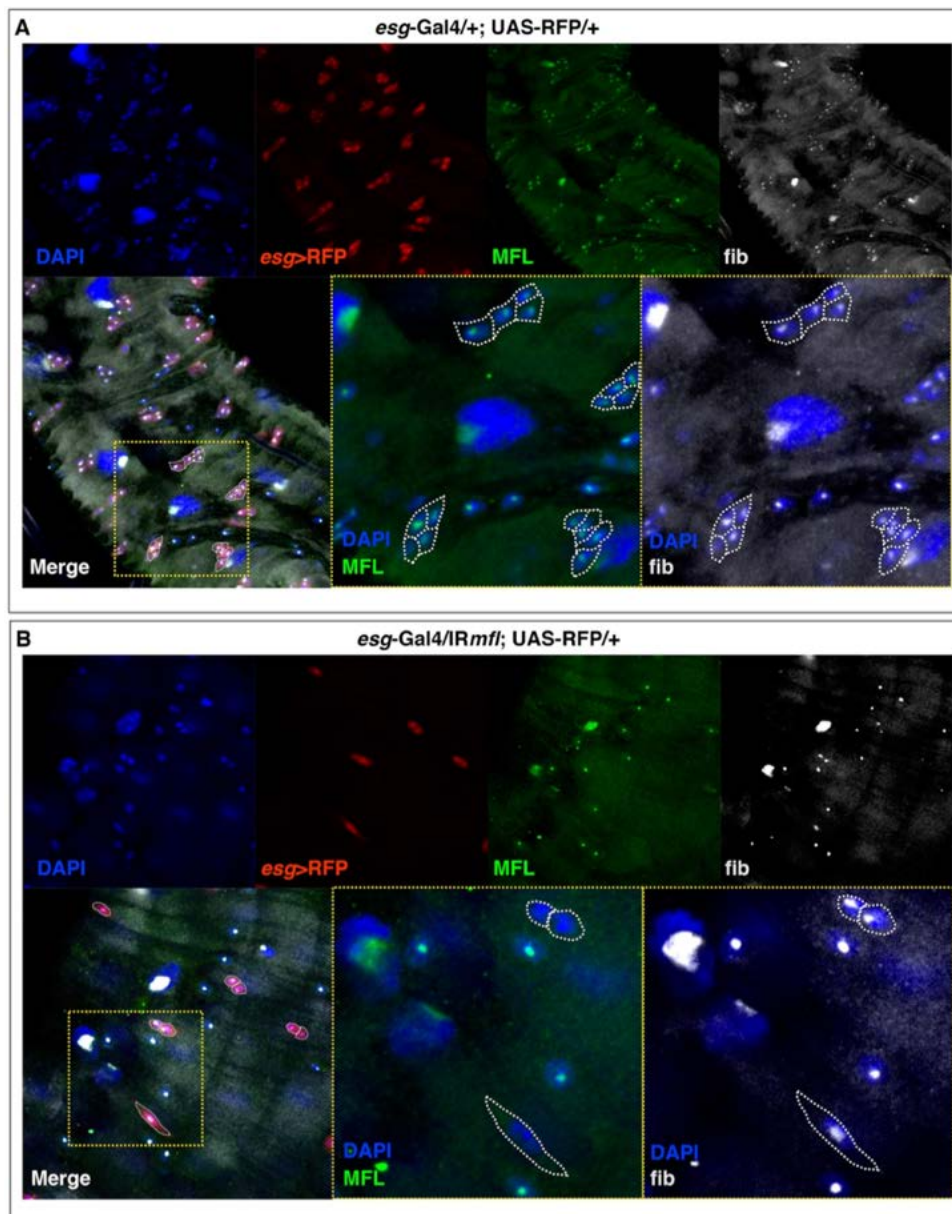


Fig. 21. Immunostaining with anti-MFL and anti-fib. A). Control midgut (*esg-Gal4/+;UAS-RFP/+*) at the third larval stage. In the enlargements on the bottom, the *esg*⁺ imaginal island cells are outlined by a dotted line. MFL and fib co-localize in the nucleolus. **B).** Silenced midgut (*esg-Gal4/UAS-IRmfl;UAS-RFP/+*) at the third larval stage. In the enlargements on the bottom, the *esg*⁺ cells (doublets or single) are outlined by a dotted line. Fibrillarlin localizes in the nucleolus of MFL-depleted *esg*⁺ cells. Dapi in blue; RFP in red marks the *esg* expression domain; anti-MFL in green; anti-fib in white.

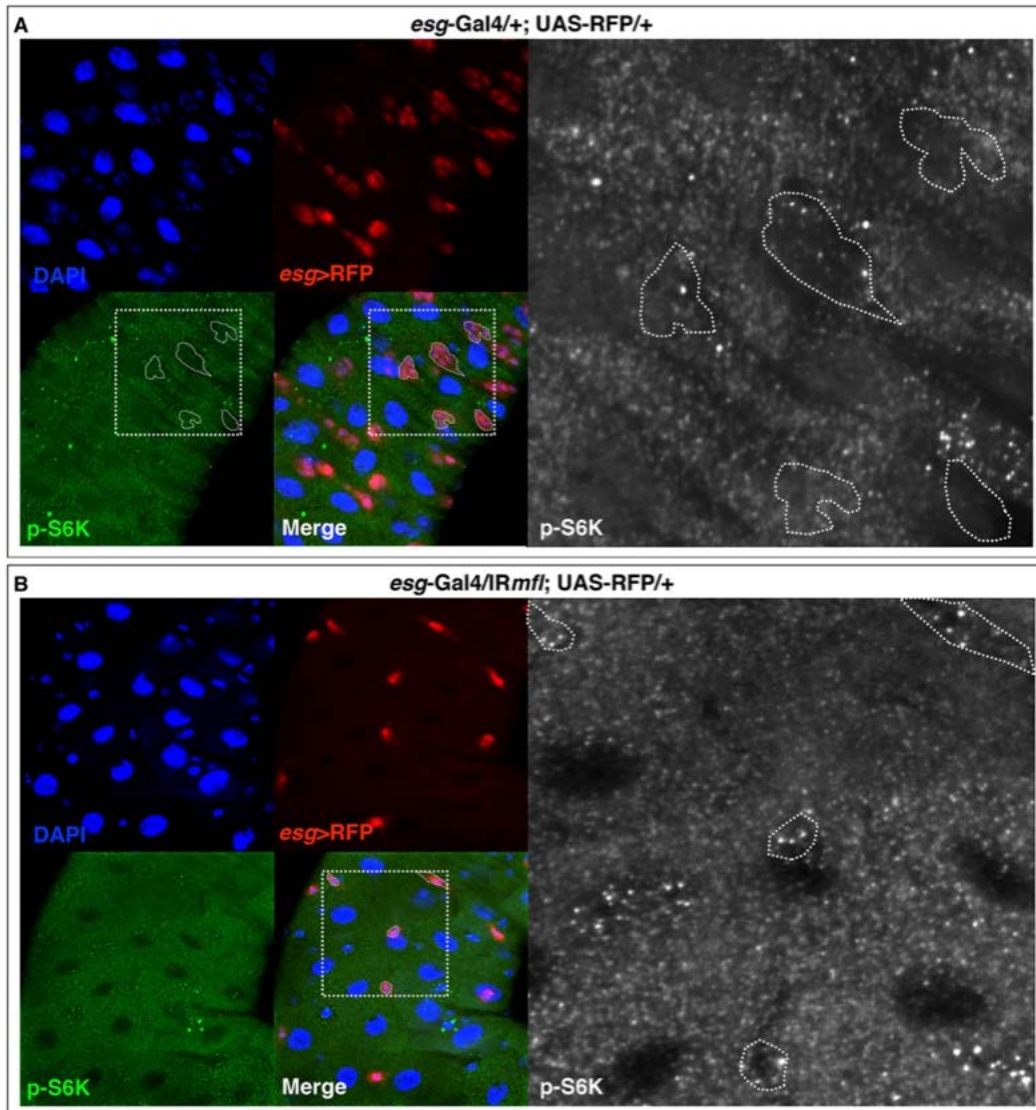


Fig. 22. Immunostaining with anti-p-S6K **A).** Control midgut (*esg-Gal4/+;UAS-RFP/+*) at the third larval stage. Low accumulation levels of p-S6K are detected in the imaginal islands (outlined by a dotted line in the enlargement on the right). **B).** Silenced midgut (*esg-Gal4/UAS-IRmfl;UAS-RFP/+*) at the third larval stage. The accumulation levels of p-S6K are not decreased in the *esg*⁺ cells (doublets or single cells, outlined by a dotted line in the enlargement on the right). Dapi is in blue; RFP in red marks the *esg* expression domain; anti-p-S6K is in green and in white in the enlargements.

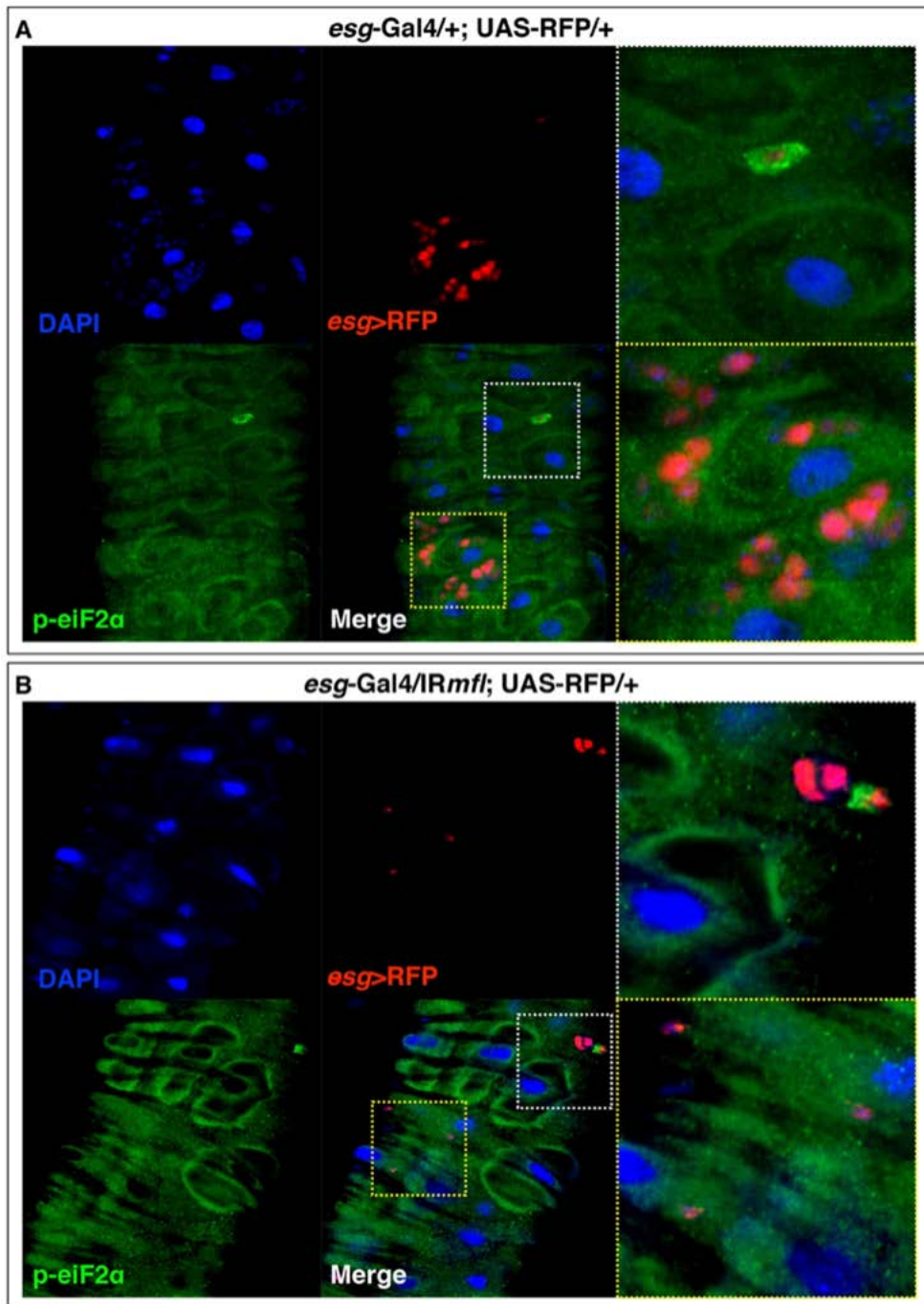


Fig. 23. Immunostaining with anti-p-eiF2 α **A).** Control midgut (*esg-Gal4/+;UAS-RFP/+*) at the third larval stage. In the yellow dashed box, imaginal islands without significant accumulation levels of p-eiF2 α . In the white dashed box, an *esg*⁺ EE cell representing an internal positive control. **B).** Silenced midgut (*esg-Gal4/UAS-IRmfl;UAS-RFP/+*) at the third larval stage. In the yellow dashed box, *esg*⁺ dispersed cells without significant accumulation levels of p-eiF2 α . In the white dashed box, an *esg*⁺ EE cell representing an internal positive control. Dapi is in blue; RFP in red marks the *esg* expression domain; anti-p-eiF2 α is in green.

4.10 Alteration of AMP maintenance is not due to apoptosis

To evaluate if *mfl* silencing could induce apoptosis of AMPs, I immunostained control and silenced midguts with an antibody against the Caspase-3 (Cas-3) activated form. However, this immunostaining did not show any apoptotic spot in the silenced midguts (genotype: *esg-Gal4/UAS-IRmfl;UAS-RFP/+*; Fig. 24). I thus utilized *Drosophila* wing discs (genotype *omb-Gal4/+* and *omb-Gal4/+;UAS-IRmfl/+*) as positive control of the staining, and observed that apoptosis of some MFL-depleted cells occurring in the central part of the wing disc was efficiently detected by the same antibody. Nevertheless, I further investigated this point by using a fluorescent reporter of Cas-3 induction, called Apoliner. This reporter involves two fused fluorescent proteins, RFP and GFP,

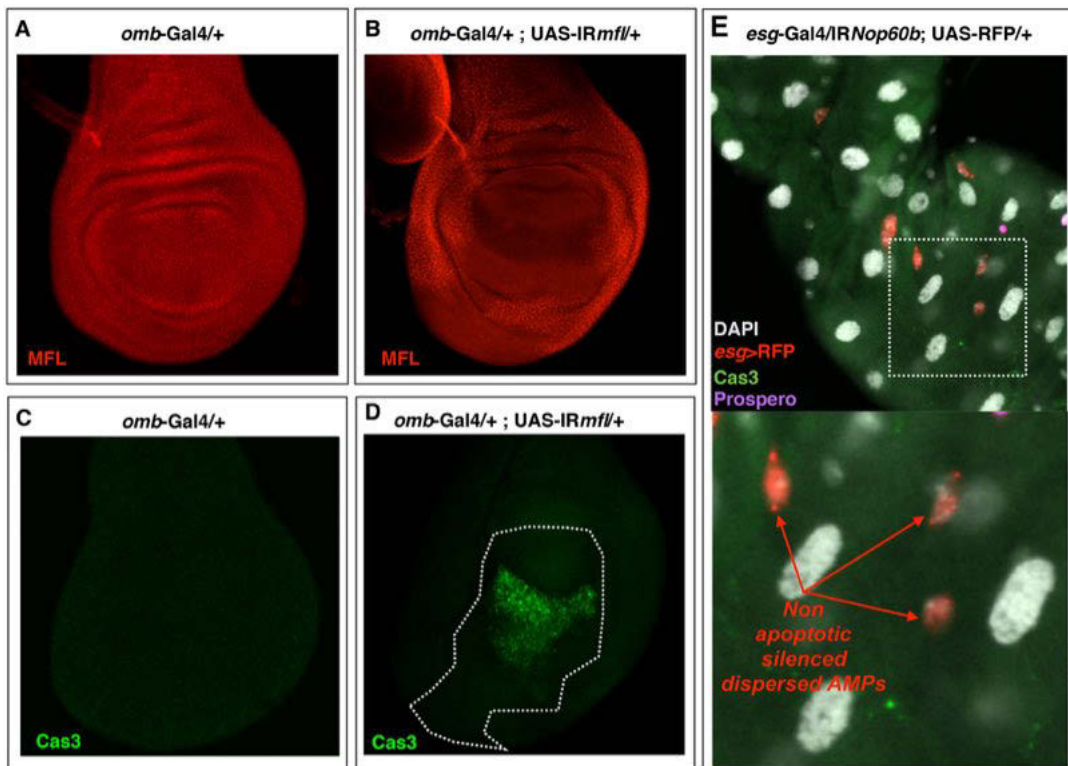


Figure 24. Caspase-3 activated form is not present in silenced AMPs. A-B-C-D). Wing discs representing positive controls of the staining. (A-C) Control wing disc of genotype *omb-Gal4/+*; (B-D) *mfl*-silenced wing disc of genotype *omb-Gal4/+;UAS-IRmfl/+*. anti-MFL in red; anti-Cas-3 activated form in green. **E)** Epifluorescence analysis of an *esg-Gal4/UAS IRmfl;UAS-RFP/+* silenced midgut at the third larval stage. DAPI is in gray; *esg*-expression domain is marked by an UAS-RFP responder line (in red); anti-Prospero, which specifically marks enteroendocrine cells, is in purple; Staining with anti-activated-Caspase-3 is shown in green. No signal of activated Caspase-3 is detected in silenced AMPs. Red arrows in the enlargement (on the bottom) indicate non apoptotic silenced and dispersed AMPs (*esg+pros-* cells).

linked by a specific Caspase-sensitive site, a fragment of the inhibitor of apoptosis DIAP1 which is cleaved by Cas-3 (Fig. 25 A). In live cells, GFP and RFP reside at the membrane, but in the presence of activated Cas-3 the GFP, that is linked to a nuclear localization sequence (NLS), is released and

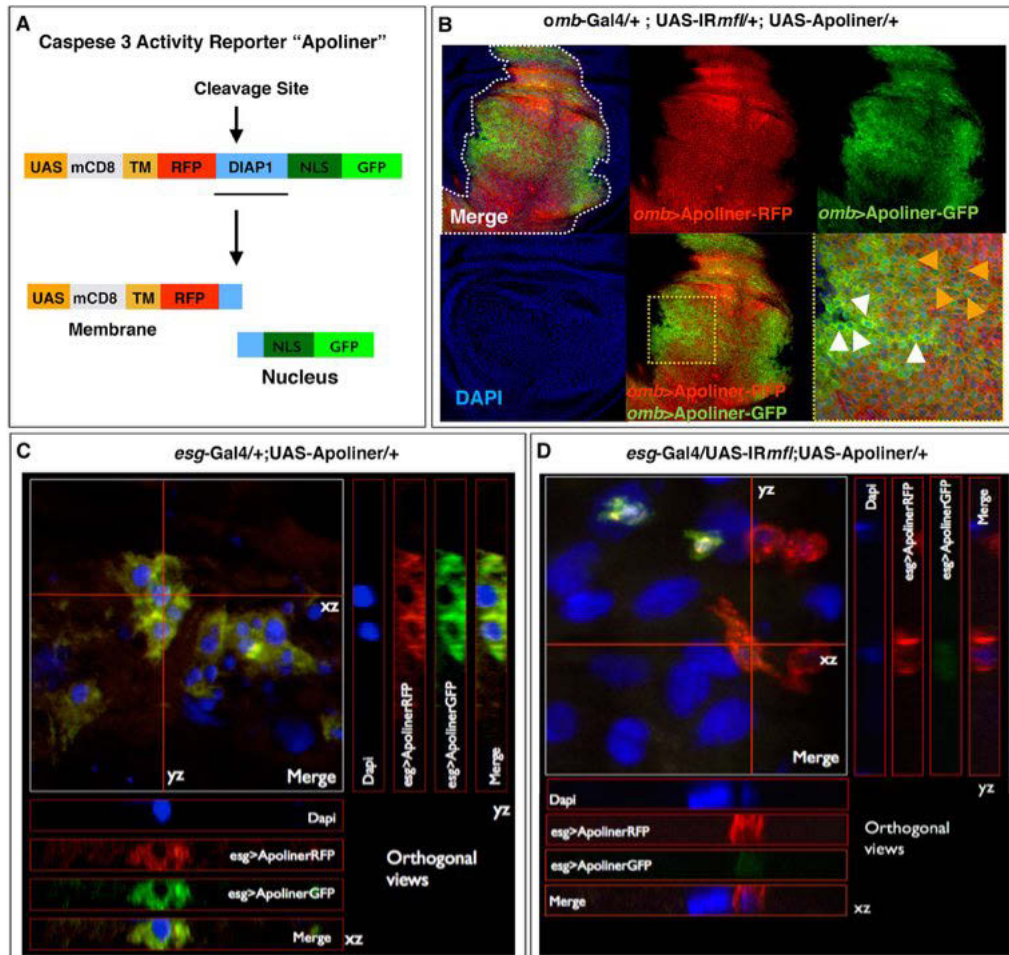


Figure 25. Apoliner reporter analysis. (A) Schematic representation of Caspase-3 activity reporter “Apoliner”. A fusion protein, under the control of UAS sequence, containing a transmembrane domain (TM), RFP, a Caspase-sensitive site (deriving from DIAP1 protein) and GFP linked to a nuclear localization signal (NLS). Activated Caspase-3 cuts in the cleavage site and separates RFP, localized in membrane, from GFP, which is translocated to the nucleus. (B) Confocal analysis of a wing disc (*omb-Gal4/+;UAS-IRmfl/+;UAS-Apoliner/+*) representing a positive control of Apoliner activity. Orange arrows indicate apoptotic cells; white arrows indicate non-apoptotic cells. (C-D) Confocal analysis of control (*esg-Gal4/+;UAS-Apoliner/+*) and silenced (*esg-Gal4/UAS-IRmfl/+;UAS-Apoliner/+*) midguts. In control midguts (C) Apoliner RFP and GFP colocalize in membrane of imaginal island cells. In silenced midguts (D) in the *esg+pros-* cells an anomalous behavior of Apoliner reporter is detected (vesicular RFP and weak GFP signal). In *esg+pros+* EE cells, Apoliner RFP and GFP colocalize in membrane. See Z-stack projections. Dapi in blue; Apoliner-RFP in red; Apoliner-GFP in green; Prospero in white.

traslocates to the nucleus of apoptotic cells (Bardet et al. 2008). Since it has been observed that wing disc cells undergo Cas-3 dependent apoptosis after *mfl* silencing, I decided to perform a confocal analysis on a silenced wing disc (genotype *omb-Gal4/+;UAS-IRmfl/+;UAS-Apoliner/+*) to have a positive control of the activity of the Apoliner sensor. As shown in Fig. 25 B, in the silenced disc apoptotic cells (yellow arrows) have RFP localized in membrane and GFP in the nucleus, whereas in non-apoptotic cells (white arrows) GFP and RFP colocalize in membrane.

I then expressed the Apoliner sensor in midgut stem cells under the control of the *esg-Gal4* driver. In control midguts (genotype: *esg-Gal4/+;UAS-Apoliner/+*) I observed that cells of the imaginal islands have RFP and GFP both localized in membranes, as expected for being non-apoptotic (Fig. 25 C). However, in the silenced midguts I observed an anomalous behavior of Apoliner reporter: RFP and GFP colocalize in the membranes of the enteroendocrine cells (which could be considered as an immunostaining internal control); in contrast, in the dispersed AMPs, the RFP appears vesicular and the GFP signal is quenched (Fig. 25 D). This results confirms that larval midgut stem cells do not die after MFL depletion, further reinforcing the idea, already sustained in previous work (Vicidomini et al. 2015), that *mfl* silencing induces context-specific effects.

4.11 MFL-depleted AMPs activate autophagy in a cell-specific manner

The anomalous behavior of Apoliner sensor (vesicular aspect of RFP and quenching of GFP signal) led to speculate that MFL depletion could activate an autophagic program in silenced AMPs. To test this hypothesis I expressed, by using the *esg-Gal4* driver, a common autophagosome reporter able to detect autophagic cells. In this reporter, ATG8a/LC3 is fused with mCherry fluorescent protein, so that autophagosomes and autolysosomes appear labeled by puncta of mCherry fluorescence (Klionsky et al. 2012). In control midguts (genotype: *esg-Gal4/+;UAS-mcherry-ATG8a/+*) the fluorescence of mCherry-Atg8a appears diffused in the imaginal island cells, as expected for non autophagic cells (Fig. 26 A). In contrast, all AMPs that are still present in the silenced midguts (genotype: *esg-Gal4/+;UAS-mcherry-ATG8a/UAS-IRmfl*) present puncta of mCherry-ATG8a, indicating a strong induction of autophagy in these cells (Fig. 26 B). Subsequently, I expressed, in the *esg+* cells, another reporter in which ATG8a/LC3 is fused with mCherry and GFP in tandem. This reporter is commonly used to monitor the autophagic flux, since GFP signal is quenched at the acidic conditions of the autolysosome lumen, whereas m-

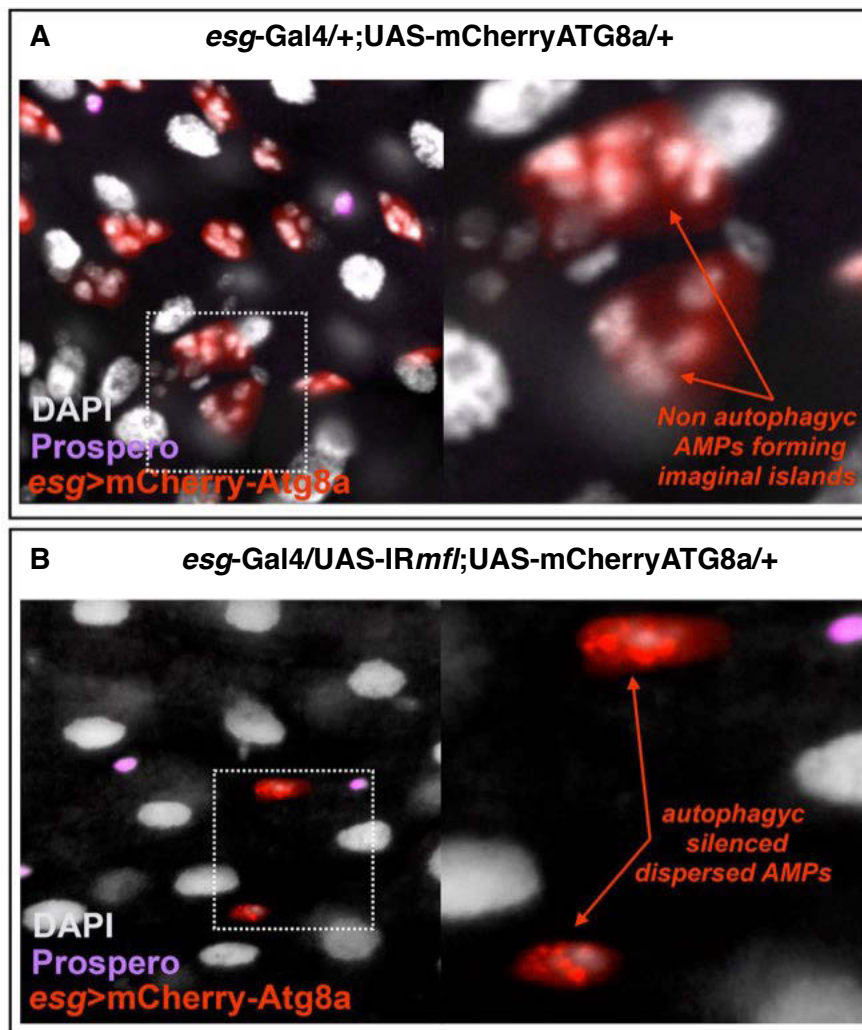


Figure 26. *mfl*-silenced AMPs activate autophagy. Confocal microscopy analysis of mcherry-ATG8a reporter expression. (A) In *esg-Gal4/+;UAS-mCherryATG8a/+* control midguts at the third larval stage, non autophagic imaginal island cells present a diffuse fluorescence of mcherry-ATG8a. (B) In *esg-Gal4/UAS-IRmfl;UAS-mCherryATG8a/+* silenced midguts at the third larval stage, dispersed AMPs present a punctuated fluorescence of mcherry-ATG8a, as expected in autophagic cells. (Red arrows (in the enlargement to the right) indicate imaginal islands in A and dispersed AMPs in B and C; DAPI is in grey; mcherryATG8a in red; anti-Prospero in magenta.

Cherry is more stable. Therefore, colocalization of both GFP and mCherry fluorescence indicates autophagosomes; in contrast, mCherry signals without GFP correspond to autolysosomes and indicates that autophagic flux is active and not blocked in the initial phases of autophagosome formation (Klionsky et al. 2012). In control midguts (*esg-Gal4/+;UAS-mCherry-GFP-ATG8a/+*) mCherry and GFP signals appear almost identical and diffused, indicating that

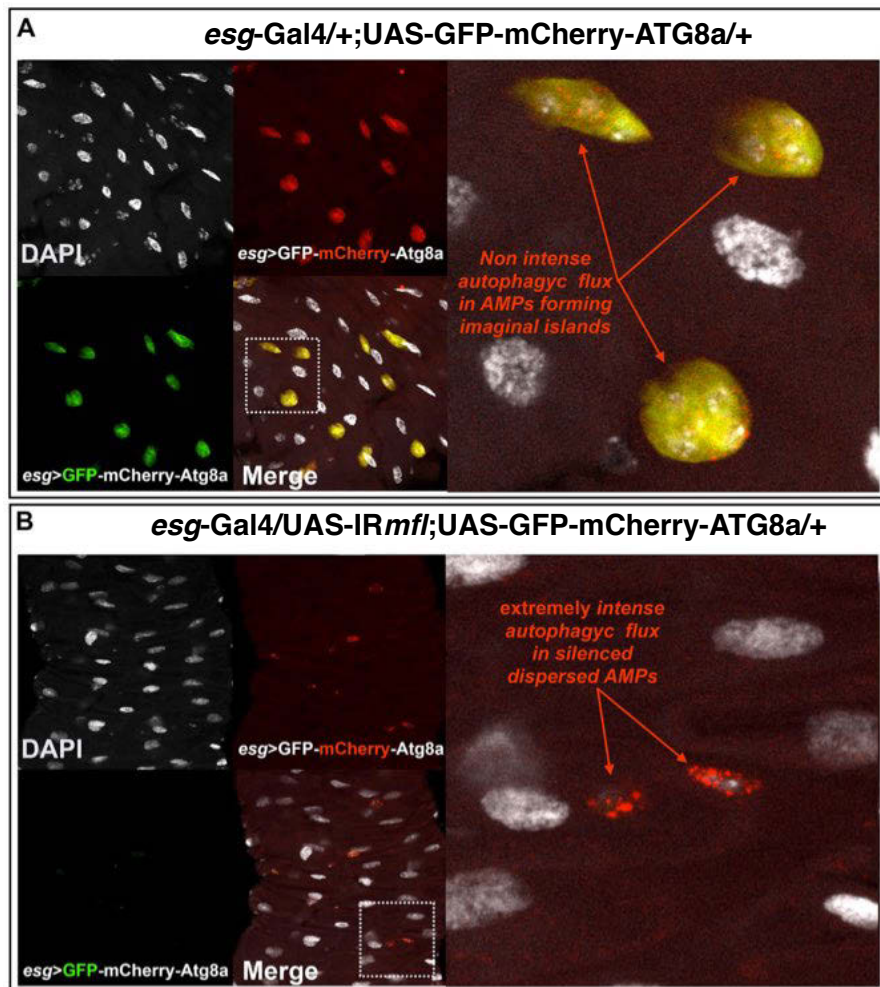


Figure 27. *mfl*-silenced AMPs exhibit an intense autophagic flux. Confocal microscopy analysis of GFP-mCherry-ATG8a reporter expression. (A) In *esg-Gal4/+;UAS-GFP-mCherryATG8a/+* control midguts at the third larval stage, GFP-mCherry-ATG8a fluorescence appears diffused (both in mCherry and GFP channels) in non autophagic imaginal island cells. (B) In *esg-Gal4/UAS-IRmfl;UAS-GFP-mCherryATG8a/+* silenced midguts at the third larval stage, puncta of ATG8a are detected in AMPs only in mCherry channel, while GFP signal is quenched, as expected in the acidic environment of autolysosomes. Red arrows (in the enlargement to the right) indicate imaginal islands in A and dispersed AMPs in B; DAPI is in grey; GFP-mCherryATG8a in red and in green.

normally autophagy is not activated in the imaginal island cells (Fig. 27 A). In silenced midguts (*esg-Gal4/+;UAS-mCherry-GFP-ATG8a/UAS-IRmfl*), instead, puncta of mCherry fluorescence are detected and GFP signals are very weak or absent (Fig. 27 B). This result reveals the presence of autolysosomes

in AMPs and confirms the activation of an intense autophagic flux in these cells after *mfl* gene silencing.

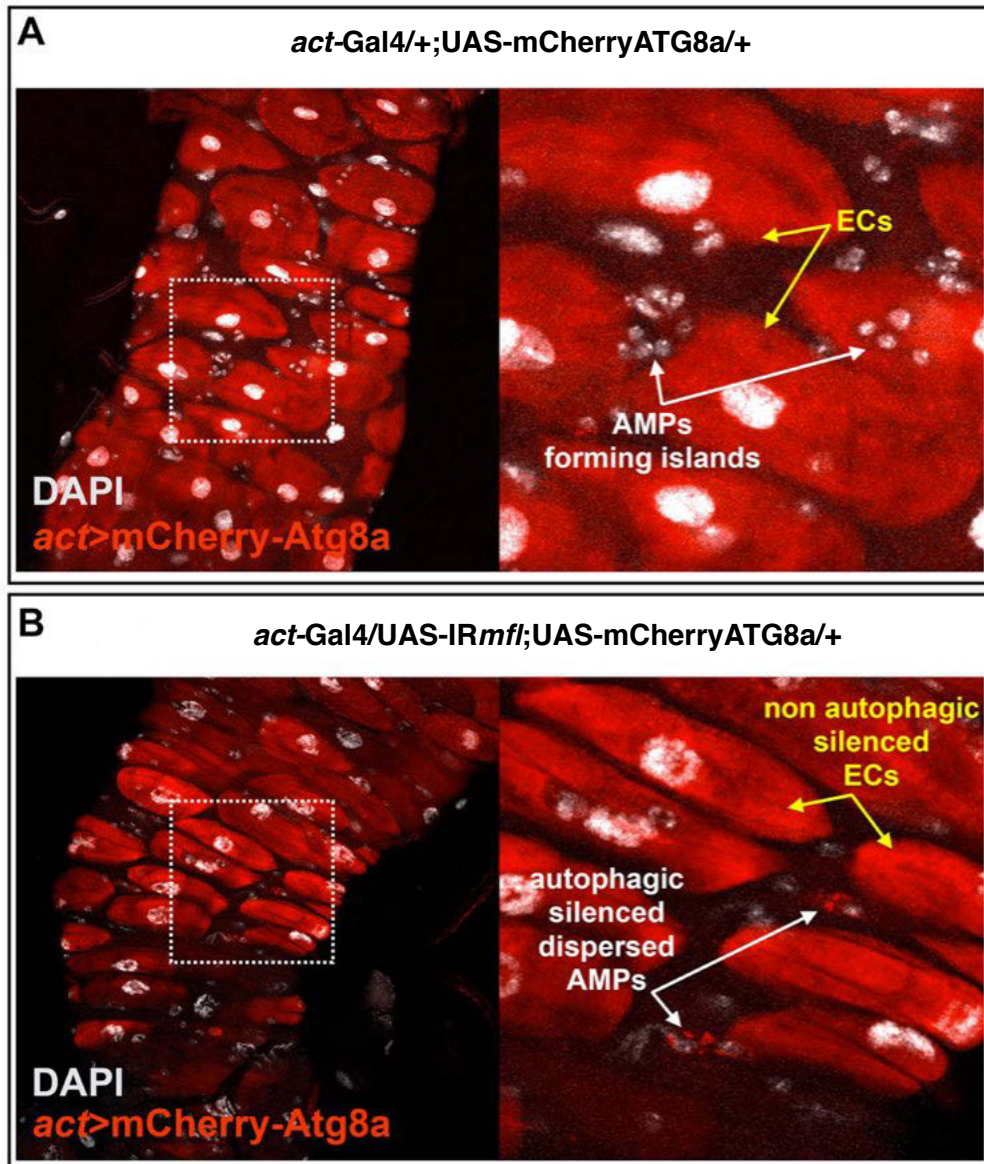


Figure 28. Ubiquitous *mfl* silencing causes autophagy in AMPs but not in enterocytes (ECs). Confocal microscopy analysis of mCherry-ATG8a reporter expression. (A) In *act-Gal4/+;UAS-mCherryATG8a/+* control midguts at the third larval stage, mCherry-ATG8a fluorescence appears diffused both in ECs and in AMPs forming islands. (B) In *act-Gal4/UAS-IRmfl;UAS-mCherryATG8a/+* silenced midguts at the third larval stage, puncta of ATG8a are detected in silenced and dispersed AMPs but not in silenced ECs. Red arrows (in the enlargement to the right) indicate imaginal islands in A and dispersed AMPs in B; DAPI is in grey; mCherryATG8a in red. In the enlargements, yellow arrows indicate ECs and white arrows indicate AMPs.

To determine whether activation of autophagy occurs specifically in the stem cell compartment of larval midgut, I decided to express the UAS-mCherry-ATG8a reporter in all midgut cells using the *act*-Gal4 driver line. In control midguts (*act*-Gal4/+;UAS-mCherry-ATG8a/+) at the third larval stage, mCherry-ATG8a fluorescence appears weak both in ECs and in AMPs aggregated into imaginal islands, confirming that autophagy is not normally activated in these cells (Fig. 28 A). In silenced midguts (*act*-Gal4/UAS-*IRmfl*;UAS-mCherry-ATG8a/+) at the third larval stage, instead, mCherry-ATG8a fluorescence appears punctuated in silenced and dispersed AMPs but not in the silenced ECs, indicating that after ubiquitous *mfl* silencing, the AMPs but not the ECs activate autophagy (Fig. 28 B). Therefore, activation of autophagy is a specific effect of *mfl* silencing in the larval midgut stem cell compartment.

To better characterize the cell-specificity of autophagy activation in AMPs, *Drosophila* transgenic embryos (genotype: *hs*-Flp;UAS-*IRmfl*; *act*>STOP>GAL4,UAS-NLS-GFP/UAS-mCherryATG8a) collected in a time of deposition of 12 hours were subjected to heat shock at 37 °C for 15 minutes. The heat shock was induced 18 hours AED, i.e. after they reach the

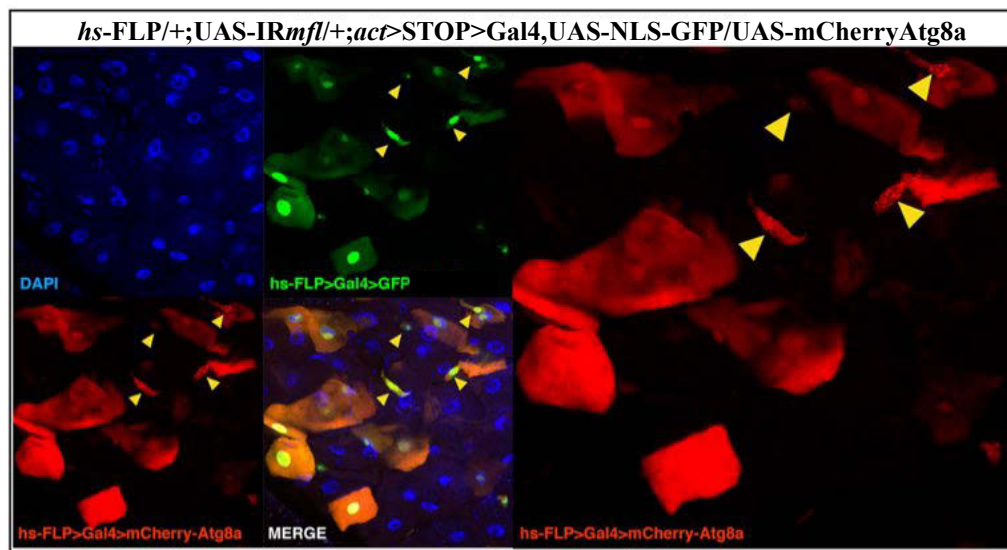


Figure 29. *mfl* silencing in mitotic clones causes autophagy in AMPs but not in enterocytes (ECs). Confocal microscopy analysis of mCherry-ATG8a reporter expression in *mfl*-silenced clones. Embryos (genotype: *hs*-Flp;UAS-*IRmfl*; *act*>STOP>GAL4,UAS-NLS-GFP/UAS-mCherryATG8a) collected in a time of deposition of 12 hours were heat-shocked for 15 min at 37 °C, 18 hours AED. Silenced midguts from heat-shocked animals were analyzed at the third larval stage. NLS-GFP+ silenced clones are formed by ECs or by dispersed AMPs (yellow arrowed). mCherry-ATG8a reporter shows a strong activation of autophagy only in *mfl*-silenced AMPs, but not in the silenced ECs. Dapi in blue; NLS-GFP in green; mCherry-ATG8a in red.

stage 10 of embryonic development, when AMPs are specified (6 hours AED). Midguts of heat-shocked animals were analyzed at the third larval stage. As shown in Fig. 29, the NLS-GFP⁺ silenced clones are formed by ECs or by dispersed diploid cells (indicated by yellow arrows) and a strong autophagy activation is revealed by mCherry-ATG8a reporter only in the dispersed diploid cells, corresponding to *mfl*-silenced AMPs, but not in the silenced enterocytes, confirming the cell-specificity of the phenomenon.

5. DISCUSSION

Drosophila melanogaster is one of the most-used animal model organisms. Many biological, physiological and neurological properties are conserved between flies and humans and about 75% of human disease genes have an ortholog in the fruit fly genome (Pandey and Nichols, 2011; Perrimon et al. 2016). In this thesis, I used *Drosophila* as model system to investigate the molecular mechanisms underlying the pathological manifestation of the X-linked Dyskeratosis congenita (X-DC), a rare human disease.

This multisystemic disorder, characterized by loss of stemness, early aging and increased susceptibility to cancer, is caused by hypomorphic alleles of the human *DKC1* gene. *hDKC1* encodes for dyskerin, a component of the H/ACA snoRNP complexes that has catalytic activity of pseudouridine synthase. The H/ACA snoRNPs are hetero-pentameric complexes evolutionary conserved from Archaea to mammals. Within these complexes, the core protein dyskerin associates with one molecule of small nucleolar RNA (snoRNA) of the H/ACA class and three highly conserved proteins, namely NOP10, NHP2 and GAR1 (Kiss et al. 2006). snoRNA H/ACA complexes are involved in several cellular functions, such as pseudouridylation of rRNAs and small nuclear RNAs (snRNAs), rRNA processing and telomere maintenance (reviewed by Angrisani et al. 2014). In recent years, an additional new role in the transcriptional control of key genes involved in mammalian embryonic stem cell maintenance has also been discovered (Fong et al. 2014).

Although many studies have been aimed at understanding the molecular basis of X-DC, several questions still remain to be answered. One of the most interesting issue is that of distinguishing the effects caused by telomere shortening from those correlated to telomerase-independent roles. Another issue is that of establishing whether loss of *hDKC1* functions is associated to growth disadvantages or to other types of dysfunctions. Finally, it remains to be clarified if dyskerin and H/ACA snoRNP complexes have cell-specific functions and how telomere shortening and alteration of ribosome biogenesis can be conciliated with the high cancer susceptibility shown by X-DC patients.

The *Drosophila Nop60b/mfl (minifly)* gene is the fly *hDKC1* orthologue, and its encoded protein, called MFL, shares 66% of identity with human dyskerin. In particular, the sequence conservation is total in the functional domains (Giordano et al. 1999). Null *mfl* alleles are lethal, whereas some hypomorphic alleles determine a pleiotropic phenotype characterized by extreme reduction of the body, developmental delay, defects in the abdominal cuticle and

alterations of bristles. One known hypomorphic allele is not associated with somatic defects, but determines the loss of male germline stem cells (Kauffman et al. 2002). All these *mfl* alleles are generated by insertional mutagenesis; the transgenes are inserted in the promoter or in the first exon of the gene, therefore causing a reduction in the levels of wild type protein. In humans, most X-DC causative mutations are missense; however, some mutations fall in the promoter, causing reduced levels of wild type protein (Knight et al. 1999; Salowsky et al. 2002). In addition, several data indicate that reduced levels of dyskerin can cause X-DC, so that induction of *hDKC1* silencing in several different cell lines is a common approach to characterize the disease (reviewed by Angrisani et al. 2014).

In my experiments, I silenced *in vivo* the *Drosophila hDKC1* orthologue, the *mfl* gene, to mimic the X-DC pathological condition. I found that the induction of *mfl* silencing, both ubiquitous or restricted specifically in the cells expressing the stem marker *esg*, impedes the formation of the larval stem niches (the imaginal islands). This result indicated that the expression of the pseudouridine synthase component of H/ACA snoRNPs is required specifically within the intestinal stem cells. Moreover, *mfl* localized silencing under the control of the *esg*-Gal4 driver not only induces loss of the imaginal islands but also strongly reduces the number of the *esg*⁺ cells. However, since the *esg*-Gal4 driver is active not only in the imaginal island cells but also in other anatomical areas (including brain, ring gland and salivary glands), I made use of the mitotic clonal analysis based on the Flp-out method (Struhl and Basler 1993) to prove that the loss of the imaginal islands is induced by MFL depletion as a cell-autonomous phenomenon. This analysis also allowed to exclude the possibility that imprecise evaluation of the larval developmental stage could have caused this effect, since in the same midgut the imaginal islands are correctly formed in the unsilenced tissue surrounding the mitotic clones. Finally, by inducing the Flp-out system silencing after that normal timing in which AMP specification occurs (i.e. after the 10th embryonic stage of development; Takashima et al. 2011), I could exclude that either the loss of the islands and the reduction in the number of the *esg*⁺ cells could be due to defective stem cell specification. Therefore, I could unequivocally conclude that MFL protein is required specifically within the AMP stem cells (the adult midgut precursors) for proper formation of the stem niches.

This result is consistent with the observation of Kauffman et al. (2002) who demonstrated that a loss of function allele of *mfl* specifically affects the maintenance of the germ-line stem cell lineage during spermatogenesis. Therefore, it is possible that a higher requirement for the canonical function of H/ACA snoRNP complexes is required into stemness compartments. An alternative explanation is that eukaryal dyskerins may play special roles in both

germ and somatic stem cell types, possibly relying on the expression of stem cell specific ncRNAs of the H/ACA class involved in regulatory networks of stem cell characteristic functions.

In every case, MFL depletion greatly alters maintenance of midgut stem cells. The counting of the *esg*⁺ cells in silenced and control entire midguts at the third larval stage revealed a drastic decline in both the total number of the *esg*⁺ cells (by 88%) and in the number of clusters formed by at least 3 *esg*⁺ cells (by about 95%). The formation of a few clusters of *esg*⁺ cells is probably due to a local low efficiency of silencing or to stochastic fluctuations that allow few cells to form imaginal islands. However, the presence of these very rare clusters does not impede to conclude that MFL depletion causes the almost total disappearance of larval intestinal stem niches. Noticeably, despite the strong reduction in the total number of the *esg*⁺ cells, I observed an increment (slightly greater than 4 folds) of single dispersed *esg*⁺ cells persisting in the silenced midguts and noticed the presence of doublet of *esg*⁺ cells, which likely represent daughter AMPs unable to further proliferate. It is well known that AMP amplification occurs in two phases: a first phase during early larval development (1-3 days AED), when AMPs increase their number and disperse into the epithelium; and a second phase during the mid-third larval stage (4 days AED), when AMPs divide into imaginal islands (Jiang and Edgar, 2009). I thus analysed midguts at two developmental stages (at 3 days AED and at the late third larval stage) and used anti-Prospero, an EE specific cell marker (Zeng et al. 2010; Micchelli et al. 2011), to exclude from counting the *esg*⁺*pros*⁺ enteroendocrine cells. Total counting led to estimate that AMP number is reduced by 60% in the early and by 50% in the later stages, indicating that only a small proportion of *esg*⁺*pros*⁻ AMP cells formed in the silenced midguts (whose number is by itself strongly reduced) is able to divide, thereby passing from single cells/doublets to clusters. Altogether, these observations suggest that MFL depletion prevents stem cells from undergoing further division cycles and confirm that stem cell reduction occurs during the first amplification phase. In the progress of this work, I also considered the possibility that several biological phenomena could be compatible with the observed phenotypes: apoptosis, decreased proliferation, or premature differentiation of AMPs may all have a role in the loss of the stem cells. Although anti-Pros immunostaining indicated that MFL-depleted *esg*⁺ cells do not differentiate into EEs, a premature differentiation toward other fates could not be excluded. To test this possibility, I performed the G-trace lineage analysis. This analysis, which allows to follow the lineage of a specific cell type (Evans et al. 2009), showed that the number of the differentiated cells derived from embryonic *esg*⁺ cells does not vary significantly after *mfl* silencing, ruling out the possibility that *esg*⁺ + depleted cells undergo premature differentiation.

Once established this point, the use of AMP common markers helped to test if these cells preserved their stem identity. I observed that *Drosophila* β -catenin (Armadillo), which accumulates at the adherence junctions of *wild type* AMPs clustered into islands, also surrounds *esg*⁺ MFL-depleted cells detected as single or doublets. This finding shows that members of the “doublet” are linked each other by adherens junctions and therefore probably derive from the division of the same “mother” cell. I noticed that the Notch ligand Delta (DI) is correctly localized in the membrane of the MFL-depleted AMPs. Moreover, in some doublets DI is highly expressed in one cell and Notch is active in the other (the peripheral cell; PC), as expected after an asymmetric division. These results confirmed that *mfl*-silenced AMPs retain their stem cell identity and keep their ability to divide asymmetrically. However, presence of some doublets lacking of Notch activation suggests possible defects in the process of division.

Since eukaryotic dyskerin loss of function have been associated with reduced efficiency of rRNA processing (Giordano et al. 1999; Ruggero et al. 2003), also cell-growth defects could have been responsible for loss of stem cells. However, I found that accumulation levels of proteins like p-S6K, p-eIF2 α and fibrillarin (and also fibrillarin localization), commonly monitored to evaluate cell-growth defects (Grewal et al. 2007; Laplante and Sabatini 2009; Gallinetti et al. 2013), were not significantly different between control and silenced midguts, indicating that cell growth ability was unaffected.

Finally, the absence of evident cell growth defects and of progressive reduction of the silenced *esg*⁺ cells during development (from 3 days AED to the late third larval stage) were not compatible with apoptotic phenomena. However, since previous works have shown that MFL depletion in other tissues can cause apoptosis (Tortoriello et al. 2010; Vicidomini et al. 2015), I checked also this hypothesis either by staining the silenced midguts for the activated Cas3 and by monitoring Caspase3 activity through the reporter “Apoliner” (Bardet et al. 2007). Both approaches indicated that apoptosis does not occur in the AMP silenced cells. However, while in the imaginal islands of control midguts Apoliner-RFP and Apoliner-GFP showed a perfect co-localization in membrane, as expected for non-apoptotic cells, in *esg*⁺*pros*⁻ silenced cells, Apoliner-RFP showed a punctuated pattern aspect and Apoliner-GFP fluorescence was very weak. This finding indicates a specific GFP quenching, suggesting that MFL-depleted AMPs may activate an autophagic program. The punctuated appearance of the Apoliner-RFP was in fact compatible with its accumulation into vesicles internal to the endoplasmic reticulum (Apoliner has in fact a transmembrane localization signal), while the specific GFP quenching was likely due to internalization into the acidic lumen of the autolysosomes (Ni et al. 2011). This unexpected behaviour of the “Apoliner” reporter allowed to

plan subsequent experiments to verify whether the silenced AMPs readily activated autophagy. To assess this point, I used the mCherry-ATG8a construct (Klionsky et al. 2012) to detect the presence of autophagosomes and autolysosomes in the silenced AMPs. Interestingly, all AMPs present in the silenced midguts exhibited punctuated fluorescence of mCherry-ATG8a already at early stages (3 AED). Since it is well known that both autophagy activation and autophagy inhibition lead to the accumulation of Atg8a/LC3 (Mizushima et al., 2010), in order to establish if *mfl* silencing induces activation or block of autophagy into AMPs, I monitored autophagic flux with a double fused reporter mCherry-GFP-Atg8a (Klionsky et al. 2012). Interestingly, activation of an intense autophagic program was observed into silenced AMPs. Noteworthy, the *mfl* ubiquitous silencing, driven by *act-Gal4*, revealed puncta of mCherry-ATG8a only into dispersed diploid cells (corresponding to AMPs) and not into polyploid enterocytes, confirming that MFL protein trigger specific effects into stemness compartments.

In synthesis, reduced levels of MFL protein into AMPs induce activation of autophagy which correlates with the reduction of the stem cell number. These data clearly indicate that MFL depletion has cell type-specific effects and that stem cells are particularly sensitive to alteration of MFL accumulation levels. Specifically, all experimental results are consistent with a reduced amplification of the silenced AMPs.

Future experiments should be addressed to the understanding of the role of the autophagy observed upon MFL silencing into larval intestinal stem cells. Since autophagy is a phenomenon implicated in several stem cell biological processes, such as self-cleaning, survival and differentiation (Guan et al. 2013; Pan et al. 2013), different scenarios are possible. For example, the silencing of *mfl* in a genetic background defective for autophagy could lead to the death of the silenced AMPs, indicating that autophagy observed after *mfl* silencing is a pro-survival signaling. Alternatively, the block of autophagy could lead to a rescue of the AMP number, leading to conclude that reduction of MFL-depleted AMP number is a direct result of the activation of the autophagic program. If *mfl* silencing in autophagy-defective conditions will not induce any changes in the number of AMPs, the autophagy induced by MFL depletion would be a secondary effect arising downstream of the block of AMP proliferation. In the latter case, the link between MFL and signaling pathways controlling AMP amplification should be deeply investigated. Since it is known that both AMPs amplification phases (that occurring before the formation of the islands and that within the islands) are controlled by EGFR/RAS (Jiang and Edgar, 2009), it is possible that the reduced number of silenced AMPs is caused by a reduction of this signaling pathway. Silencing of *mfl* in a background over-expressing a constitutively activated form of EGFR (EGFR^{gof}) or an

activated form of RAS (RASV12) will clarify whether MFL-depleted AMPs can rescue their proliferation ability under stimulation of the EGFR/RAS signaling.

6. CONCLUSIONS

All the data shown here indicate that *Drosophila* dyskerin protein (MFL, Minify) is required in a cell-autonomous manner to allow formation of larval midgut stem niches and to ensure the proper amplification of the larval midgut stem cells (AMPs), since the first phases of amplification in the embryonic-larval development. The observed decline of midgut stem cell number is not caused by premature differentiation of these cells, which do not become polyploid enterocytes and do not express a differentiation marker like *prospero*, but preserve their stem nature and biology. Indeed, MFL-depleted AMPs retain the expression of common midgut stem cell markers, such as *escargot*, *Delta* and *Armadillo* and seem to preserve the ability to divide asymmetrically, generating doublets of cells in which one activates Notch signaling. However, silenced AMPs appear to divide in a delayed and asynchronous manner, suggesting an alteration of their division rate. Indeed, all the obtained results indicates that AMPs amplification is altered upon *mfl* silencing.

The analysis of cell growth markers, like p-S6K, p-eIF2 α and fibrillarlin, led to assert that MFL depletion is not perceived as a condition that impairs the ability of AMPs to grow. Moreover, the observation that MFL-depleted wing disc cells undergo apoptosis but larval midgut stem cells do not die supports the idea, already sustained in our previous work (Vicidomini et al. 2015), that *mfl* silencing induces context-specific effects, in the same way as human dyskerin loss of function in X-DC. Furthermore, the activation of an intense autophagic flux is generated in the larval midgut stem cells but not in the enterocytes, reinforcing the belief that cell-type specific effects occur after MFL depletion. In conclusion, the results reported in this thesis established for the first time a link among loss of function of an eukaryotic snoRNP pseudouridine synthase, defects into stem cell maintenance and autophagy.

Given the high degree of conservation in the structure and functions of the snoRNP complexes of *Drosophila* and humans and the previous characterization of *Drosophila* as a good animal model for X-linked dyskeratosis syndrome (Giordano et al. 1999; Tortoriello et al. 2010; Vicidomini et al, 2015), the present work provides new interesting insights into the molecular mechanisms that could underlie the loss of stemness observed in X-DC patients.

7. AKNOWLEGMENTS

I thank M. Furia for her help in experimental planning and for constructive discussions. I thank R. Vicidomini for his essential contribution to this work and also A. Di Giovanni, L. Cassese and all the students of M. Furia's "Drosophila laboratory" for the wonderful work days spent together.

8. REFERENCES

Angrisani A, Vicidomini R, Turano M, Furia M. Human dyskerin: beyond telomeres. *Biol Chem*. 2014 Jan 28. pii:/j/bchm.just-accepted/hsz-2013-0287/hsz-2013-0287.xml. doi:10.1515/hsz-2013-0287

Arnez and Steitz. Crystal structure of unmodified tRNA (Gln) complexed with glutaminyl-tRNA synthetase and ATP suggests a possible role for pseudouridines in stabilization of RNA structure. *Biochemistry* 1994; 21;33:24:7560-7.

Axe EL, SA Walker, Manifava M, Chandra P, Roderick HL, Habermann A, Griffiths G, Ktistakis NT. Autophagosome formation from membrane compartments enriched in phosphatidylinositol 3-phosphate and dynamically connected to the endoplasmic reticulum. *JCB* 2008;182(4):685-701.

Bardet PL, Kolahgar G, Mynett A, Miguel-Aliaga I, Briscoe J, Meier P, Vincent JP. A fluorescent reporter of caspase activity for live imaging. *Proc Natl Acad Sci U S A* 2008; 105(37):13901-5.

Bellodi C, McMahon M, Contreras A, Juliano D, Kopmar N, Nakamura T, Maltby D, Burlingame A, Savage SA, Shimamura A, Ruggero D. H/ACA small RNA dysfunctions in disease reveal key roles for noncoding RNA modifications in hematopoietic stem cell differentiation. *Cell Rep*. 2013;3(5):1493-502

Bjørkøy G, Lamark T, Brech A, Outzen H, Perander M, et al. p62/SQSTM1 forms protein aggregates degraded by autophagy and has a protective effect on huntingtin-induced cell death. *J Cell Biol* 2005; 171:603–14.

Boisvert FM, van Koningsbruggen S, Navascues J, Lamond AI. The multifunctional nucleolus. *Nat Rev Mol Cell Biol* 2007; 8:574–585.

Brand AH, Perrimon N. Targeted gene expression as a means of altering cell fates and generating dominant phenotypes. *Development* 1993 Jun;118(2):401-15.

Canada Y, Funakoshi T, Shintani T, Nagano K, Ohsumi M, Ohsumi Y. Tor-Mediated Induction of Autophagy via an Apg1 Protein Kinase Complex. *JCB* 2000; 150(6):1507-1513

Chintapalli VR, Wang J, Herzyk P, Dow JAT. (2010.9.17). FlyAtlas: survey of adult and larval expression. <http://www.flyatlas.org/>

Choi NH, Lucchetta E, Ohlstein B. Nonautonomous regulation of *Drosophila* midgut stem cell proliferation by the insulin-signaling pathway. *Proc Natl Acad Sci USA* 2011; 108:18702–18707

Clarke PGH. Developmental cell death: Morphological diversity and multiple mechanisms. *Anat Embryol* 1990; 181:195–213.

Cohen SB, Graham ME, Lovrecz GO, Bache N, Robinson PJ, Reddel RR. Protein composition of catalytically active human telomerase from immortal cells. *Science* 2007;315:1850-53

Das G, Shrivage BV, Bachrecke EH. Regulation and Function of Autophagy during Cell Survival and Cell Death. *Cold Spring Harb Perspect Biol* 2012; 4:a008813

De Celis J F, Bray S. Feed-back mechanisms affecting Notch activation at the dorsoventral boundary in the *Drosophila* wing. *Development* 1997; 124, 3241-3251.

De Duve C, Wattiaux R. Functions of lysosomes. *Annu Rev Physiol.* 1966;28:435-92.

Denton D, Shrivage B, Simin R, Mills K, Berry DL, Baehrecke EH et al. Autophagy, not apoptosis, is essential for midgut cell death in *Drosophila*. *Curr Biol* 2009; 19:1741–1746.

Derenzini M, Trere D, Pession A, Govoni M, Sirri V, et al. Nucleolar size indicates the rapidity of cell proliferation in cancer tissues. *J Pathol* 2000; 191:181–186.

Ender C, Krek A, Friedländer MR, Beitzinger M, Weinmann L, Chen W, Pfeffer S, Rajewsky N, Meister G. A Human snoRNA with MicroRNA-Like Functions. *Molecular Cell* 2008;32:519-28

Evans CJ, Olson JM, Ngo KT, Kim E, Lee NE, Kuoy E et al. G-TRACE: rapid Gal4-based cell lineage analysis in *Drosophila*. *Nat Methods* 2009; 6:603–605.

Fernández García MS, Teruya-Feldstein J. The diagnosis and treatment of dyskeratosis congenita: a review. *J Blood Med*. 2014; 21;5:157-67.

Filimonenko M, Isakson P, Finley KD, Anderson M, Jeong H, Melia TJ, Bartlett BJ, Myers KM, Birkeland HC, Lamark T, Krainc D, Brech A, Stenmark H, Simonsen A, Yamamoto A. The selective macroautophagic degradation of aggregated proteins requires the PI3P-binding protein Alfy. *Mol Cell*. 2010; 38(2):265-79.

Fischer JA, Giniger E, Maniatis T, Ptashne M. GAL4 activates transcription in *Drosophila*. *Nature*. 1988;332(6167):853-6.

Fong YW, Ho JJ, Inouye C, Tjian R. The dyskerin ribonucleoprotein complex as an OCT4/SOX2 coactivator in embryonic stem cells. *Elife*. 2014;19;3.

Gallinetti J ,Harputlugil E.,Mitchell JR. Amino acid sensing in dietary-restriction-mediated longevity: roles of signal-transducing kinases GCN2 and TOR. *Biochem J* 2013; 449(1):1-10.

Giordano E, Peluso I, Senger S, Furia M. minifly, a *Drosophila* gene required for ribosome biogenesis. *J Cell Biol*. 1999;144(6):1123-33

Graveley BR, Brooks AN, Carlson JW, Cherbas L, Choi J, Davis CA, Dobin A, Duff M, Eads B, Hansen KD, Landolin J, Langton L, Malone J, Miller D, Roberts J, Sandler J, Sturgill D, Tang H, van Baren MJ, Wan KH, Xiao S, Yang L, Zhang D, Zhang Y, Zou Y, Andrews J, Brenner SE, Brent M, Cherbas P, Dudoit S, Gingeras TR, Hoskins R, Kaufman T, Oliver B, Celniker SE. The *D. melanogaster* transcriptome: modENCODE RNA-Seq data. 2010. <http://www.modencode.org/celniker/>

Grewal SS, Li L, Orian A, Eisenman RN, Edgar BA. Myc-dependent regulation of ribosomal RNA synthesis during *Drosophila* development. *Nat Cell Biol* 2005; 7:295–302.

Grewal SS, Evans JR, Edgar BA. *Drosophila* TIF-IA is required for ribosome synthesis and cell growth and is regulated by the TOR pathway. *J Cell Biol* 2007; 179(6):1105-13.

Guan J, Simon AK, Prescott M, Menendez JA, Liu F, Wang F, Wang C, Wolvetang E, Vazquez-Martin A and Zhang J. Autophagy in stem cells. *Autophagy Landes Bioscience* 2013; 9:6, 830–849.

Guo Z, Ohlstein B. Stem cell regulation. Bidirectional Notch signaling regulates *Drosophila* intestinal stem cell multipotency. *Science*. 2015;350(6263).

Hartenstein AY, Rugendorff A, Tepass U, Hartenstein V. The function of the neurogenic genes during epithelial development in the *Drosophila* embryo. *Development* 1992;116:1203–1220.

Hayashi S, Hirose S, Metcalfe T, Shirras AD. Control of imaginal cell development by the escargot gene of *Drosophila*. *Development* 1993; 118(1): 105-115.

Heiss NS, Knight SW, Vulliamy TJ, Klauck SM, Wiemann S, Mason PJ, Poustka A, Dokal I. X-linked dyskeratosis congenita is caused by mutations in a highly conserved gene with putative nucleolar functions. *Nat Genet*. 1998;19(1):32-8

Hilla Weidberg, Elena Shvets, Tomer Shpilka, Frida Shimron, Vera Shinder, Zvulun Elazar LC3 and GATE-16/GABARAP subfamilies are both essential yet act differently in autophagosome biogenesis. *The EMBO Journal* 2010; 29:1792-1802

Hou YC, Chittaranjan S, Barbosa SG, McCall K, Gorski SM. Effector caspase Dcp-1 and IAP protein Bruce regulate starvation-induced autophagy during *Drosophila melanogaster* oogenesis. *J Cell Biol* 2008; 182:1127–1139.

Issigonis M, Matunis E. Previews. Niche today, gone tomorrow--progenitors create short-lived niche for stem cell specification. *Cell Stem Cell*. 2010;6(3): 191-3.

Jacinto E, Hall MN. Tor signalling in bugs, brain and brawn. *Nat Rev Mol Cell Biol* 2003; 4:117–126.

Jiang C, Baehrecke EH, Thummel CS. Steroid regulated programmed cell death during *Drosophila* metamorphosis. *Development* 1997;124:4673–4683.

- Jiang H, Edgar BA. EGFR signaling regulates the proliferation of *Drosophila* adult midgut progenitors. *Development* 2009;136:483–493.
- Johansen T, Lamark T. Selective autophagy mediated by autophagic adapter proteins. *Autophagy* 2011; 7(3):279-96.
- Juhász G, Csikós G, Sinka R, Erdélyi M, Sass M. The *Drosophila* homolog of Atg1 is essential for autophagy and development. *FEBS letters* 2003; 543:154-158.
- Juhász G, Hill JH, Yan Y, Sass M, Baehrecke EH, Backer JM, Neufeld TP. The class III PI(3)K Vps34 promotes autophagy and endocytosis but not TOR signaling in *Drosophila*. *J. Cell Biol* 2008; 181:655–66.
- Kamada Y, Funakoshi T, Shintani T, Nagano K, Ohsumi M, Ohsumi Y. Tor-mediated induction of autophagy via an Apg1 protein kinase complex. *J Cell Biol* 2000;150: 1507–1513.
- Kauffmann T, Tran J, Di Nardo S. Mutations in Nop60B, the *Drosophila* homolog of human dyskeratosis congenita 1, affect the maintenance of the germ-line stem cell lineage during spermatogenesis. *Dev Biol* 2003; 253:189-199.
- Kaushik S, Cuervo AM. Chaperones in autophagy. *Pharmacol Res.* 2012;66(6): 484-93.
- Khanna A, Stamm S. Regulation of alternative splicing by short non-coding nuclear RNAs. *RNA Biol.* 2010;7(4)480-5
- Kiran M and Dokal I. Dyskeratosis congenita, stem cells and telomeres. *Biochimica Biophysica Acta* 2009;1792:371-79
- Kirisako T, Baba M, Ishihara N, Miyazawa K, Ohsumi M, Yoshimori T et al. Formation process of autophagosome is traced with Apg8/Aut7p in yeast. *J Cell Biol* 1999; 147: 435–446.
- Kirkin V, Lamark T, Johansen T, Dikic I. NBR1 cooperates with p62 in selective autophagy of ubiquitinated targets. *Autophagy.* 2009; 5(5):732-3.
- Kiss, T., E. Fayet, B. E. Jány, P. Richard and M. Weber. Biogenesis and intranuclear trafficking of human box C/D and H/ACA RNPs. *Cold Spring Harb. Symp. Quant.Biol.* 2006; 71:407-417.

Klionsky DJ. Autophagy: from phenomenology to molecular understanding in less than a decade. *Nature Reviews Molecular Cell Biology* 2007; 8:931-937.

Klionsky DJ, Abdalla FC, Abeliovich H et al. Guidelines for the use and interpretation of assays for monitoring autophagy. *Autophagy* 2012; 4(8):445–544.

Knight SW, Heiss NS, Vulliamy TJ, Aalfs CM, McMahon C, Richmond P, Jones A, Hennekam RC, Poustka A, Mason PJ, Dokal I. Unexplained aplastic anaemia, immunodeficiency, and cerebellar hypoplasia (Hoyeraal-Hreidarsson syndrome) due to mutations in the dyskeratosis congenita gene, DKC1. *Br J Haematol.* 1999;107(2):335-9

Lafontaine DL, Tollervey D. Birth of the snoRNPs: the evolution of the modification-guide snoRNAs. *Trends Biochem Sci.* 1998;23(10):383-8

Laplante M. and Sabatini DM. mTOR signaling at a glance. *Journal of Cell Science* 2009; 122:3589-3594.

Lestrade L, Weber MJ. snoRNA-LBME-db, a comprehensive database of human H/ACA and C/D box snoRNAs. *Nucleic Acids Res.* 2006;34(Database issue):D158-62

Levine B, Klionsky DJ. Development by self-digestion: molecular mechanisms and biological functions of autophagy. *Dev Cell* 2004; 6:463–477.

Lucchetta EM1, Ohlstein B. The *Drosophila* midgut: a model for stem cell driven tissue regeneration. *Wiley Interdiscip Rev Dev Biol.* 2012;1(5):781-8.

Lum JJ, Bauer DE, Kong M, Harris MH, Li C, Lindsten T, Thompson CB. Growth factor regulation of autophagy and cell survival in the absence of apoptosis. *Cell* 2005; 120: 237–248.

Mathur D, Bost A, Driver I, Ohlstein B. A transient niche regulates the specification of *Drosophila* intestinal stem cells. *Science* 2010;327:210–213.

Matsushita M, Suzuki NN, Obara K, Fujioka Y, Ohsumi Y, Inagaki F. Structure of Atg5·Atg16, a Complex Essential for Autophagy. *The Journal of Biological Chemistry* 2007; 282:6763-6772.

Melendez A, Neufeld TP. The cell biology of autophagy in metazoans: a developing story. *Development* 2008; 135:2347-2360.

Micchelli CA, Perrimon N. Evidence that stem cells reside in the adult *Drosophila* midgut epithelium. *Nature* 2006;439(7075):475-9.

Micchelli CA, Sudmeier L, Perrimon N, Tang, S, Beehler-Evans R. Identification of adult midgut precursors in *Drosophila*. *Gene Expr Patterns* 2011;11:12–21.

Micchelli CA. The origin of intestinal stem cells in *Drosophila*. *Dev Dyn*. 2012;241(1):85-91.

Mijaljica D, Prescott M, Devenish RJ. Microautophagy in mammalian cells: revisiting a 40-year-old conundrum. *Autophagy*. 2011;7(7):673-82.

Mizushima N, Yoshimori T, Levine B. Methods in mammalian autophagy research. *Cell* 2010; 140(3):313-26.

Mizushima N, Komatsu M. Autophagy: renovation of cells and tissues. *Cell*. 2011;147(4):728-41.

Mochizuki, Y., He, J., Kulkarni, S., Bessler, M., Mason, P.J. Mouse dyskerin mutations affect accumulation of telomerase RNA and small nucleolar RNA, telomerase activity, and ribosomal RNA processing. *Proc. Natl. Acad. Sci. USA* 2004; 101:10756-10761

Mohseni N, McMillan SC, Chaudhary R, Mok J, Reed BH. Autophagy promotes caspase-dependent cell death during *Drosophila* development. *Autophagy* 2009; 5:329–338.

Nair U, Jotwani A, Geng J, Gammoh N, Richerson D, Yen WL, Griffith J, Nag S, Wang K, Moss T, Baba M, McNew JA, Jiang X, Reggiori F, Melia TJ, Klionsky DJ. SNARE proteins are required for macroautophagy. *Cell*. 2011; 146(2):290-302.

Newby and Greenbaum. Sculpting of the spliceosomal branch site recognition motif by a conserved pseudouridine. *Nat Struct Biol*. 2002 ;9(12):958-65.

Nezis IP, Lamark T, Velentzas AD, Rusten TE, Bjørkøy G, Johansen T, Papassideri IS, Stravopodis DJ, Margaritis LH, Stenmark H, et al. Cell death

during *Drosophila melanogaster* early oogenesis is mediated through autophagy. *Autophagy* 2009; 5:298–302.

Nezis IP, Shrivage BV, Sagona AP, Lamark T, Bjørkøy G, Johansen T, Rusten TE, Brech A, Baehrecke EH, Stenmark H. Autophagic degradation of dBruce controls DNA fragmentation in nurse cells during late *Drosophila melanogaster* oogenesis. *J Cell Biol* 2010; 190: 523–531.

Ohlstein B, Spradling A. The adult *Drosophila* posterior midgut is maintained by pluripotent stem cells. *Nature*. 2006 Jan 26;439(7075):470-4. Epub 2005 Dec 7.

Ohsumi Y. Molecular dissection of autophagy: Two ubiquitin-like systems. *Nat Rev Mol Cell Biol* 2001; 2:211 – 216.

Pan H, Cai N, Li M, Liu G, Izpisua Belmonte JC. Autophagic control of cell ‘stemness’. *EMBO Mol Med* 2013; 5, 327–331.

Pandey UB, Nichols CD. Human disease models in *Drosophila melanogaster* and the role of the fly in therapeutic drug discovery. *Pharmacol Rev* 2011; 63(2):411-36.

Pardue ML, Rashkova S, Casacuberta E, DeBaryshe PG, George JA, Traverse KL. Two retrotransposons maintain telomeres in *Drosophila*. *Chromosome Res.* 2005;13(5):443-53

Perrimon N, Bonini NM, Dhillon P. Fruit flies on the front line: the translational impact of *Drosophila*. *Dis Model Mech* 2016; 9(3):229-31.

Pignoni, F. and Zipursky, S. L. Induction of *Drosophila* eye development by decapentaplegic. *Development* 1997; 124, 271-278.

Podlevsky JD, Bley CJ, Omana RV, Qi X, Chen JJ. The telomerase database. *Nucleic Acids Res.* 2008;36(Database issue):D339-43.

Riccardo S, Tortoriello G, Giordano E, Turano M, Furia M. The coding/non-coding overlapping architecture of the gene encoding the *Drosophila* pseudouridine synthase. *BMC Mol Biol* 2009; 8:15.

Richard P, Darzacq X, Bertrand E, Jády BE, Verheggen C, Kiss T. A common sequence motif determines the Cajal body-specific localization of box H/ACA scaRNAs. *EMBO J.* 2003 Aug;22(16):4283-93

Ruggero D, Grisendi S, Piazza F, Rego E, Mari F, Rao PH, Cordon-Cardo C, Pandolfi PP. Dyskeratosis Congenita and Cancer in Mice Deficient in Ribosomal RNA Modification. *Science* 2003;299:259-62

Saj A, Arziman Z, Stempfle D, van Belle W, Sauder U, Horn T, Durrenberger M, Paro R, Boutros M, Merdes G. A Combined Ex Vivo and In Vivo RNAi Screen for Notch Regulators in *Drosophila* Reveals an Extensive Notch Interaction Network. *Developmental Cell* 2010; 18:862–876.

Salowsky R, Heiss NS, Benner A, Wittig R, Poustka A. Basal transcription activity of the dyskeratosis congenita gene is mediated by Sp1 and Sp3 and a patient mutation in a Sp1 binding site is associated with decreased promoter activity. *Gene.* 2002;293(1-2):9-19

Savage SA, Giri N, Baerlocher GM, Orr N, Lansdorp PM, Alter BP. TINF2, a component of the shelterin telomere protection complex, is mutated in dyskeratosis congenita. *Am J Hum Genet.* 2008;82(2):501-9

Schwartz S, Bernstein DA, Mumbach MR, Jovanovic M, Herbst RH, León-Ricardo BX, Engreitz JM, Guttman M, Satija R, Lander ES, Fink G, Regev A. Transcriptome-wide mapping reveals widespread dynamic-regulated pseudouridylation of ncRNA and mRNA. *Cell.* 2014;159(1):148-62.

Scott RC, Schuldiner O, Neufeld TP. Role and regulation of starvation-induced autophagy in the *Drosophila* fat body. *Dev Cell* 2004; 7:167–178.

Shimizu S, Kanaseki T, Mizushima N, Mizuta T, Arakawa-Kobayashi S, Thompson CB and Tsujimoto Y. Role of Bcl-2 family proteins in a non-apoptotic programmed cell death dependent on autophagy genes. *Nat Cell Biol* 2004; 6:1221–1228.

Simonsen A, Tooze SA. Coordination of membrane events during autophagy by multiple class III PI3-kinase complexes. *JCB* 2009; 186(6):773-782

Skaer H. The alimentary canal. In: Bate, M., Martinez-Arias, A. (Eds.). *The Development of Drosophila melanogaster.* 1993. pp. 941–1012.

Struhl G, Basler K. Organizing activity of wingless protein in *Drosophila*. *Cell* 1993;72, 527-540.

Taft RJ, Glazov EA, Lassmann T, Hayashizaki Y, Carninci P, Mattick JS. Small RNAs derived from snoRNAs. *RNA* 2009;15:1233-40

Takashima S, Adams KL, Ortiz PA, Ying CT, Moridzadeh R, Younossi-Hartenstein A, Hartenstein V. Development of the *Drosophila* enteroendocrine lineage and its specification by the Notch signaling pathway. *Dev Biol* 2011;353:161–172.

Technau G, Campos-Ortega JA. Lineage analysis of transplanted individual cells in embryos of *Drosophila melanogaster*. III. Commitment and proliferative capabilities of pole cells and midgut progenitors. *Wilhelm Roux' Arch Devl Biol* 1986;195:489–498.

Tepass U, Hartenstein V. Epithelium formation in the *Drosophila* midgut depends on the interaction of endoderm and mesoderm. *Development* 1994;120:579–590.

Tepass U, Hartenstein V. Neurogenic and proneural genes control cell fate specification in the *Drosophila* endoderm. *Development* 1995;121:393–405.

Tollervey D, Lehtonen H, Jansen R, Kern H, Hurt EC. Temperature-sensitive mutations demonstrate roles for yeast fibrillarin in pre-rRNA processing, pre-rRNA methylation, and ribosome assembly. *Cell* 1993; 72:443–457.

Tortoriello G, de Celis JF, Furia M. Linking pseudouridine synthases to growth, development and cell competition. *The FEBS Journal* 2010;277:3249- 63

Vulliamy TJ, Marrone A, Knight SW, Walne A, Mason PJ, Dokal I. Mutations in dyskeratosis congenita: their impact on telomere length and the diversity of clinical presentation. *Blood*. 2006;107(7):2680-5.

Vulliamy T, Beswick R, Kirwan M, Marrone A, Digweed M, Walne A, Dokal I. Mutations in the telomerase component NHP2 cause the premature ageing syndrome dyskeratosis congenita. *Proceedings of the National Academy of Sciences of the United States of America* 2008;105:8073-78

Walne AJ, Vulliamy T, Marrone A, Beswick R, Kirwan M, Masunari Y, Al-Qurashi F-h, Aljurf M, Dokal I. Genetic heterogeneity in autosomal recessive

dyskeratosis congenita with one subtype due to mutations in the telomerase-associated protein NOP10. *Human Molecular Genetics* 2007;16:1619-29

Walne AJ, Vulliamy T, Beswick R, Kirwan M, Dokal I. TINF2 mutations result in very short telomeres: analysis of a large cohort of patients with dyskeratosis congenita and related bone marrow failure syndromes. *Blood* 2008;112:3594-600

Wei Y, Pattingre S, Sinha S, Bassik M, Levine B. JNK1-mediated phosphorylation of Bcl-2 regulates starvation-induced autophagy. *Mol Cell* 2008; 30:678–688.

Wong and Collins. Telomerase RNA level limits telomere maintenance in X-linked dyskeratosiscongenita. *Genes Dev.* 2006;20(20):2848-58.

Yu L, McPhee CK, Zheng L, Mardones GA, Rong Y, Peng J, Mi N, Zhao Y, Liu Z, Wan F, Hailey DW, Oorschot V, Klumperman J, Baehrecke EH, Lenardo MJ. Termination of autophagy and reformation of lysosomes regulated by mTOR. *Nature* 2010; 465:942–946

Zeng X, Chauhan C, Hou SX. Characterization of midgut stem cell and enteroblast-specific Gal4 lines in drosophila. *Genesis* 2010; 48:607–611.

Zhou Y, Li Y, Jiang W, Zhou L. MAPK/JNK signalling: a potential autophagy regulation pathway. *Bioscience Reports* 2015; 35:e00199.

Loss of *Drosophila* pseudouridine synthase triggers apoptosis-induced proliferation and promotes cell-nonautonomous EMT

R Vicidomini^{1,4}, A Di Giovanni^{1,4}, A Petrizzo¹, LF Iannucci¹, G Benvenuto², AC Nagel³, A Preiss³ and M Furia^{4*}

Many developing tissues display regenerative capability that allows them to compensate cell loss and preserve tissue homeostasis. Because of their remarkable regenerative capability, *Drosophila* wing discs are extensively used for the study of regenerative phenomena. We thus used the developing wing to investigate the role played in tissue homeostasis by the evolutionarily conserved eukaryotic H/ACA small nucleolar ribonucleoprotein pseudouridine synthase. Here we show that localized depletion of this enzyme can act as an endogenous stimulus capable of triggering apoptosis-induced proliferation, and that context-dependent effects are elicited in different sub-populations of the silenced cells. In fact, some cells undergo apoptosis, whereas those surrounding the apoptotic foci, although identically depleted, overproliferate. This overproliferation correlates with ectopic induction of the Wg and JAK-STAT (Janus kinase-signal transducer and activator of transcription) mitogenic pathways. Expression of a p35 transgene, which blocks the complete execution of the death program and generates the so-called 'undead cells', amplifies the proliferative response. Pseudouridine synthase depletion also causes loss of apicobasal polarity, disruption of adherens cell junctions and ectopic induction of JNK (c-Jun N-terminal kinase) and Mmp1 (matrix metalloproteinase-1) activity, leading to a significant epithelial reorganization. Unexpectedly, cell-nonautonomous effects, such as epithelial mesenchymal transition in the contiguous unsilenced squamous epithelium, are also promoted. Collectively, these data point out that cell-cell communication and long-range signaling can take a relevant role in the response to pseudouridine synthase decline. Considering that all the affected pathways are highly conserved throughout evolution, it is plausible that the response to pseudouridine synthase depletion has been widely preserved. On this account, our results can add new light on the still unexplained tumor predisposition that characterizes X-linked dyskeratosis, the human disease caused by reduced pseudouridine synthase activity. *Cell Death and Disease* (2015) 6, e1705; doi:10.1038/cddis.2015.68; published online 26 March 2015

The control of cell growth and proliferation is a fundamental aspect of tissue homeostasis. To maintain homeostatic conditions, different subsets of cells are continuously required to respond coordinately to external and intrinsic stimuli, to keep the appropriate balance between death, proliferation and differentiation.

The overall capacity of the protein synthetic machinery has an obvious rate-limiting regulatory role in cell growth and division, and production of ribosomes is directly coupled with these processes. Moreover, in a growing number of cases mutations in ribosome components proved to regulate not only the overall translational capacity but also to affect specific developmental or differentiative events, revealing more specialized functions in translational regulation.^{1,2} Mutations in factors that allow synthesis, processing and modification of rRNA, assembly and nuclear export of preribosomal particles or ribosome translational efficiency also cause tissue- or cell-specific phenotypes and produce a variety of diseases,

collectively indicated as ribosomopathies.³ Eukaryotic rRNA pseudouridine synthases are among these factors. These ubiquitous nucleolar proteins are conserved from Archaea to man and associate with other conserved core proteins and H/ACA small nucleolar RNAs (snoRNAs) to compose the functional H/ACA snoRNP complexes, whose activity is known to be involved in rRNA processing and site-specific pseudouridylation of rRNA and snRNAs,⁴ as well as of mRNAs and additional classes of noncoding RNAs.⁵

Well-established, rRNA undergoes extensive modifications that influence its processing, folding and functionality. For example, reduction of rRNA pseudouridylation affects ribosome translation fidelity⁶ and modulates the efficiency of internal ribosome entry site-dependent translation,^{7–10} outlining a crucial role in the regulation of translation specificity. The high biological relevance of rRNA pseudouridine synthases is further testified by the fact that reduced levels or hypomorphic mutations in the human coding gene

¹Dipartimento di Biologia, Università di Napoli 'Federico II', via Cinthia, Naples 80126, Italy; ²Stazione Zoologica Anton Dohrn, Villa Comunale, Napoli 80121, Italy and ³Institut für Genetik, Universität Hohenheim, Garbenstrasse 30, Stuttgart 70599, Germany

*Corresponding author: M Furia, Dipartimento di Biologia, Università di Napoli 'Federico II', via Cinthia, Naples 80126, Italy. Tel. +39 081 679072; Fax +39 081 679233; E-mail: mfuria@unina.it

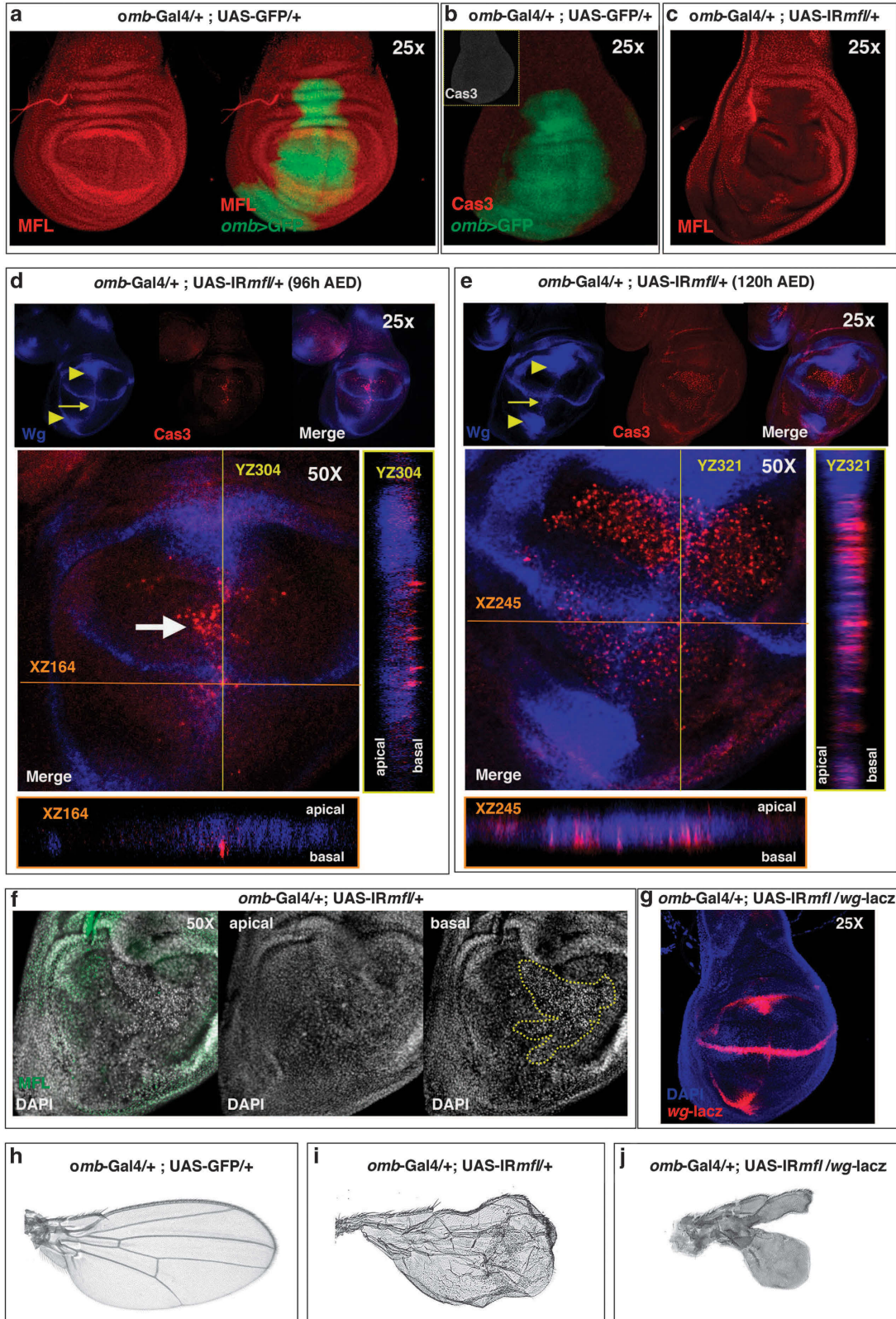
⁴These authors contributed equally to this work.

Abbreviations: H/ACA snoRNP, H/ACA box small nucleolar ribonucleoprotein; snoRNA, small nucleolar RNA; X-DC, X-linked dyskeratosis congenita; Omb, optomotor blind; En, engrailed; Dpp, decapentaplegic; Wg, Wingless; Arm, Armadillo/ β -catenin; Cas3, caspase-3; pH3, phosphohistone H3; EdU, 5-ethynyl-2'-deoxyuridine; JAK-STAT, Janus kinase-Signal Transducer and Activator of Transcription; JNK, c-Jun N-terminal kinase; Puc, puckered; Mmp1, matrix metalloproteinase-1; Ubx, ultrabithorax; EMT, epithelial–mesenchymal transition

Received 20.10.14; revised 11.2.15; accepted 12.2.15; Edited by N Tavernarakis

cause the human X-linked dyskeratosis (X-DC) multisystemic disorder.¹¹ Beside H/ACA snoRNPs, the human pseudo uridine synthase, called dyskerin, is also a component of the

active telomerase complex; this dual role makes it difficult to distinguish between the effects related to loss of snoRNP functions and those caused by telomere attrition. As a



consequence, whether X-DC must be regarded primarily as a ribosomopathy or as a telomere disease is still being debated. Considering the availability of sophisticated genetic tools, *Drosophila melanogaster* can represent an advantageous model organism to dissect the multiple roles played by pseudouridine synthases. *Drosophila dyskerin* is 66% identical and 79% similar to human dyskerin, and is equally involved in rRNA processing and pseudouridylation;¹² however, it has no established role in the maintenance of telomere integrity, as fly telomeres are maintained by insertion of specific retrotransposons at chromosome ends.¹³ This divergent procedure of telomere maintenance makes *Drosophila* an ideal organism to delineate the range of biological effects specifically triggered by loss of H/ACA snoRNP activity, especially focusing at the interface among cell growth, proliferation and differentiation. Because of their striking capacity of undergoing regenerative growth,¹⁴ the imaginal wing disc provides an ideal system in which to investigate how growth, proliferation and differentiation are coordinated in the context of a developing organ. In fact, cell proliferation is essentially uniform across the whole disc¹⁵ and is controlled by the same morphogens that govern wing patterning. Gradients of two morphogens, decapentaplegic (Dpp), a member of the transforming growth factor- β family, and wingless (Wg), a member of the Wnt family, establish a tight link between cell proliferation and developmental programs. During disc development, a gradient of Dpp determines the anterior/posterior (A/P) axis, whereas a gradient of Wg subsequently defines the dorsal/ventral (D/V) axis, giving rise to the A/P and D/V compartments.¹⁶ We previously showed that localized depletion of *Drosophila dyskerin* in the wing discs not only caused cell death but also additionally triggered a variety of developmental defects.¹⁷ Here, we further investigated the role of *Drosophila dyskerin* in wing disc homeostasis and demonstrate that its loss can induce regenerative growth and extensive tissue remodeling, as well as stimulate cell-nonautonomous events of cell fate changes that result in epithelial–mesenchymal transition (EMT).

Results

Effect of *mfl* silencing on wing growth and patterning.

Drosophila dyskerin, called Mfl, is encoded by the *Nop60B/minify (mfl)* gene.^{12,18,19} To define in more detail how Mfl loss can affect growth and development, we silenced Mfl activity in

the area of the wing disc that flanks the A/P border and includes the main organization center of patterning. Gene silencing made use of the Gal4/UAS system²⁰ and was directed by the *omb* (optomotor blind)-Gal4 driver line, which is expressed in the wing central domain from between presumptive veins 1 and 2 in the A compartment to presumptive veins 4 and 5 in the P compartment.²¹ Two different UAS-*IRmfl* target lines were used (v46282 and no. 36595); both lines had no predicted off-targets and gave identical results. The v46282 line already proved to knock down efficiently all *mfl* mRNAs.¹⁷ The effects of *mfl* silencing were then carefully followed within the *omb* domain of silenced discs (Figures 1a–c). Discs were collected at two developmental times during the third larval instar, that is, at 96 and 120 h after egg deposition (AED), and costained with anti-caspase-3 (Cas3) to follow cell death and with anti-Wingless (Wg) to monitor wing patterning and growth. Control discs at 96 h AED did not show any significant Cas3 staining (Figure 1b), whereas clusters of Cas3-positive cells arised along the A/P boundary in the silenced discs (Figure 1d), confirming that cell death is a major consequence of *mfl* downregulation.¹⁷ However, in the same discs Wg was strongly upregulated at the center of the inner ring, in both D and V compartments, and ectopically expressed along the A/P boundary (Figure 1d). At the later developmental time (120 h AED), the number of Cas3 spots further increased, massively spreading from A/P border throughout the wing pouch. In parallel, Wg accumulation at the inner ring became more conspicuous (Figure 1e). As shown by confocal Z-stack analysis, Wg staining at the D/V border flanked the Cas3 apoptotic signals, most of which were located more basally (Figures 1d and e). The presence of dying cells was further confirmed by a large number of pyknotic nuclei detected basally in the pseudostratified epithelium (Figure 1f). To mark precisely the cells that were actively producing the Wg proliferative signal, we followed the expression of the *wg-lacZ* transcriptional reporter. Activity of the reporter increased in the silenced background, and stained the same areas previously marked by Wg accumulation (Figure 1g). This observation confirmed that the silenced cells surrounding the apoptotic foci were actively producing high level of Wg. Ectopic secretion of Wg at the edge of the dying tissue has been reported by several authors,^{22–24} and in some cases has been described to be essential for regenerative growth.²⁴ Consistent with this view, we noticed that most of the silenced larvae carrying the *wg-lacZ* reporter died at the pupal stage,

Figure 1 Mfl depletion induces both Cas3 and Wg activation in the wing discs. (a–g) Confocal analysis of control and *omb > IRmfl* silenced wing discs (v46282 line). (a) Ubiquitous expression of Mfl protein (in red) in an *omb > GFP* control disc, in which GFP (green) marks the *omb* expression domain. (b) Cas3-positive spots are not present in the *omb > GFP* controls. GFP in green and Cas3 in red (gray in the inset). (c) An *omb > IRmfl* silenced disc showing efficient and localized Mfl depletion within the *omb* domain (Mfl in red). (d and e) *omb > IRmfl* discs collected at 96 h (d) and 120 h AED (e). At 96 h AED, clusters of Cas3-positive spots mark the A/P boundary (white arrow), flanked by Wg ectopic induction (see yellow arrow at the top); Wg accumulates also at the middle of the inner ring (see yellow arrowheads on the top). At 120 h AED, the number of Cas3-positive spots increased, concomitantly with Wg ectopic induction along the A/P border (see yellow arrow at the top) and Wg upregulation at the inner ring (see yellow arrowheads at the top). Z-stack confocal analysis showed that most Cas3 signals lie basally and do not overlap Wg staining (see XZ and YZ projections). Cas3 in red and Wg in blue. (f) DAPI (4',6-diamidino-2-phenylindole) staining of an *omb > IRmfl* disc shows basal clusters of pyknotic nuclei within the silenced domain (area encircled by the yellow line); DAPI is in gray and Mfl in green. (g) Expression of *wg-lacZ* reporter in *omb > IRmfl* silenced discs confirms that *wg* expression is transcriptionally upregulated compared with controls (see Figure 4d) and marks the same areas where Wg protein accumulates (DAPI in blue and β -gal in red). (h–j) Comparison of an *omb > GFP* adult wing, taken as control (h), with an *omb > IRmfl* silenced wing, whose blade appears crumpled and highly disorganized (i), and an *omb > IRmfl;wg-lacZ* wing (j), in which Wg haploinsufficiency strongly enhances the growth defects (see also Supplementary Figure 1)

whereas rare adult escapers all display underdeveloped/deformed wings that miss the central *omb* domain (Figures 1h–j and Supplementary Figure 1). As the *wg-lacZ* allele is mutant owing to the *lacZ* insertion,²⁵ silenced larvae carrying this allele have only one active copy of the *wg* gene. With respect to *mfl* silencing alone, which led to disturbed wing morphology with detachment of the two epithelial layers and blistering, the heterozygous *wg* background markedly worsened the silenced phenotype (Figures 1h–j and Supplementary Figure 1). This enhancement is consistent with a dose effect, and suggests that the level of *wg* activation in these silenced flies is inadequate to counteract the developmental defects caused by Mfl depletion.

Finally, we analyzed by phalloidin staining the structure of the silenced disc. As shown in Figure 2, the tissue appeared wrinkled, folded and fractured along the A/P border, where clusters of Cas3-positive cells were observed. These local fractures were strongly enhanced in the presence of an UAS transgene that expresses the baculovirus p35 protein, known to inhibit the function of Cas3 but not its activation.^{26,27} UAS-p35 expression has no effect on the epithelium structure in a wild-type background (Figure 2a), whereas in the silenced discs it generates along the A/P margin patches of large ‘undead cells’ that, as typical,²⁸ secrete high levels of Wg (Figures 2b and c). The alignment of undead cells along the A/P boundary indicated that these margin cells exhibit a particular sensitivity to Mfl depletion, and first undergo apoptosis. This susceptibility may be an indirect consequence of abnormal formation of the A/P border, possibly due to defects in cell adhesion and/or cell communication.

***mfl* Silencing elicits context-dependent effects and apoptosis-induced proliferation.** A proliferative role has generally been attributed to Wg in regenerative phenomena.²⁹ Indeed, we noticed that at both 96 and 120 h AED the silenced discs exhibited morphological alterations in shape, including an evident bending of the A/P boundary that was indicative of localized overgrowth (see Figure 1 and Supplementary Video 1).

In previous experiments, we triggered *mfl* silencing by the *en-Gal4* (engrailed-Gal4) driver, whose expression specifically marks the P compartment. Despite the induction of apoptosis, no reduction in the number of phosphohistone H3 (pH3)-positive mitotic cells was noted in the silenced domain.¹⁷ To further check this aspect, we stained the *en-Gal4* silenced discs by EdU (5-ethynyl-2'-deoxyuridine) incorporation, to mark with higher sensitivity DNA synthesis and label S-phase cells. This approach highlighted a significant enhancement of the proliferative activity in the silenced P compartment (Figure 3a). According to the previous data,¹⁷ the A/P boundary was discontinuous and deformed and, upon p35 expression, undead cells that overexpress Wg were detected close to this irregular border (Figure 3b). Note that these cells are located basally, whereas Wg upregulation at the A/P margin is detected only apically.

Enhanced proliferative activity was similarly observed in the *omb* silenced domain. In fact, despite the massive apoptosis (see Figure 1), the overall proliferation rate was not reduced. pH3-positive dividing cells were visualized inside and around Wg-secreting regions, and their number markedly augmented upon p35 expression (Supplementary Figure 2). Consistent with this observation, EdU labeling of S-phase cells was markedly enhanced with respect to controls, and even further by p35 expression (Figures 4a and c; note that in the silenced discs the *omb* domain is expanded and bent). Reliably, upon UAS-p35 expression the rare adult escapers develop wings typified by epithelial refolding, as it occurs upon excessive and hyperplastic overgrowth (Supplementary Figure 3).

Proliferation of the silenced cells also correlated with upregulation and ectopic induction of JAK-STAT, another proliferative pathway associated with apoptosis-induced proliferation and regeneration.^{30,31} As shown in Figure 5, this pathway is upregulated at the center of the inner ring, and ectopically activated at specific regions of the silenced domain. In the V compartment, its induction surrounded the areas showing Wg accumulation, whereas in the dorsal part it encircled and in part overlapped Wg ectopic expression. Altogether, these data indicate that Mfl depletion induces a regenerative response,

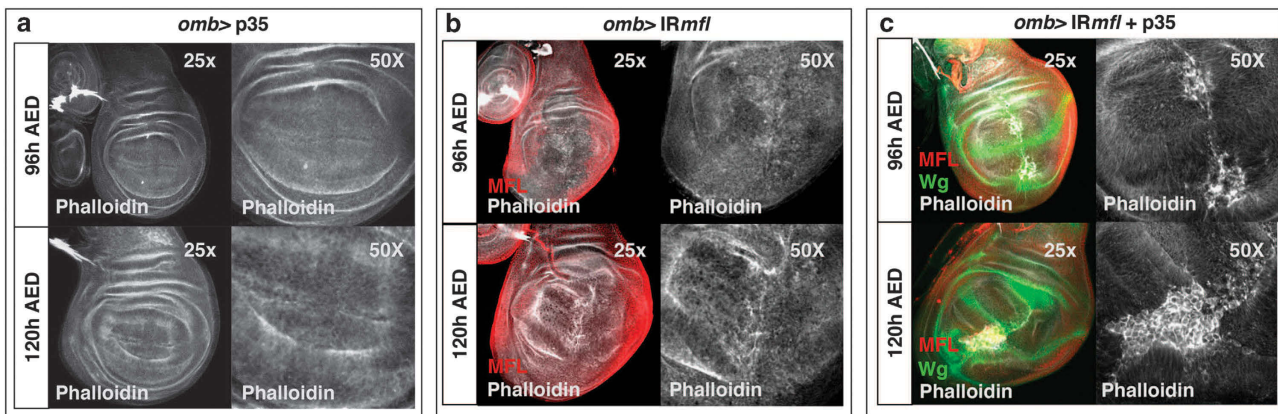


Figure 2 Epithelial remodeling and formation of p35-induced undead cells in the *omb* silenced domain. Confocal analysis of wing discs at 96 and 120 h AED upon phalloidin staining. (a) An *omb* > p35 control disc. Phalloidin is in gray. (b) An *omb* > *IRmfl* silenced disc (no. 36595 line) exhibiting a strong tissue disorganization. Phalloidin is in gray and Mfl in red. (c) Expression of p35 in the silenced discs causes formation of big patches of large undead cells that secrete high level of Wg (in green) and cluster along the A/P border

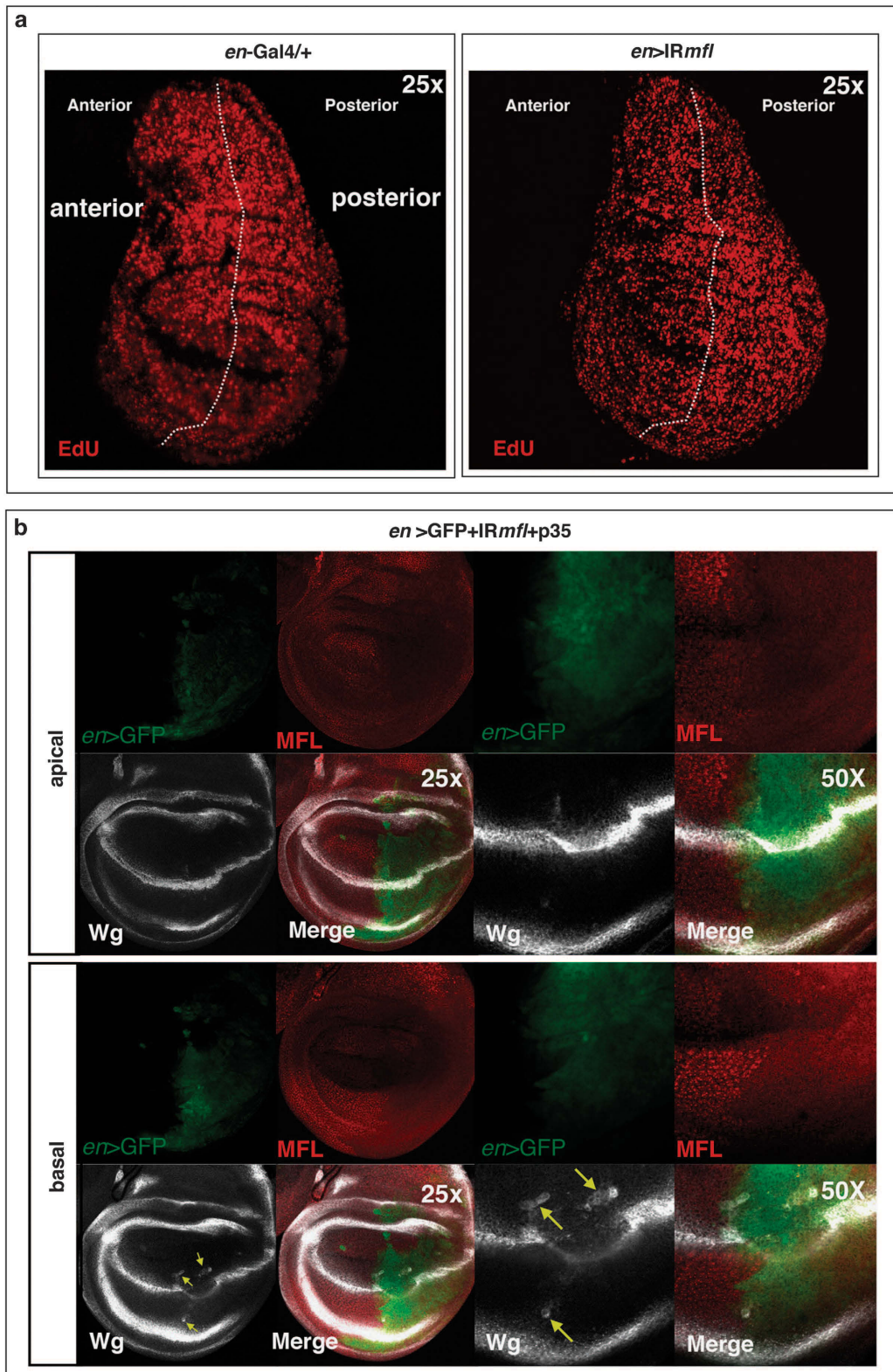


Figure 3 Enhanced proliferation and formation of p35-induced undead cells in the silenced P compartment. Confocal analysis of wing discs at 96 h AED. (a) On the left, an *en/+* control disc, in which EdU labeling marks S-phase cells; on the right, an *en > IRmfl* silenced discs (v46282 line) in which EdU labeling stains more intensely the P silenced compartment, indicating that the silenced cells overproliferate. The A compartment serves as internal control. (b) Expression of p35 causes formation of undead cells that secrete high level of Wg (in gray) and are dispersed along the irregular A/P border. Note that Wg accumulation at the D/V boundary is detected apically, whereas deformation of the A/P margin is more evident basally, in keeping with previous data¹⁷

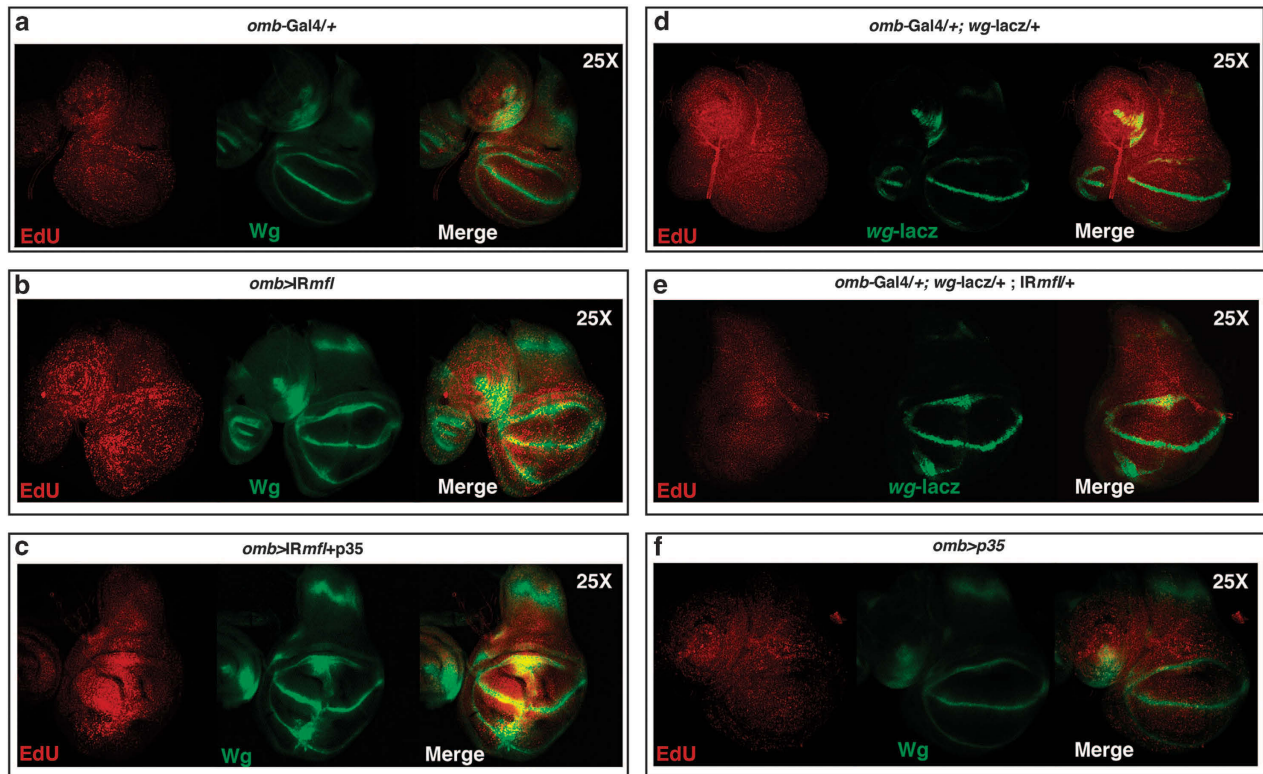


Figure 4 *mfl* Silencing causes apoptosis-induced proliferation. Confocal analysis of wing discs at 96 h AED. (a) An *omb*^{-/-} control disc labeled by EdU incorporation to mark specifically DNA synthesis and label S-phase cells. (b) An *omb* > *IRmfl* silenced disc (no. 36595 line) showing a significant increase of proliferating cells. (c) P35 expression further boosts proliferation and elicits a more pronounced hyperplastic overgrowth. EdU is in red and Wg in green. (d and e) EdU labeling of *omb*^{-/-}, *wg-lacZ* (d) and *omb* > *IRmfl*, *wg-lacZ* discs (e), both carrying a single active copy of the *wg* gene (β -gal is in green). Note that in the *wg-lacZ* background the proliferative activity of the silenced domain is significantly reduced compared with that of *omb* > *IRmfl* discs (b). (f) Expression of p35 in unsilenced discs has no effect on the proliferation rate (Wg in green)

which, as observed in other cases,³² in the presence of p35 results in a pronounced hyperplastic phenotype.

Intriguingly, the emerged scenario pointed out that Mfl depletion elicits opposite outcomes in diverse wing territories. Although some cells (those at the A/P boundary first) activate Cas3 and undergo apoptosis, other silenced cells undergo robust proliferation.

The silenced discs show extensive epithelial remodeling and JNK and Mmp1 ectopic activation. As shown above, the silenced discs appeared crumpled and folded (Figure 1 and Supplementary Video 1), indicating the occurrence of extensive tissue reorganization and remodeling. As regenerative processes require widespread tissue restoration, we followed in detail the expression of two typical markers of epithelial restructuring: the apicobasal distribution of the *Drosophila* β -catenin/Armadillo (Arm) and the levels of polymerized F-actin. Within the wing discs, Arm and F-actin are ubiquitously expressed, but they are both strongly stabilized in two stripes surrounding the D/V boundary.^{33,34}

The Arm protein is a known effector of Wg signaling and has a dual role: as a component of the cell adherens junctions on the one hand and as a nuclear transcription factor transducing Wg signal on the other hand.³⁵ Within the wing disc, Arm concentrates apically, in which it binds transmembrane cadherins to build up the adherens junctions that connect actin filaments across polarized epithelial cells³⁶

(see Figure 6a). Interestingly, upon *mfl* silencing directed by *en*-Gal4, Arm accumulation was strongly reduced in the whole silenced area, and most evidently at the D/V boundary. Moreover, confocal Z-stack analysis revealed a reduction of apical Arm accumulation, so that cells had lost their polarity (Figure 6b). Identical results were obtained when silencing was directed by the *omb*-Gal4 driver (Supplementary Figure 4). Reduction of apical Arm is consistent with the observation that Wg overexpression in the wing discs induces a transient reduction of membrane-associated Arm, this way allowing an immediate decline of cell adhesion that facilitates structural reorganization of the cytoskeleton.³⁷ Similarly to Arm, F-actin accumulation was also heavily reduced, and accumulation at the D/V boundary disrupted (Figures 6c and d and Supplementary Videos 2 and 3). Hence, the concomitant induction of cell death and proliferation is accompanied by extensive cytoskeletal remodeling. The involvement of pseudouridine synthase activity in cytoskeletal dynamics and cell adhesion is worth noting, and it has previously been described also in human cells.³⁸

Given that the JNK pathway is known to be involved in cytoskeletal remodeling during both apoptotic^{39,40} and regenerative processes,^{41–45} we checked whether it was specifically induced upon Mfl depletion. We then followed the expression of *puckered* (*puc*), a JNK downstream effector,⁴⁶ taking advantage of the widely used *puc-lacZ* reporter. As described,⁴⁷ *puc-lacZ* expression in wild-type discs is

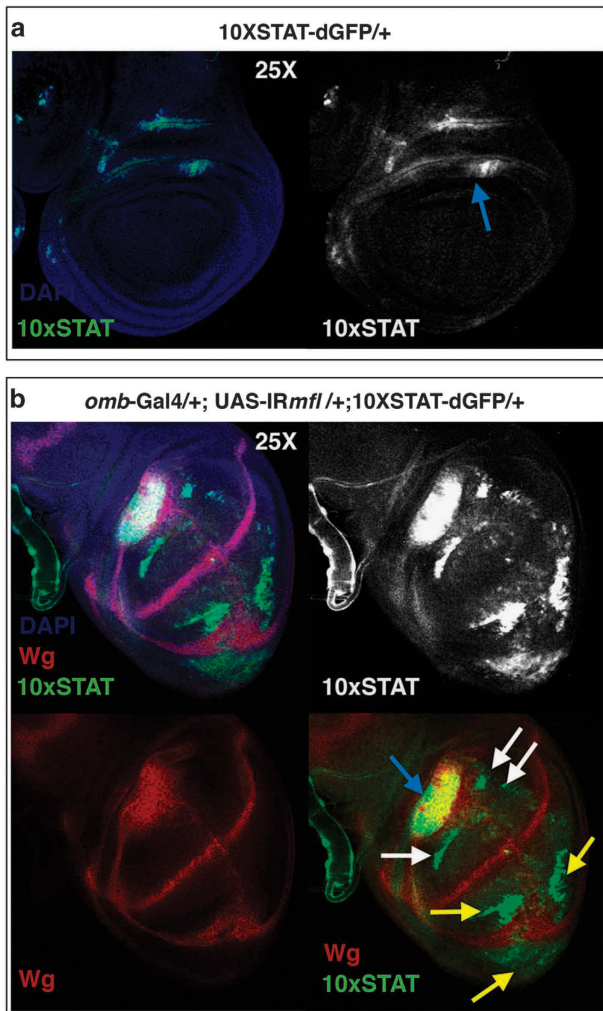


Figure 5 Mfl depletion triggers ectopic activation of JAK-STAT signaling. Confocal analysis of wing discs collected at 120 h AED carrying the 10XSTAT-dGFP reporter (the use of destabilized dGFP⁶⁹ allows to visualize real-time activation of the reporter). (a) No activity of the reporter was detectable in the wing pouch of control discs, whereas JAK-STAT expression is detected in the presumptive wing hinge (blue arrow). (b) In *omb > IRmfl* silenced discs (v46282 line in the picture), the reporter was overexpressed in the wing hinge (blue arrow) and ectopically induced in the dorsal area of the *omb* domain (white arrows), where it, in part, surrounded and overlapped the domain of Wg induction. In the ventral region (yellow arrows), JAK-STAT ectopic induction encircled Wg accumulation. DAPI (4',6-diamidino-2-phenylindole) is in blue, Wg in red and GFP in green

restricted to the stalk region, where wing discs are connected to the larval epidermis (Figure 7a). In contrast, expression of this reporter was found strongly induced within the silenced discs (Figure 7b). Along the A/P border, JNK ectopic induction matched the local clusters of pyknotic nuclei, suggesting that it resulted in a local cell death. However, in the ventral regions it overlapped the areas of Wg accumulation, suggesting that in these regions JNK activity could instead promote proliferation, in keeping with the dual role recently suggested for this pathway.⁴⁵ JNK also has a well conserved role in the induction of Mmps that degrade the extracellular matrix and are strongly expressed during regeneration.^{48,49} Specifically, *Drosophila* Mmp1 is directly involved in re-epithelialization after wound healing, remodeling of the basement membrane and

cytoskeletal reorganization.^{50,51} Not surprisingly, Mmp1 was strongly induced along the A/P border and ventrally, where it matched the area of Wg overexpression at the middle of the inner ring (Figures 7c and d).

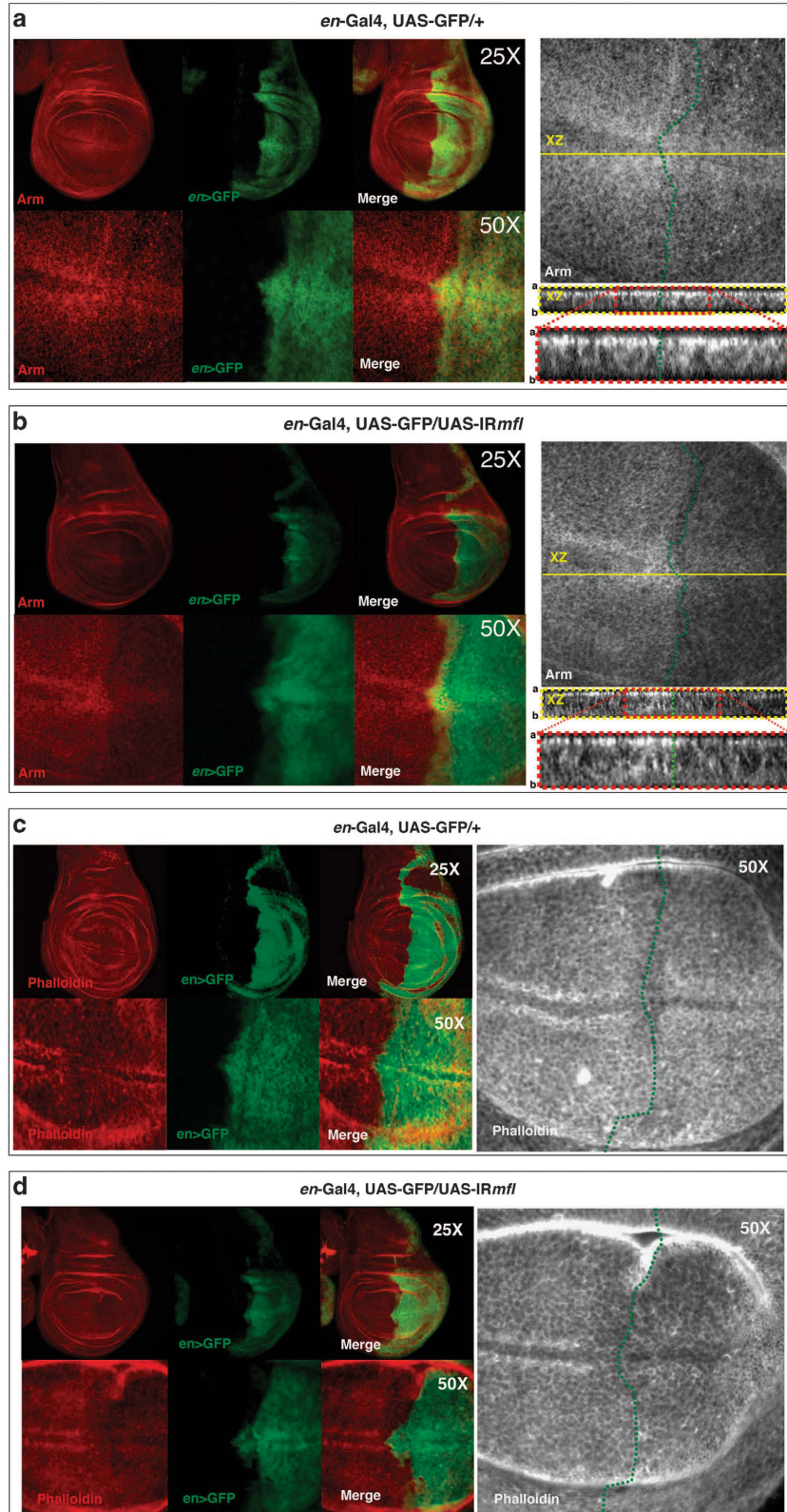
Mfl depletion promotes EMT in a cell-nonautonomous manner.

The concomitant occurrence of Wg overexpression, reduction of adherens junctions, loss of apicobasal polarity, JNK and Mmp1 induction raised the intriguing possibility that Mfl depletion could also trigger changes in cell fate, and possibly give rise to EMT. EMT occurs in many developmental events but, if induced by pathological conditions, can lead to tumourigenesis.⁵² As X-DC is characterized by a still unexplained susceptibility to malignancy, the possibility that pseudouridine synthase depletion could trigger EMT was of great interest. We thus stained the silenced discs with an antibody directed against Twist, a typical marker for mesenchymal cells known to be involved in EMT.^{53,54} Twist is expressed in presumptive mesodermal cells and not in epithelia,⁵⁵ and thus no disc cell was expected to be positively stained. Intriguingly, patches of Twist-positive cells were instead detected in about 95% of the silenced discs (Figure 8a). These cells also ectopically expressed Cut, an additional marker of myoblasts,^{55,56} further confirming the acquisition of mesoderm identity and the occurrence of EMT. Surprisingly, Z-stack confocal analysis lead to locate these myoblasts within the peripodial membrane, that is, the overlying squamous epithelium that lies outside the *omb* expression domain and thus was not silenced (Figure 8b). Note that, as awaited, Cut-positive cells are never present in the peripodial membrane of control discs (Supplementary Figure 5). We then wondered whether the observed myoblasts originated from the underlying silenced epithelium and then migrated above or, alternatively, directly arose from the unsilenced tissue. To investigate this aspect, we performed a lineage-tracing experiments by using the G-TRACE system, which is based on the expression of a pair of GFP-RFP Stinger reporters.⁵⁷ In this system, cells that had a previous Gal4-dependent activation of the GFP reporter, even if transient, remain GFP-labeled; conversely, cells showing only an active real-time expression of the Stinger vector become RFP-labeled. In our experiments, Twist/Cut-positive cells were never GFP- or RFP-labeled, clearly indicating that they were not expressing the *omb*-Gal4 driver nor activated it at any previous developmental stage (Figure 8c). This result confirmed that these cells derive from the peripodial membrane. To learn more, we used an anti-Ubx antibody that marks the majority of peripodial cells.^{58,59} Intriguingly, the Twist/Cut-positive cells faintly expressed also Ubx, indicating that they are in a state of cell fate transition (Figure 8d). This result ruled out also the possibility that these myoblasts could derive from the ad epithelial cells abutting the wing disc in the notum region, as those myoblasts do not express Ubx.⁵⁸ EMT in the peripodial membrane was identically induced in a different *mfl* silencing line (no. 36595; Supplementary Figure 6), confirming the occurrence of cell-nonautonomous fate changes.

Discussion

In *Drosophila* wing discs, cell death provoked by a variety of approaches, including disc transplantation, exogenous

injuries or localized induction of proapoptotic genes, can induce regenerative growth.⁶⁰ In response to death, neighboring cells are stimulated to proliferate and reconstitute tissue loss,



a process defined as apoptosis-induced proliferation.^{28,61,62} Here we show that the level of expression of pseudouridine synthase is crucial for tissue homeostasis and that its local reduction triggers apoptosis-induced proliferation, as typically observed during regeneration.⁶³ This regenerative stimulus is enhanced by blocking the execution of death by p35 expression, which, as occurring after several different types

of tissue injuries, elicits hyperplastic overgrowth.⁶⁴ As both apoptotic and proliferating cells are identically Mfl-depleted, our results outlined an unexpected context-dependent effect of pseudouridine synthase level. Possibly, as a consequence of their differentiation status, different cell sub-populations respond in a reverse manner to lessening of this enzyme: those more susceptible undergo apoptosis, whereas others

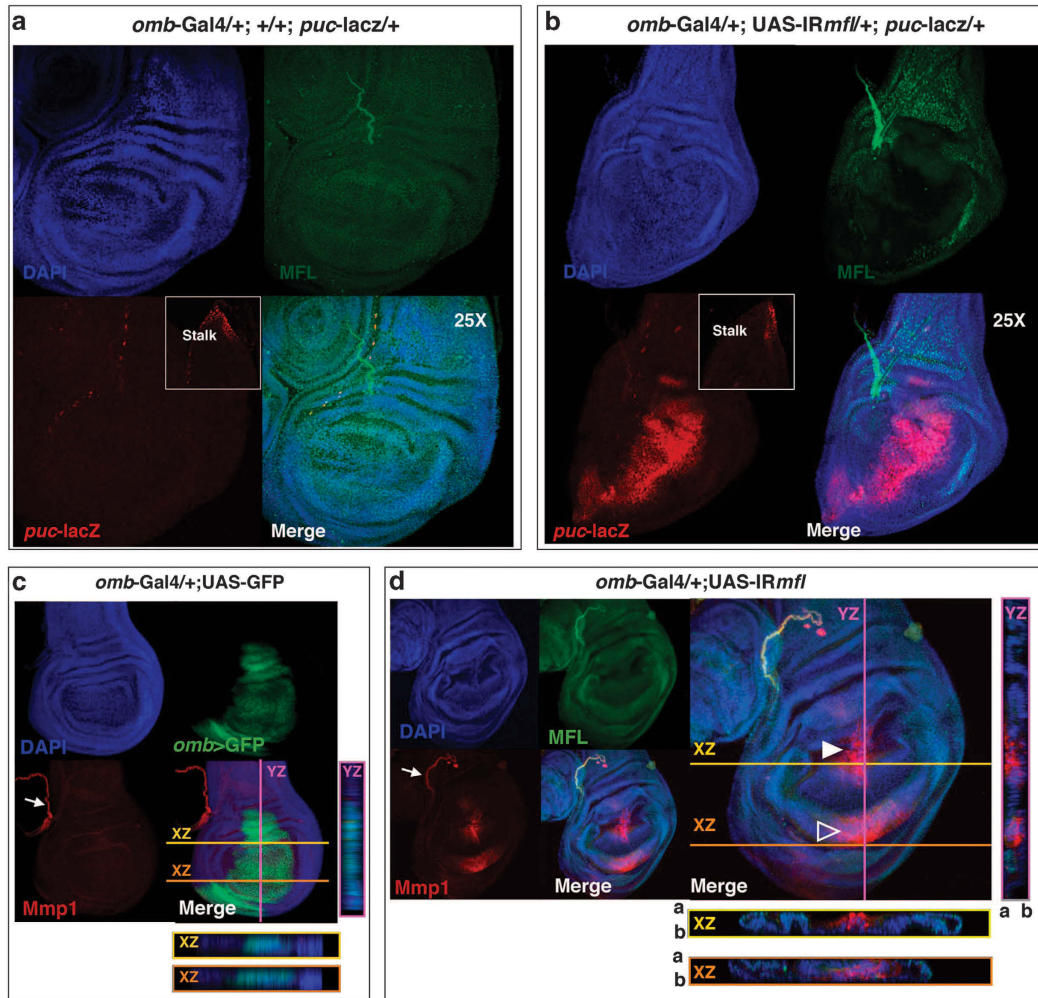
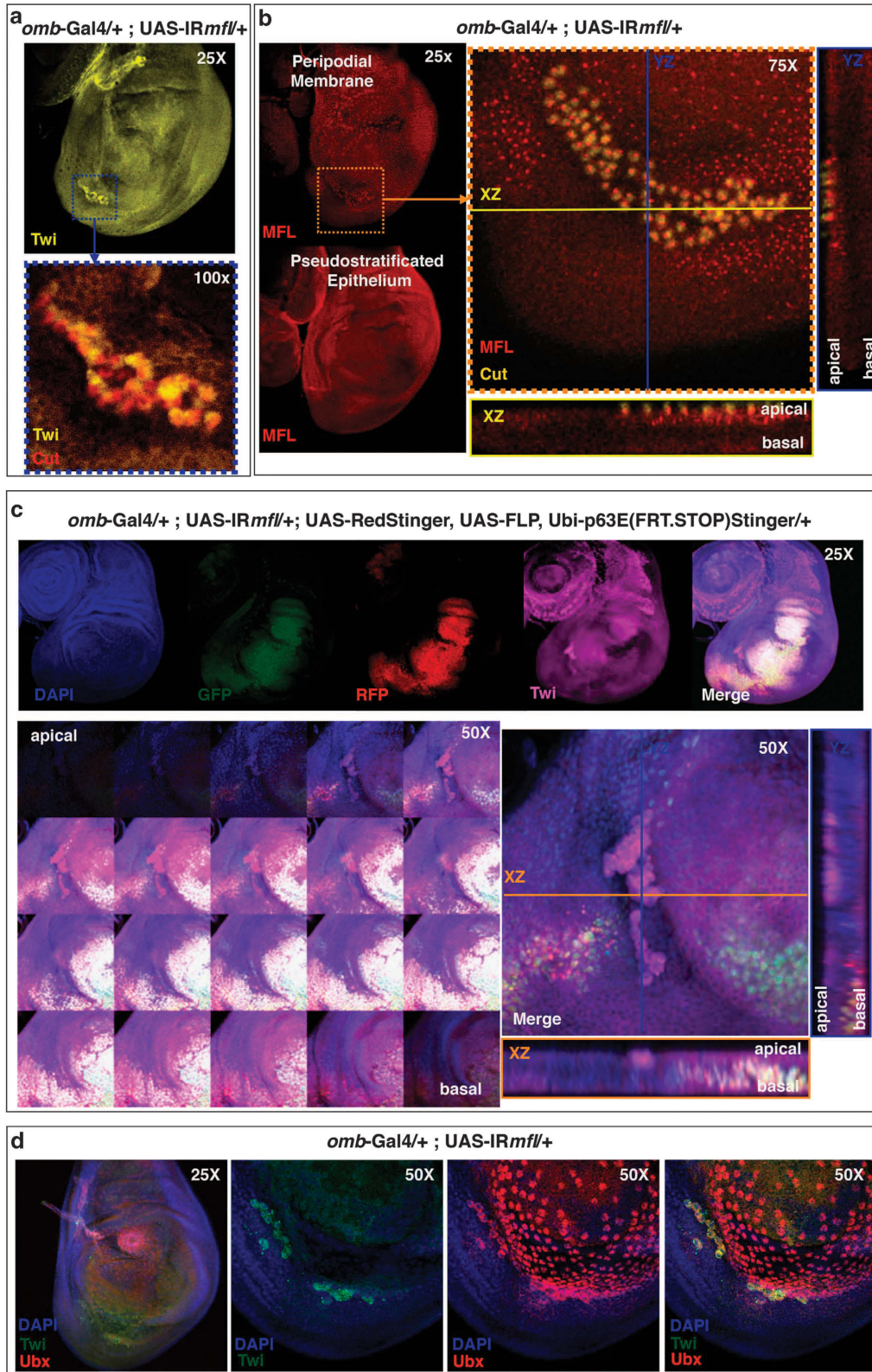


Figure 7 Mfl depletion induces JNK and Mmp1 ectopic activation. Confocal analysis of wing discs collected at 120 h AED. (a) In *omb*> *puc-lacZ* control discs, activation of the JNK pathway, marked by the *puc-lacZ* reporter, is restricted to the stalk cells (inset) and to some dispersed cells.⁴⁷ (b) In *omb*> *IRmfl*; *puc-lacZ* silenced discs (v46282 line in the picture), JNK is ectopically and strongly activated. In (a and b), DAPI (4',6-diamidino-2-phenylindole) is in blue, Mfl in green and β -gal in red. (c) Mmp1 expression in *omb*> GFP control discs marks the trachea (arrow) and the stalk cells (not in frame), where it overlaps *puc-lacZ* expression. Z-stack analysis (see XZ and YZ projections) confirms Mmp1 absence in the *omb* domain. (d) In *omb*> *IRmfl* silenced discs (v46282 line in the picture), Mmp1 is strongly and ectopically induced in the MFL-depleted domain; in the D compartment, Mmp1 enrichment flanks the A/P border (closed arrowhead) within the area of JNK activation (compared with b), whereas in the V compartment, Mmp1 concentrates in a small domain (open arrowhead) overlapping the Wg-expressing inner ring. In both areas, Z-stack analysis (see XZ and YZ projections) confirms Mmp1 active secretion within the silenced domain. DAPI is in blue; GFP (c) and Mfl (d) in green and Mmp1 in red. a, Apical; b, basal

Figure 6 Loss of Arm/ β -catenin apical localization and reduced F-actin accumulation in the silenced discs. Confocal analysis of wing discs collected at 120 h AED and stained with Arm antibody (in red or gray) or phalloidin (red or gray). (a) Localization of Arm protein in *en*> GFP control discs, in which GFP (green) marks the *en* posterior domain. Note that Arm is strongly concentrated in two stripes of cells adjacent to the D/V boundary, and Z-stack analysis (right panels) shows its uniform apical localization in both A/P compartments. (b) Localization of Arm in an *en*> *IRmfl* silenced disc (v46282 line). *mfl* silencing causes a strong reduction of Arm protein, with Z-stack analysis (right panels) demonstrating loss of apical localization (right panel). In a and b, green dots mark the boundary between the A and P compartments within the enlargements; red dots mark XZ projection enlargements. (c and d) Confocal analysis of wing discs stained with phalloidin. (c) In *en*> GFP control discs, F-actin concentrates in two stripes of cells adjacent to the D/V boundary. (d) In *en*> GFP; *en*> *IRmfl* silenced discs (v46282 line in the picture), F-actin accumulation is strongly reduced within the whole silenced domain, and particularly at the D/V margin. GFP is in green and phalloidin in red or gray. Green dots mark the A/P boundary. a, Apical; b, basal



hyperproliferate, acting as a blastema.²⁹ This dual effect also establishes for the first time that pseudouridine synthase depletion *per se* does not hamper proliferation, as generally considered; on the contrary, under mitogenic stimuli the

depleted cells are able to overproliferate vigorously. This finding further supports the view that this enzyme has a more specialized than a general effect on ribosome functionality.

Figure 8 Mfl depletion promotes EMT in the contiguous peripodial membrane. Confocal analysis of wing discs collected at 120 h AED. (a) An *omb* > *IRmfl* silenced disc (v46282 line) costained with anti-Twist (on the top) and anti-Cut antibodies, showing an islet of double positive cells (enlargement at the bottom; Twist is in yellow and Cut in red). (b) Z-stack images captured at different planes show that the Twist-Cut-positive islet lies apically, in the peripodial membrane. As this membrane is not included in the *omb* silenced domain, these cells were actively accumulating the Mfl protein within their nucleoli; conversely, cells of the underlying silenced pseudostratified epithelium are efficiently depleted (Mfl in red and Cut in yellow). (c) G-TRACE experiments in which the *omb* silenced domain was labeled by GFP and RFP expressed by UAS-Stinger vectors and stained with DAPI (4',6-diamidino-2-phenylindole) and Twist antibody (top panel). In the middle, Z-stack images captured at different focal planes (left) and orthogonal projections (right). Note that Twist-positive cells (in magenta) remain fully unstained by both GFP and RFP and lie apically, within the peripodial membrane. DAPI is in blue, GFP in green, RFP in red and Twist in magenta. (d) Twist-positive cells faintly express also Ubx, a typical marker of the peripodial membrane, indicating that they are in a state of fate transition. DAPI is in blue, Twist in green and Ubx in red. Twi, Twist

As described in regenerative processes, massive epithelial remodeling occurs in the silenced tissue. Loss of Arm apical localization, reduction of F-actin polymerization and JNK and Mmp1 ectopic activation, altogether converged to underscoring cytoskeletal rearrangement dynamics and massive epithelium reorganization. In our experiments, the sustainment of the proliferative activity correlates with the activation of Wg and JAK-STAT mitogenic pathways, both of which are found ectopically induced in the depleted areas. However, the Wg signal was actively produced not only by the apoptotic but also by surrounding cells, where it partially overlapped with JAK-STAT ectopic induction. These features suggest the involvement of long-range intercellular signaling in response to pseudouridine synthase depletion. Indeed, an interesting conclusion that can be drawn by our experiments is that cell-cell communication is likely to have a key role in the pseudouridine synthase loss-of-function phenotype. This conclusion is further supported by the striking discovery that depletion of *Drosophila* dyskerin can trigger cell fate changes in a cell-nonautonomous manner. Unexpectedly, in response to Mfl silencing, EMT occurs in the adjacent unsilenced peripodial membrane, where groups of cells exhibited ectopic expression of myoblast markers. Considering the pivotal role played by EMT in development, regeneration and stem cell behavior,⁶⁵ this result is of utmost importance. Moreover, it emphasizes the important role of dyskerin, which is also reflected by extensive consequences of its depletion on many processes during fly development.¹⁷ Indeed, the regenerative growth described here is likely to reflect a general intrinsic homeostatic mechanism occurring in the context of physiological metabolic perturbation. In developing tissues, a local decrease in the amount of pseudouridine synthase, or in its activity, can occur stochastically or be caused by developmentally or metabolically regulated processes. Our results show that such variations can act not only as an apoptotic trigger but also as a regenerative stimulus, and thus nicely fit with the general observation that a tight control of the level of this enzyme is crucial in human cultured cells⁶⁶ and developing organisms as well.^{4,17}

Collectively, the effects observed upon Mfl depletion all converge to make the tumor predisposition observed in the X-DC patients⁶⁷ much easier to understand. Indeed, considering the high degree of conservation of all the pathways affected by Mfl reduction, we foresee that the core wiring diagram of pseudouridine synthase tasks might be conserved between flies and mammals. We surmise that *in vivo* experimental approaches in this animal model may help to better define the wide range of biological processes that interlace with these multifunctional proteins, and that perturbation of cell-cell

interactions, so far largely ignored in the studies of X-DC pathogenesis, may represent a relevant aspect of the disease.

Materials and Methods

Fly stocks. Flies were raised on standard *Drosophila* medium at 25 °C. The *en-Gal4*, *omb-Gal4/FM7*, UAS-GFP/CyO, 10XSTAT92E-dGFP/TM6C, *puc-lacZ/TM3Sb*, UAS-2XEGFP, UAS-RedStinger, UAS-FLP, Ubi-p63E(FRT.STOP)Stinger and UAS-*IRmfl* (no. 36595) strains were obtained from the Bloomington Drosophila Stock Center at Indiana University (BDSC, Bloomington, IN, USA); UAS-*IRmfl* RNAi (v46282) was obtained from the Vienna Drosophila RNAi Center (VDRC, Vienna, Austria). *wg-lacZ/CyO* and UAS-*p35/TM3Sb* stocks were kindly provided by L Johnston (Columbia University, New York, NY, USA).

Mounting adult wings. Wings were removed from adult flies, dehydrated in 100% ethanol for 5 min and placed on a microscope slide to allow ethanol to evaporate. A small drop of Euparal Mounting Medium (Roth, Karlsruhe, Germany) was dropped onto the wing and a glass coverslip placed on top. Images were captured with a Spot digital camera and a Nikon E1000 microscope (Nikon Instruments Europe, Tokyo, Japan).

Immunofluorescence stainings. Wing discs were dissected, fixed and immunostained as described in Tortoriello *et al.*¹⁷ Antibodies used were as follows: customer rabbit polyclonal antibody against Mfl (Sigma-Aldrich Inc., St. Louis, MO, USA; dilution 1:100); mouse monoclonal antibodies against Wingless, Cut, Arm, Mmp1, β -galactosidase, ultrabithorax (Ubx; Hybridoma Bank, University of Iowa, Iowa City, IA, USA; dilution 1:50 anti-Wg, 1:100 anti-Cut, 1:50 anti-Arm, 1:50 anti-Mmp1 mixture of 5H7B11, 3B8D12 and 3A6B4, 1:250 anti- β -Gal and 1:50 anti-Ubx); rabbit polyclonal antibody against Twist (Yin *et al.*,⁶⁸ dilution 1:50; gift from M Frasch); rabbit polyclonal antibodies against pH3 and cleaved Cas3 (Cell Signaling Technology, Danvers, MA, USA; dilutions 1:100 anti-pH3 and 1:500 anti-Cas3). Fluorescent secondary antibodies were from Jackson ImmunoResearch (Dianova, Hamburg, Germany) and used at a final dilution of 1:200. Rhodamine phalloidin conjugate for actin cytoskeleton staining were obtained from Molecular Probes (Eugene, OR, USA; dilution 1:250). Confocal images were obtained with a Bio-Rad MRC1024 (Bio-Rad, Munich, Germany) or Zeiss LSM510 (Carl Zeiss, Jena, Germany) confocal microscope.

Labeling of S-phase cells. For EdU immunohistochemistry, the Click-iT EdU Imaging Kit (Invitrogen, Carlsbad, CA, USA) was used. Discs were dissected and incubated in 10 μ M EdU in Ringer's for 20 min or 2 h and, following EdU labeling, fixed and immunostained as described in Tortoriello *et al.*¹⁷ Afterwards, they were incubated in 1x Click-iT reaction cocktail for 30 min, washed thoroughly in PBS and mounted.

Z-stack analysis. All captured pictures (in RAW format) have been analyzed and processed with ImageJ v1.440 software (National Institutes of Health, Bethesda, MD, USA). Z-stack analysis was performed by using STACK > ZProjection and STACK > Orthogonal views ImageJ plug-in.

Conflict of Interest

The authors declare no conflict of interest.

Acknowledgements. This work was supported by University Federico II of Naples and by POR Campania FSE 2007-2013 Project CREMe CUP B25B0900050007, which funded Rosario Vicidomini, Arianna Petrizzo and Liliana

Felicia Iannucci with research fellowships. A Di Giovanni PhD fellowship was supported by POR Campania FSE 2007-2013 Project 'Dottorato in Azienda' c/o Microtech srl.

1. Kondrashov N, Pusic A, Stumpf CR, Shimizu K, Hsieh AC, Xue S *et al*. Ribosome-mediated specificity in Hox mRNA translation and vertebrate tissue patterning. *Cell* 2011; **145**: 383–397.
2. McGowan KA, Li JZ, Park CY, Beaudry V, Tabor HK, Sabinis AJ *et al*. Ribosomal mutations cause p53-mediated dark skin and pleiotropic effects. *Nat Genet* 2008; **40**: 963–970.
3. McCann KL, Baserga SJ. Mysterious ribosomopathies. *Science* 2013; **341**: 849–5.
4. Angrisani A, Vicidomini R, Turano M, Furia M. Human dyskerin: beyond telomeres. *Biol Chem* 2014; **395**: 593–610.
5. Schwartz S, Bernstein DA, Mumbach MR, Jovanovic M, Herbst RH, León-Ricardo BX *et al*. Transcriptome-wide mapping reveals widespread dynamic-regulated pseudouridylation of ncRNA and mRNA. *Cell* 2014; **159**: 148–162.
6. Jack K, Bellodi C, Landry DM, Niederer RO, Meskauskas A, Musalgaonkar S *et al*. rRNA pseudouridylation defects affect ribosomal ligand binding and translational fidelity from yeast to human cells. *Mol Cell* 2011; **44**: 660–666.
7. Yoon A, Peng G, Brandenburg Y, Zollo O, Xu W, Rego E *et al*. Impaired control of IRES-mediated translation in X-linked dyskeratosis congenita. *Science* 2006; **312**: 902–906.
8. Bellodi C, Krasnykh O, Haynes N, Theodoropoulou M, Peng G, Montanaro L *et al*. Loss of function of the tumor suppressor DKC1 perturbs p27 translation control and contributes to pituitary tumorigenesis. *Cancer Res* 2010; **70**: 6026–6035.
9. Montanaro L, Calienni M, Bertoni S, Rocchi L, Sansone P, Storci G *et al*. Novel dyskerin-mediated mechanism of p53 inactivation through defective mRNA translation. *Cancer Res* 2010; **70**: 4767–4777.
10. Rocchi L, Pacilli A, Sethi R, Penzo M, Schneider RJ, Treré D *et al*. Dyskerin depletion increases VEGF mRNA internal ribosome entry site-mediated translation. *Nucleic Acids Res* 2013; **41**: 8308–8318.
11. Heiss NS, Knight SW, Vulliamy TJ, Klauk SM, Wiemann S, Mason PJ *et al*. X-linked dyskeratosis congenita is caused by mutations in a highly conserved gene with putative nucleolar functions. *Nat Genet* 1998; **19**: 32–38.
12. Giordano E, Peluso I, Senger S, Furia M. Minify, a *Drosophila* gene required for ribosome biogenesis. *J Cell Biol* 1999; **144**: 1123–1133.
13. Pardue ML, Rashkova S, Casacuberta E, DeBaryshe PG, George JA, Traverse KL. Two retrotransposons maintain telomeres in *Drosophila*. *Chromosome Res* 2005; **13**: 443–453.
14. Ryoo HD, Bergmann A. The role of apoptosis-induced proliferation for regeneration and cancer. *Cold Spring Harb Perspect Biol* 2012; **4**: a008797.
15. Potter CJ, Xu T. Mechanisms of size control. *Curr Opin Genet Dev* 2001; **11**: 279–286.
16. Dahmann C, Oates AC, Brand M. Boundary formation and maintenance in tissue development. *Nat Rev Genet* 2011; **12**: 43–55.
17. Tortoriello G, de Celis JF, Furia M. Linking pseudouridine synthases to growth, development and cell competition. *FEBS J* 2010; **277**: 3249–3263.
18. Phillips B, Billin AN, Cadwell C, Buchholz R, Erickson C, Merriam JR *et al*. The Nop60B gene of *Drosophila* encodes an essential nucleolar protein that functions in yeast. *Mol Gen Genet* 1998; **260**: 20–29.
19. Riccardo S, Tortoriello G, Giordano E, Turano M, Furia M. The coding/non-coding overlapping architecture of the gene encoding the *Drosophila* pseudouridine synthase. *BMC Mol Biol* 2007; **8**: 15.
20. Brand AH, Perrimon N. Targeted gene expression as a means of altering cell fates and generating dominant phenotypes. *Development* 1993; **118**: 401–415.
21. Grimm S, Pflugfelder GO. Control of the gene optomotor-blind in *Drosophila* wing development by decapentaplegic and wingless. *Science* 1996; **271**: 1601–1604.
22. Pérez-Garijo A, Martín FA, Morata G. Caspase inhibition during apoptosis causes abnormal signalling and developmental aberrations in *Drosophila*. *Development* 2004; **131**: 5591–5598.
23. Ryoo HD, Gorenc T, Steller H. Apoptotic cells can induce compensatory cell proliferation through the JNK and the wingless signaling pathways. *Dev Cell* 2004; **7**: 491–501.
24. Smith-Bolton RK, Worley MI, Kanda H, Hariharan IK. Regenerative growth in *Drosophila* imaginal discs is regulated by Wingless and Myc. *Dev Cell* 2009; **16**: 797–809.
25. Oh SW, Kingsley T, Shin HH, Zheng Z, Chen HW, Chen X *et al*. A P-element insertion screen identified mutations in 455 novel essential genes in *Drosophila*. *Genetics* 2003; **163**: 195–201.
26. Hay BA, Wolff T, Rubin GM. Expression of baculovirus P35 prevents cell death in *Drosophila*. *Development* 1994; **120**: 2121–2129.
27. Callus BA, Vaux DL. Caspase inhibitors: viral, cellular and chemical. *Cell Death Differ* 2007; **14**: 73–78.
28. Martín FA, Pérez-Garijo A, Morata G. Apoptosis in *Drosophila*: compensatory proliferation and undead cells. *Int J Dev Biol* 2009; **53**: 1341–1347.
29. Sun G, Irvine KD. Control of growth during regeneration. *Curr Top Dev Biol* 2014; **108**: 95–120.
30. Wu M, Pastor-Pareja JC, Xu T. Interaction between Ras(V12) and scribbled clones induces tumour growth and invasion. *Nature* 2010; **463**: 545–548.
31. Rodríguez AB, Zoranovic T, Ayala-Camargo A, Grewal S, Reyes-Robles T, Krasny M *et al*. Activated STAT regulates growth and induces competitive interactions independently of Myc, Yorkie, Wingless and ribosome biogenesis. *Development* 2012; **139**: 4051–4061.
32. Pérez-Garijo A, Shlevkov E, Morata G. The role of DPP and Wg in compensatory proliferation and in the formation of hyperplastic overgrowths caused by apoptotic cells in the *Drosophila* wing disc. *Development* 2009; **136**: 1169–1177.
33. Couso JP, Bishop SA, Martínez Arias A. The wingless signalling pathway and the patterning of the wing margin in *Drosophila*. *Development* 1994; **120**: 621–636.
34. Major RJ, Irvine KD. Influence of Notch on dorsoventral compartmentalization and actin organization in the *Drosophila* wing. *Development* 2005; **132**: 3823–3833.
35. Valenta T, Hausmann G, Basler K. The many faces and functions of β -catenin. *EMBO J* 2012; **31**: 2714–2736.
36. Somorjai IM, Martínez-Arias A. Wingless signalling alters the levels, subcellular distribution and dynamic of Armadillo and E-cadherin in third instar larval wing imaginal discs. *PLoS One* 2008; **3**: e2893.
37. Wodarz A, Stewart DB, Nelson WJ, Nusse R. Wingless signaling modulates cadherin-mediated cell adhesion in *Drosophila* imaginal disc cells. *J Cell Sci* 2006; **119**: 2425–2434.
38. Angrisani A, Turano M, Paparo L, Di Mauro C, FFuria M. A new human dyskerin isoform with cytoplasmic localization. *Biochim Biophys Acta* 2011; **1810**: 1361–1368.
39. Adachi-Yamada T, Fujimura-Kamada K, Nishida Y, Matsumoto K. Distortion of proximodistal information causes JNK-dependent apoptosis in *Drosophila* wing. *Nature* 1999; **400**: 166–169.
40. McEwen DG, Peifer M. Puckered, a *Drosophila* MAPK phosphatase, ensures cell viability by antagonizing JNK-induced apoptosis. *Development* 2005; **132**: 3935–3946.
41. Bosch M, Serras F, Martín-Blanco E, Baguña J. JNK signaling pathway required for wound healing in regenerating *Drosophila* wing imaginal discs. *Dev Biol* 2005; **280**: 73–86.
42. Bosch M, Baguña J, Serras F. Origin and proliferation of blastema cells during regeneration of *Drosophila* wing imaginal discs. *Int J Dev Biol* 2008; **52**: 1043–1050.
43. Mattila J, Omelyanchuk L, Kytälä S, Turunen H, Nokkala S. Role of Jun N-terminal Kinase (JNK) signaling in the wound healing and regeneration of a *Drosophila melanogaster* wing imaginal disc. *Int J Dev Biol* 2005; **49**: 391–399.
44. Bergantiños C, Corominas M, Serras F. Cell death-induced regeneration in wing imaginal discs requires JNK signalling. *Development* 2010; **137**: 1169–1179.
45. Rudrapatna VA, Bangi E, Cagan RL. Caspase signalling in the absence of apoptosis drives Jnk-dependent invasion. *EMBO Rep* 2013; **14**: 172–177.
46. Ring JM, Martínez Arias A. Puckered, a gene involved in position-specific cell differentiation in the dorsal epidermis of the *Drosophila* larva. *Dev Suppl* 1993; **121**: 251–259.
47. Agnès F, Suzanne M, Noselli S. The *Drosophila* JNK pathway controls the morphogenesis of imaginal discs during metamorphosis. *Development* 1999; **126**: 5453–5462.
48. Reuben PM, Cheung HS. Regulation of matrix metalloproteinase (MMP) gene expression by protein kinases. *Front Biosci* 2006; **11**: 1199–1215.
49. Fanjul-Fernández M, Folgueras AR, Cabrera S, López-Otín C. Matrix metalloproteinases: evolution, gene regulation and functional analysis in mouse models. *Biochim Biophys Acta* 2010; **1803**: 3–19.
50. Stevens LJ, Page-McCaw A. A secreted MMP is required for reepithelialization during wound healing. *Mol Biol Cell* 2012; **23**: 1068–1079.
51. Uhlirova M, Bohmann D. JNK- and Fos-regulated Mmp1 expression cooperates with Ras to induce invasive tumors in *Drosophila*. *EMBO J* 2006; **25**: 5294–5304.
52. Radisky ES, Radisky DC. Matrix metalloproteinase-induced epithelial–mesenchymal transition in breast cancer. *J Mammary Gland Biol Neoplasia* 2010; **15**: 201–212.
53. Ghazi A, Anant S, Vijay Raghavan K. Apterous mediates development of direct flight muscles autonomously and indirect flight muscles through epidermal cues. *Development* 2000; **127**: 5309–5318.
54. Khan MA, Chen HC, Zhang D, Fu J. Twist: a molecular target in cancer therapeutics. *Tumour Biol* 2013; **34**: 2497–2506.
55. Sudarsan V, Anant S, Guptan P, Vijay Raghavan K, Skaer H. Myoblast diversification and ectodermal signaling in *Drosophila*. *Dev Cell* 2001; **1**: 829–839.
56. Roy S, Vijay Raghavan K. Muscle pattern diversification in *Drosophila*: the story of imaginal myogenesis. *BioEssays* 1999; **21**: 486–498.
57. Evans CJ, Olson JM, Ngo KT, Kim E, Lee NE, Kuoy E *et al*. G-TRACE: rapid Gal4-based cell lineage analysis in *Drosophila*. *Nat Methods* 2009; **6**: 603–605.
58. Pallavi SK, Shashidhara LS. Egr/Ras pathway mediates interactions between peripodial and disc proper cells in *Drosophila* wing discs. *Development* 2003; **130**: 4931–4941.
59. Pallavi SK, Shashidhara LS. Signaling interactions between squamous and columnar epithelia of the *Drosophila* wing disc. *J Cell Sci* 2005; **118**: 3363–3370.
60. Worley MI, Setiawan L, Hariharan IK. Regeneration and transdetermination in *Drosophila* imaginal discs. *Annu Rev Genet* 2012; **46**: 289–310.
61. Mollereau B, Pérez-Garijo A, Bergmann A, Miura M, Gerlitz O, Ryoo HD *et al*. Compensatory proliferation and apoptosis-induced proliferation: a need for clarification. *Cell Death Differ* 2013; **20**: 181.
62. Sun G, Irvine KD. Regulation of Hippo signaling by Jun kinase signaling during compensatory cell proliferation and regeneration, and in neoplastic tumors. *Dev Biol* 2011; **350**: 139–151.
63. Repiso A, Bergantiños C, Corominas M, Serras F. Tissue repair and regeneration in *Drosophila* imaginal discs. *Dev Growth Differ* 2011; **53**: 177–185.
64. Bergmann A, Steller H. Apoptosis, stem cells and tissue regeneration. *Sci Signal* 2010; **3**: re8.

65. Lamouille S, Xu J, Derynck R. Molecular mechanisms of epithelial–mesenchymal transition. *Nat Rev Mol Cell Biol* 2014; **15**: 178–196.
66. Parry EM, Alder JK, Lee SS, Phillips JA III, Loyd JE, Duggal P *et al*. Decreased dyskerin levels as a mechanism of telomere shortening in X-linked dyskeratosis congenita. *J Med Genet* 2011; **48**: 327–333.
67. Alter BP, Giri N, Savage SA, Rosenberg PS. Cancer in dyskeratosis congenita. *Blood* 2009; **113**: 6549–6557.
68. Yin Z, Xu XL, Frasch M. Regulation of the twist target gene tinman by modular cis-regulatory elements during early mesoderm development. *Development* 1997; **124**: 4971–4982.
69. Bach EA, Ekas LA, Ayala-Camargo A, Flaherty MS, Lee H, Perrimon N *et al*. GFP reporters detect the activation of the *Drosophila* JAK/STAT pathway *in vivo*. *Gene Expr Patterns* 2007; **7**: 323–331.



Cell Death and Disease is an open-access journal published by **Nature Publishing Group**. This work is licensed under a **Creative Commons Attribution 4.0 International License**. The images or other third party material in this article are included in the article's Creative Commons license, unless indicated otherwise in the credit line; if the material is not included under the Creative Commons license, users will need to obtain permission from the license holder to reproduce the material. To view a copy of this license, visit <http://creativecommons.org/licenses/by/4.0/>

Supplementary Information accompanies this paper on Cell Death and Disease website (<http://www.nature.com/cddis>)